INFORMATION TO USERS

This material was produced from a microfilm copy of the original document. While the most advanced technological means to photograph and reproduce this document have been used, the quality is heavily dependent upon the quality of the original submitted.

The following explanation of techniques is provided to help you understand markings or patterns which may appear on this reproduction.

1. The sign or "target" for pages apparently lacking from the document photographed is "Missing Page(s)". If it was possible to obtain the missing page(s) or section, they are spliced into the film along with adjacent pages. This may have necessitated cutting thru an image and duplicating adjacent pages to insure you complete continuity.

2. When an image on the film is obliterated with a large round black mark, it is an indication that the photographer suspected that the copy may have moved during exposure and thus cause a blurred image. You will find a good image of the page in the adjacent frame.

3. When a map, drawing or chart, etc., was part of the material being photographed the photographer followed a definite method in "sectioning" the material. It is customary to begin photoing at the upper left hand corner of a large sheet and to continue photoing from left to right in equal sections with a small overlap. If necessary, sectioning is continued again — beginning below the first row and continuing on until complete.

4. The majority of users indicate that the textual content is of greatest value, however, a somewhat higher quality reproduction could be made from "photographs" if essential to the understanding of the dissertation. Silver prints of "photographs" may be ordered at additional charge by writing the Order Department, giving the catalog number, title, author and specific pages you wish reproduced.

5. PLEASE NOTE: Some pages may have indistinct print. Filmed as received.

University Microfilms International
300 North Zeeb Road
Ann Arbor, Michigan 48106 USA
St. John's Road, Tyler's Green
High Wycombe, Bucks, England HP10 8HR

Downloaded from SHAREOK. Persistent Handle URL: https://hdl.handle.net/11244/4471

7824607

MORIYAMA, KOJI
ELECTROMAGNETIC PROPERTIES OF THIN FILM LEAD SUPERCONDUCTORS.

THE UNIVERSITY OF OKLAHOMA, PH.D., 1978

University Microfilms International 300 N. ZEEB ROAD, ANN ARBOR, MI 48106

© 1978

KOJI MORIYAMA

ALL RIGHTS RESERVED

THE UNIVERSITY OF OKLAHOMA

GRADUATE COLLEGE

ELECTROMAGNETIC PROPERTIES OF THIN FILM LEAD SUPERCONDUCTORS

A DISSERTATION

SUBMITTED TO THE GRADUATE FACULTY

in partial fulfillment of the requirements for the

degree of

DOCTOR OF PHILOSOPHY

BY

KOJI MORIYAMA

Norman, Oklahoma

1977

ELECTROMAGNETIC PROPERTIES OF

THIN FILM LEAD SUPERCONDUCTORS

APPROVED BY:

D E Dolde

Stephen Whitmore

Stanley E. Babb, Jr.

C. K. Hulen

Robert M. St. John

DISSERTATION COMMITTEE

TABLE OF CONTENTS

Page

List of Tables iv

List of Figures. v

Chapter

I. Introduction. 1

II. Historical Survey 8

III. Theory. 22

IV. Ultra-High-Vacuum (UHV) System. 75

V. Results and Discussion. 123

VI. Conclusions 176

References 178

Appendix I 185

Appendix II. 188

LIST OF TABLES

Page

5-1. Measured values of thickness d, critical magnetic field H_{cF} and critical temperature T_c, and calculated values of penetration depth $\lambda(0,d)$, coherent length ξ_0 for thin films and ξ_0' for thick films and mean free path ℓ of lead films. 153

5-2. Measured resistance R of lead films at $4.2^{\circ}K$ and $295^{\circ}K$ are given in second and third columns respectively. Resistivity ρ calculated from R and nominal thickness d by Eq. (151) are in fourth and fifth columns. Nominal thickness d in seventh column is from deposition rate. The last column gives the thickness d (electrical) calculated by Eq. (151) 154

5-3. Values of the penetration depth $\lambda(0)$ and the coherent length ξ_0 calculated and observed by other groups. 163

LIST OF FIGURES

Page

3-1. Magnetic distribution in a superconduction plate placed in a magnetic field H parallel to its surface (a) $d>>\lambda$; (b) $d<<\lambda$. 25

3-2. Magnetization curves of lead films at $4.2^{o}K$ 27

3-3. In parallel field geometry, vortices are limited by film thickness. 33

3-4. The case of an infinitely wide film with thickness $\underline{d}$ 58

3-5. (a) Current densities vs. distance from center of film. (b) Direction and magnitude of field in and around superconducting film 62
(c) Horizontal component of magnetic field in plane of top surface of film vs. distance from center of film. (d) Normal component of magnetic field in plane of top surface of film vs. distance from center of film. 63

3-6. Current distribution in a superconducting film with rectangular cross-section 66

3-7. Cross section of film in tangential external field and carrying transport current. 67

Page

3-8. Magnetic field and applied current profiles for a cross section near the center of the sample. 70

4-1. PHI Cylindrical-Auger Electron Optics system and associated electronics 78

4-2. Gas manifold schematic 83

4-3. Distribution of sputtered materials. 88

4-4a. Automatic pressure control schematic 93

4-4b. Residual gases of the ultra high vacuum system at $3x10^{-7}$ torr. 98

4-5. Thin film pattern used to make electrical measurement. 99

4-6. Vacuum system used in the calibration of millitorr ionization gauge 103

4-7. A block diagram of the experimental arrangement of the cryogenic apparatus 107

4-8. The fundamental stru-ture of the Dektak system . . 112

4-9. A typical surface profile of a sapphire substrate. 114

4-10. A typical surface profile of a lead film 115

4-11. Profile of a typical film, showing the lead. . . . 114

4-12. A histogram of y_i-h vs. frequency for the smooth side of the sapphire single crystal plate. 118

4-13. The surface simplified with triangle valleys and peaks, and the profile of the surface with the stylus as the round circle 120

Page

4-14. (a) The stylus climbs over a distance of 1.6 microns. (b) The distance of 1.6 microns at the magnification of 20,000x. (c) The vertical magnification is much higher than the horizontal 121

4-15. The broadening of the step of the profile of the surface by the horizontal magnification 122

5-1. The definition of T_c for low H. 124

5-2. The definition of T_c for high H 124

5-3. The definition of H_{cF} 124

5-4. (a) H vs. T^2 for the lead film roughened by sand paper of #180 126

(b) H vs. T^2 for the lead film roughened by #320 sand paper. 127

(c) H vs. T^2 for the lead film roughened vertically 129

(d) H vs. T^2 for the film roughened horizontally. . 130

5-5. Data for sample S1 is plotted by Eq. (27) of the thin film approximation 131

5-6. Data for sample R1 is plotted by Eq. (27) of the thin film approximation 132

5-7. Data for sample S2 is plotted by Eq. (27) of the thin film approximation 133

5-8. Data for sample S3 is plotted by Eq. (27) of the thin film approximation 134

5-9. Data for sample S4 is plotted by Eq. (27) of the thin film approximation 135

Page

5-10. (a) Data for sample S5 is plotted by Eq. (27) of the thin film approximation. 137

(b) Data for sample S5 is plotted by Eq. (27) of the thin film approximation. 138

5-11. (a) Data for sample S6 is plotted by Eq. (26) of the thick approximation. 139

(b) Data for sample S6 is plotted by Eq. (27) of the thin film approximation. 140

5-12. (a) Data for sample R6 is plotted by Eq. (26) of the thick film approximation 141

(b) Data for sample R6 is plotted by Eq. (27) of the thin film approximation. 142

5-13. (a) Data for sample S7 is plotted by Eq. (26) of the thick film approximation 143

(b) Data for sample S7 is plotted by Eq. (27) of the thin film approximation. 144

5-14. (a) Data for sample S8 is plotted by Eq. (26) of the thick film approximation 145

(b) Data for sample S8 is plotted by Eq. (27) of the thin film approximation. 146

5-15. Data for sample R8 is plotted by Eq. (26) of the thick film approximation 147

5-16. Data for sample S9 is plotted by Eq. (26) of the thick film approximation 148

5-17. Data for sample R9 is plotted by Eq. (26) of the thick film approximation 149

Page

5-18. (a) A typical surface profile of the smooth side of a sapphire substrate. (b) A typical surface profile of the rough side of a sapphire substrate. 151

5-19. Auger spectra of a lead film 156

5-20. Auger spectra of the lead film of Fig. 5-19 taken six months later 157

5-21. The critical magnetic field H_{cF} vs. the film thickness d for thin films 159

5-22. H_{cF}/H_c - 1 vs. the film thickness d for thick films. 160

5-23. The critical magnetic field H_{cF} vs. the film thickness. 161

5-24. Critical current I_c vs. temperature t where $t = T/T_c$ 165

5-25. Critical current I_c vs. critical magnetic field H_{cF} of sample S10. 168

5-26. (a) I_c vs. H_{cF} for sample S11. 169

(b) I_c vs. H_{cF} for sample R11. 170

5-27. (a) I_c vs. H_{cF} for sample S13. 171

(b) I_c vs. H_{cF} for sample R12. 172

5-28. (a) I_c vs. H_{cF} for sample S14. 173

(b) I_c vs. H_{cF} for sample R14. 174

5-29. I_c vs. H_{cF} for sample S15. 175

ABSTRACT

The dependence of critical film magnetic field H_{cf} on temperature, thickness, and surface texture of lead superconducting films was investigated, as well as the relationship between the applied magnetic field and the applied current at the critical field. Temperature and thickness dependence data were consistent with the predictions of London, of Ginzburg, and of Bardeen, Cooper, and Schreiffer. The values of H_{cf} of lead films deposited on a rough surface were consistently lower than for those on a smooth surface and so were not in agreement with any currently accepted theory. The degree of lowering of H_{cf} by a rough surface was greater in thin films than in thick films. The expected dependence of penetration depth λ on thickness d was not observed, and the range of λ was somewhat greater than expected. The range of coherence length was greater than predicted. The prediction for temperature dependence of critical current by Glover and

Coffey was found to involve some oversimplification, and a suggested correction is supported by the data. For applied magnetic fields perpendicular to the applied current and parallel to the film surface, the relationship between the critical values of the magnetic field and the current was as predicted for lead films by Alphonse and Bergstein.

ELECTROMAGNETIC PROPERTIES OF THIN FILM LEAD SUPERCONDUCTORS

CHAPTER I

INTRODUCTION

The resistivity of a normal metal decreases with decreasing temperature, approaching a constant value at a temperature less than 10°K. For instance, the resistivities of aluminum and copper with purity of 99.999% are the order of 10^{-9} ohm-cm at 4.2°K. However, the resistivity of very pure mercury suddenly decreases to zero at 4.15°K. Measurements with a sensitivity of 10^{-9} ohm-cm fail to indicate any resistivity.[1] This phenomenon is called "superconductivity". Since superconductivity was discovered in 1911 by Kammerligh Onnes,[2] twenty-four elements and well over a thousand compounds and alloys have been shown to be superconductors with transition temperatures ranging from 0.0002°K for rhodium[3] to 22.3°K for Nb_3Ge.[4] The superconducting properties of alloys and intermetallic compounds

in an applied magnetic field are quite different from those of elements. The latter are called type I and the former type II superconductors. Theoretical and experimental work into the nature and origin of superconductivity has resulted in several successful theories: the microscopic theory by Bardeen, Cooper and Schreiffer (1957),[5] and the phenomenological theories earlier by F. and H. London (1935),[6] and later by Ginzburg and Landau (1950).[7] Superconductivity is now well established as a macroscopic manifestation of a quantum effect.

The behavior of superconducting films is of basic interest and of considerable technological importance. When a superconducting specimen is placed in a magnetic field, the field strength within the film decays very rapidly with distance inward from the surface. The behavior of the uppermost layer, which is called the penetration depth, λ, differs from that of the bulk. Therefore, measurements on thin films of superconductors could lead to information valuable for the development of theories. Practical applications of superconducting films include the development of high-speed memory storage devices utilizing the field induced superconducting-normal transition in type I superconducting films such films as Pb, Sn and In, and electrical power transmission lines which consist of fibers of alloyed metals such as Nb_3Sn.

Film Thickness Dependence of a Critical Magnetic Field of a Film

The transition of a superconductor to the normal state occurs when the magnetic energy resulting from the diamagnetic flux exclusion overcomes the condensation energy of the superconducting state. It is well known that the critical magnetic field of a superconducting film, H_c, at which the transition to the normal state occurs, is higher than the critical magentic field of a bulk specimen, H_c, when the film thickness, d, becomes comparable to the penetration depth, λ, and the field is applied parallel to the film surface. The same functional forms for H_c (with different coefficients) are predicted by the London, Ginzburg-Landau and BCS theories, discussed in Chapter III. The thickness ranges are usually discussed for $d>>\lambda$, the thick film region and $d<<\lambda$, the thin film region. Although Ginzburg[8] derived the critical thickness, d_c, as $d_c=\sqrt{5}\lambda$, the actual value of d_c is not clear, since λ varies with d. There is no equation to represent the intermediate thickness region, i.e., the region around d_c. So far, no study has been in this area.

Temperature Dependence of a Critical Magnetic Field of a Film

The previous section mentioned two quantities, the bulk critical magnetic field H_c and penetration depth λ, which are dependent on temperature. The temperature dependence of H_c and λ will be indicated in Chapter III.

However, the temperature dependence of λ and the critical magentic field of a thin film, H_{cf}, in the intermediate thickness region is not clear. Studies of thickness and temperature dependence of H_{cf} of lead films are reported by Lock (1951),[9] Mydosh and Meissner (1965),[10] Cody and Miller (1968),[11] Kratzig, Walther and Shilz (1969),[12] and Huebner (1970).[13] However, their work were done on thick films. Cody and Miller, who did intensive work on lead film, used only two thicknesses, 500Å and 900Å, for thin films.

Influence of Surface Roughness on Critical Magnetic Field of a Film

Recent experiments show that surface abrasion results in the persistence of superconductivity at enhanced magnetic fields. Hill, Kohr and Rose (1969),[14] Fink and Joiner (1969),[15] Morrison and Rose (1970),[16] and Melville (1971, 1972)[17] reported that superconducting films with rough surfaces had higher critical magnetic fields, H_{cf}. Only one case reported by Easson and Hlawiczka (1968)[18] associated a rough surface with a lower value of sheath current, which is related to magnetic fields, than that of a smooth surface. Bussiere and Suenage (1975)[19] reported that, in order to get low a.c. loss in Nb_3Sn while high critical current are maintained, the best results were obtained from the surface treatment of an initial mechanical polish followed by electropolishing or annealing. The surface conditions for these experiments, except for

Morrison and Rose,[16] were not specified. However, all these reports were for type II superconductors. There is no report concerning influence of surface roughness on critical magnetic field for type I superconductor.

The Relationship Between Applied Magnetic Field and Current of a Film

There are a great deal of data concerning I versus H curves for type I and type II materials, but no theoretical curves for them, except for the work of Mydosh and Meissner.[10] Their work was done for tin deposited on hollow glass tubing with I parallel to H. Their theoretical curve is based on Ginzburg's theoretical equation:[20]

$$I = (a - bH^2)^{3/2}$$

Their data closely agree with Ginzburg's prediction. However, Ginzburg's equation cannot be applied to this present work because I is perpendicular to H. Alphonse and Bergstein[21] derived the equation for the case of I perpendicular to H in terms of applied magnetic fields and magnetic fields due to applied currents. It is based on Ginzburg-Landau theory.[7] When it is rewritten in terms of I and H, it gives the same form of the equation as above with different constants a and b. So far, there are no experimental data to prove or disprove the modified Alphonse and Bergstein equation.[21]

The Present Work

In view of the questions outlined above, the purpose of this work was of basic interest and was to determine empirical relationships between the variables critical magnetic field and critical current, and the thickness, temperature and surface texture of superconducting lead films. In this work, the specimens used were lead, a type I superconductor. Thickness and temperature dependence of H_{cf} were investigated and data obtained were fitted to equations predicted by Ginzburg. Lead was deposited on smooth or rough surfaces of substrates. To specify the surface texture of films, or in this work, the surface texture of substrates, surfaces were profiled mechanically by the stylus system and their roughness determined. Chemical components of a surface of the film were determined by an Auger Electron Spectrometer. In this present work, the value of H_{cf} of lead films deposited on a rough surface was consistently lower than that for films deposited on a smooth surface. The results obtained did not agree with any current explanation.

The final part of this present work was to determine the relationship between the applied magnetic field and applied current at the critical field. The applied magnetic field is parallel to the surface of the film, but perpendicular to the applied current. Experimental data of I versus H are plotted in semi-log graph

sheets for smooth and rough surface films. The plotted curves are analyzed with the equation predicted by Alphonse and Bergstein.[21] Plotted curves also showed that critical currents are depressed. However, the explanation for this depression of H_{cf} is not known at this time. The author of this work feels that the measurement of I versus H for specimens of this type is the first reported in this field.

CHAPTER II

HISTORICAL SURVEY

Historical Background of the Study of Thin Film Superconductors

The first studies of very small superconductors such as thin films or wires began in the middle of the 1930's. Meissner and Ochsenfield (1933)[22] discovered the complete exclusion of magnetic flux from a pure bulk specimen in the superconducting state, known as the Meissner effect. By examining an old theory of Becker, Heller and Sauter (1933),[23] F. and H. London (1935)[6] not only succeeded in explaining the Meissner effect theoretically but predicted many electromagnetic properties of superconductors. Works of critical magnetic field and critical current are listed chronologically.

a) Critical Magnetic Field

One prediction of the London theory was "a very small superconductor should have a much higher magnetic

threshold value than a bulky one,[11] which was also derived by M. von Laue (1938)[24] from a different concept. This prediction was subsequently confirmed experimentally by Pontius (1937),[25] Shalnikov (1938),[26] Appleyard and co-workers (Appleyard and Lowell, 1937;[27] Appleyard and Misener, 1938;[28] Appleyard, Bristow and London, 1939;[29] Appleyard, Bristow, London and Meissner, 1939[30]), and Alekseyevsky (1941).[31] In these works lead wires (Pontius), tin and lead films (Shalnikov), mercury film (Appleyard et. al.) and tin film (Alekseyevsky) were used. The results of these works provided the first indication that the penetration effect of the magnetic field was important for thin specimens in producing a very high critical field. Appleyard et. al. and Alekseyevsky found the temperature dependence of parallel magnetic critical fields, H_C , for films of various thickness, d. The empirical relation between the critical magnetic field, H_{CF}, and film thickness, d, is given as

$$H_{CF} = H_C \left(1 + \frac{C}{d}\right) \qquad \text{(A)}$$

where H_C is the critical magnetic field of bulk material and C is a constant, about 1×10^{-5} cm. However, the interpretation of the measurements of these works was not straightforward.

Shoenberg (1940),[32] by using mercury colloids, obtained direct evidence that a magnetic field penetrates a superconductor appreciably. He also proved that the penetration depth λ or the constant c in equation (A) varies with temperature, which was predicted by Casimir (1940)[33] using the two-fluid model which was developed by C. Gorter and H. Casimir (1934).[34] Andrew (1941),[35] with rolled tin films, verified equation (A) and the temperature dependence of thin films. Ginzburg (1945)[36] suggested that if the penetration depth is independent of field strength, then the constant C is $\lambda + \beta$ instead of λ, where

$$\beta = \frac{8\pi}{H_c^2} (\alpha_n - \alpha_s)$$

and α_n, α_s are the surface energies per unit ares between the normal metal and insulator, and the superconducting metal and insulator respectively. A similar argument was given thermodynamically by Pippard (1951).[37] Andrew (1949)[38] with rolled tin films and Lock (1950)[39] with tin, lead and indium films evaporated on mica, verified equation (A) with interpretations of the constant C by Ginzburg and Pippard. Shoenberg (1952)[40] pointed out that thick speciments ($d>>\lambda$) or very thin ones ($d<<\lambda$) can be treated independently by calculating the thickness dependence of the ratio of magnetic suceptibility χ of a sample into which the applied field penetrates, to the susceptibility χ_o of an

identical sample from which the field is entirely excluded.

Pippard (1950,[41] 1953[42]) initiated experiments on the surface impedance of superconductors at microwave frequencies. One result of his measurements was that the value of λ for a tin -3% indium alloy was nearly twice its value for pure tin, even though all thermodynamic properties changed by only a few percent upon alloying. This result is contrary to the prediction of the London theory that λ is a function of only the electron effective mass and density, neither of which would be strongly changed by the introduction of small amount of impurity. In order to explain the impurity effect upon λ, Pippard introduced a new parameter, the coherence length ξ (about 10^{-4} cm in a bulk superconductors), over which superconducting electrons do not behave completely independently of each other, but exhibit strong correlation or "long range order". He also derived the relation between the coherence length ξ and the electron mean free path ℓ. This modification of the London theory is called the "Pippard non-local theory".

Meanwhile Ginzburg and Landau (1950)[7] developed a new phenomenological theory which was based on the work of Landau (1973)[43] on second-order phase transitions. Ginzburg and Landau noticed certain inadequacies of the London theory: (a) the critical fields of thin films were correctly predicted only by assuming that λ varied with film thickness, (b) there

was no explanation of the enormous positive surface energy which appeared to be associated with the normal-superconducting interface in superconductors; and (c) the theory did not allow a description of the critical current in thin films. In order to explain these inadequacies, they introduced a complex order parameter $\psi(r)$ with amplitude and phase such that $|\psi(r)|^2$ may be considered as the density of superconducting electrons, and developed a nonlinear Schrödinger-like equation which $\psi(r)$ satisfies. The Ginzburg-Landau theory correctly predicted the change from first-order to second-order transitions with decreasing thickness d, and derived the dependency of H_{cf} upon $(T_c - T)^{1/2}$ and $\lambda(T)/d$. Gor'kov (1960),[44] using the microscopic theory based upon the Green's function method, obtained the same results as Ginzburg and Landau.

The Ginaburg-Landau theory of the film thickness and temperature dependencies of H_c was elaborated upon by Douglass (1961),[45] Douglass and Blumberg (1962),[46] and de Gennes and Tinkham (1964).[47] Bardeen (1962),[48] and Hauser and Helfand (1962)[49] derived the relationship between H_{cf} and d based on modification of the BCS theory by Miller (1959).[50] The variation of the penetration depth by thickness was considered by Tinkham (1958)[51] who used the Pippard equations (1953).[42] Miller calculated λ as a function ξ/λ from the BCS theory. Douglas (1961)[45] combined Tinkham and Miller's relationships and derived

the expression for the dependence of λ on d and ℓ. These theoretical investigations were verified empirically by Zavaritskii with tin films (1951),[52] with thallium films (1952),[53] Khukhareva (1961)[54] with thin mercury films, Douglass and Blumberg (1962)[46] with tin films deposited on glass substrates at 77°K, Toxen (1962)[46] with tin films Douglass and Meservey (1964)[56] with aluminum films and Glover (1964)[57] who compiled the data of Zavaritskii, and Douglass and Blimberg's. There was a general agreement between theory and experiment.

Shubnikov, Khotkevich, Shepelev and Riabinin (1936,[58] 1937,[59]) discovered a new class of superconductors, the type II superconductor, by observing the magnetization curves of lead-indium and lead-thallium alloys. However, this pioneering work went unrecognized until Abrikosov (1952,[60] 1957[61]) and Zavaritskii (1952)[53] proposed the structure of the mixed state consisting of a periodic array of quantized vortex lines threading the superconductor, based on the Ginzburg and Landau theory, and applied it to Shubnikov's data. Abrikosov also predicted the thickness and temperature dependence of the upper critical field for a film in parallel field. These papers were overlooked in the flurry over microscopic theories started in 1957.[5] Renewed interest in type II superconductors was initiated by Goodman (1961)[62] who suggested that Nb_3Sn with very high

critical magnetic field (2×10^5 gauss), might be a type II superconductor. Nb_3Sn was discovered by Kunzler (1961).[63]

All work on thin films done before 1961 was on type I superconductors. However, it may be pointed out that, although the criterion for the type classification of superconductors is the same for both bulk and films, a thin film prepared from a type I superconductor may behave as type I or type II, depending on the effective value of the electron mean path, which is strongly influenced by its thickness, impurities, imperfections, and grain size. For example, by increasing the mean free path by annealing a vapor-quenched film, its type II behavior may be changed to type I.

Saint James and de Gennes (1963)[64] calculated universal curves for the critical parallel magnetic field of thick and thin type II films as a function of d and λ. They also showed that, as a magnetic field approached H_{cf}. volume superconductivity is destroyed, however, superconductivity in a sheath, with a thickness of about ξ, parallel to the applied magnetic field continues to exist up to a third critical field H_{c_3}, which is $1.69H_{c_2}$. This is called the "surface superconductivity". It occurs in every type II superconductor. However, Cardona and Rosedblum (1964)[65] mentioned that type I superconductors, with the exception of lead and tantalum (and possibly vanadium and lanthanum), do not exhibit surface superconductivity.

Due to the massive amount of research on superconductors after the discovery of type II superconductors and surface superconductivity it is impossible to conveniently list all the work about magnetic properties of superconducting films in parallel magnetic fields. For this reason, only those relating more directly to my project will be mentioned by name.

The following are papers used in this work for studying lead film, which is a type I superconductor. Rhoderick (1962)[66] studied the vertical magnetic field dependency on thickness of tin films in parallel magnetic field. Burger, Deutschen, Guyon and Martinent (1965)[67] studied $\lambda(T)$ and $\xi(T)$ of type I and type II superconducting films as a function of the film thickness with films of tin and tin-indium, indium-lead and lead-bismuth alloys. Seidel and Meissner (1965)[68] measured thermal and electrical conductivity of lead films. Alphonse and Bergstein (1967)[69] solved the Ginzburg and Landau equations for arbitrary parallel magnetic field and showed the relationship between the external field and field generated by supercurrents. Baldwin (1963),[70] and Tilley, Baldwin and Robinson (1966)[71] discussed hysteresis in magnetic field phase transition curve of tin films. A third critical magnetic field (or surface nucleation field), Hc_3, of lead films was measured for two different rough surfaced films by Fischer (1968).[72] Cody and Miller measured critical magnetic fields as a function of temperature and thickness for lead films

evaporated onto glass substrates (1968)[73] and for tin films evaporated onto glass substrates at 77°K (1968),[74] and their experimental data generally agreed with the Ginzburg and Landau, and Saint James and de Gennes theories. A comparison of the Ginzburg and Landau parameter K for lead, tin and indium, made by Cody and Miller (1970).[75]. Experimental data of H_{cf} dependency on d of aluminum films by Khuskhareva (1962),[76] and Douglass and Meservey (1964)[56] were compiled with Tedow and Meservey's data by Tedow and Meservey (1973).[77] They also obtained H_{cf} as a function of temperature and field direction and discussed their results with the theory of high-field superconductors. The apparatus which Hayler, Geppert, Chen and Kim (1975)[78] used for Quantum-resistance states of lead film was very similar to the one which was used in my project.

The following are papers used in this work for films of niobium which is a type II superconductor. DeSorbe (1964)[79] showed the influence of gasses in the film on electromagnetic properties. Neugebauer and Ekvall (1964)[80] studied films of niobium, tantalum, and vanadium evaporated on quartz substrates. By changing the coherence length, Sosniak and Hull (1967)[81] produced niobium films by dc diode sputtering and compared them with those produced by the evaporation method. Hlawiczka and Rose (1967)[82] measured the thickness on non-superconducing niobium films by a Taysurf gauge and compared the results with thickness estimated from

the weight of niobium deposited by sputtering on the inner surface of a quartz tubular substrate. Ward and Tilley (1971)[83] studied rolled niobium foils in parallel magnetic fields.

b) Critical Current

The destruction of superconductivity by current was discovered by K. Onnes (1913).[84] After the discovery of a critical magnetic field (Hc), Silsbee (1916)[85] pointed out that the critical current Ic restoring the resistance will be that current which generates the critical magnetic field at the surface of the conductor if there is no applied magnetic field. This is known as "Silsbee's hypothesis". H. London (1935)[86] showed that the critical current density Jc of thick wire has the same value as Silsbee's hypothesis but those of thin wire and thin film have smaller values than Silsbee's hypothesis.

Schubnikov and Alekseyeusky (1936)[87] showed that there was a discontinuous restoration of resistance of tin wire at exactly the current strength predicted by Silsbee's hypothesis as $R/R_o \approx 0.8$ where R_o is the full normal resistance of the wire, and R, the resistance with current. F. London (1937)[88] predicted the restoration curve of resistance of a wire by a current at constant temperature, influence of current strength on the curve, and the intermediate state structure of a current carrying wire. Shalnikov (1938)[26]

measured the critical current density for lead and tin films. However, London's prediction for wire could not be applied to Shalnikov's thin film results. Scott (1948)[89] found that the ratio R/R_o of indium wire varies inversely with the wire diameter. Kuper (1952)[90] attributed this divergence of Scott's results to increased resistance introduced by the scattering of conduction electrons at interphase boundaries of normal and superconducting states. Makei (1958)[91] confirmed experimentally the intermediate state structure of wire postulated by F. London by inserting a bismuth magnetoresistive probe into a slot cut into current-carrying wire. Baird and Mukherjee (1967,[92] 1970[93]) revised the London theory of the curve of the restoration of resistance of a wire by a current, and of the intermediate state structure of the wire. Their improved model was in good agreement with experimental values for the restoration curve by Freud, Sulkowski and Makiej (1968).[94]

Glover (1958)[95] measured the critical current dependency on the temperature for lead and tin films with 50Å thickness. Bremer and Newhouse (1958)[96] pointed out that if small regions are present, the Joule heating due to the high current densities would lead to an abrupt transition to the normal state at lower current values than the predicted critical current value, J_c. Using short current pulses and a substrate such as single-crystal sapphire, which has a high thermal conductivity to suppress Joule heating phenomena,

Bremer and Newhouse (1959)[97] obtained current induced-transition curves of tin films and that the transition curve is still very broad and J_c is substantially lower than the prediction. Smallman, Slade and Cohen (1960),[98] and Schimidlin, Learn, Critten and Cooper (1960)[99] also obtained the value of J_c five to thirty five times lower than the prediction. These results indicate that the current distribution across the width of a film is not uniform as mentioned by Schoenberg (1952).[40]

Shoenberg (1952)[40] pointed out that the current in a film is concentrated in the edge and the current distribution in a film according to the London's equation has not yet been solved because of mathematical difficulty. Marcus (1961)[100] obtained the numerical distributions of currents and magnetic fields in and around a superconducting film carrying a steady current. In the discussion of communications of Marcus' paper, Glover (1961)[101] quoted the current density distribution derived by Bowers, which was unpublished. Rhoderick and Wilson (1962)[102] and Broom and Rhoderick (1961)[103] measured the perpendicular component of the magnetic field due to a current through a lead film of 2000Å thickness and showed that the measured field agreed well with that calculated from the non-uniform current distribution predicted by Bowers. By using the Bowers' distribution in tin films evaporated on a quartz substrate. Glover and Coffey (1964)[104] found that both the magnitude

and temperature dependence of J_c over a substantial temperature range were in good agreement with the theory predicted by Bardeen (1962).[105] Mydosh and Meissner (1965)[10] used the pulse method to measure the temperature dependence of critical currents of a planar tin film and reported the same results as those Glover and Coffey observed. Huebener and Gallus (1973)[106] proposed the model of the nucleation of the current-induced intermediate state in lead and indium films, which was analogous to the kink instability in magnetohydrodynamics.

In order to avoid non-uniform current distribution of films, Feigin and Shalnikow (1956),[107] Ginzburg and Shalnikov (1959),[108] and Alekseevskii and Mikheeva (1960)[109] used a compensated geometry with tin films deposited on the outside of cylinders, which eliminate the edge effect. Their results were in poor agreement with the magnitude of J_c, but showed that the temperature dependency of I_c predicted by the Ginzburg and Landau theory. Edwards and Newhouse (1962)[110] used another compensated geometry. A tin film was deposited on a flat insulated "shield plane" made of lead which has higher critical temperature. The J_c of the double shield tin increased by a factor of 2.5 times the J_c of the unshielded tin film. However, the observed magnitude of J_c is still smaller than the predicted one. Bardeen (1962)[105] calculated a more exact equation of the temperature dependency of J_c including the equation from the Ginzburg and Landau

theory as limit $T \approx T_c$. Extensive dc and pulse measurements of J_c were reported by Mydosh and Meissner (1965)[10] on cylindrical tin film deposited on Hollow glass tubes. They obtained close agreement in the temperature dependence of J_c with Bardeen's calculation.

Critical currents measurements were also taken with external magnetic field on cylindrical tin films by Mydosh and Meissner (1965).[10] Their I_c versus H curves closely agreed with the theoretical predictions of Ginzburg (1958).[20]

Papers used for studying niobium films are listed below. Neugebauer and Ekvall (1963)[111] measured the I_c-H curve for niobium films deposited on quartz substrates with varying thickness. Fowler (1963)[112] produced noibium films vapor-deposited on quartz and copper substrates by using electron bombardment technique and noted the aging effect for the current-carrying capacity. Using the laminar model that the alternating layers of normal and superconducting states are parallel to the external field, based on Abrikosov (1957)[61] and Goodman (1961),[62] El Bindari and Litvak (1964)[113] derived the relationship between I/I_c and H/H_c, where H and I are the applied magnetic field.

CHAPTER III

THEORY

I. Introduction

To describe electromagnetic properties of superconductors, three theories, London, BCS and Ginzburg-Landau theories are used often. When a specimen becomes small, the ratio of surface area to volume becomes large and the mean free path of electrons, ℓ, becomes comparable to the size of the specimen, in the case of a film, the thickness of the film. Under this configuration, electromagnetic properties of small specimens become quite different from those of bulk specimens. For instance, the thinner the superconducting film is, the higher the critical magnetic field. For normal metal film, surface roughness and scattering of electrons from surfaces are taken into account by the electrical conductivity, σ, and approximate equations of σ in terms of d/ℓ for thick and thin films agree with experimental results. However, an equation for the intermediate thickness is not established yet. In addition

to ℓ, the coherence length ξ and the penetration length λ must be considered for superconducting films. The equations derived from the three theories give the same results qualitatively for the thick and thin regions under certain conditions. However, all these equations neglect the scattering of electrons from the surface and the critical structures of films which depend on the process of deposition of films. Also, the current density distribution is assumed constant in all these equations. Ginzburg-Landau theory gives the critical thickness $d_c=\sqrt{5}\lambda$ which distinguishes between thick films and thin films. However, the thin and thick film limits obtained by substituting d_c into equations for thin and thick films do not have good agreement. Coherence length ξ_o and penetration depth λ_L predicted from these theories give quite different values. A complete discussion of existing theories is given in Section II, III and IV for the cases of applied field with no applied current, of applied current with no applied field and of applied field and current respectively. The equations used in the analysis of this work are then summarized in Section V.

II. The Critical Magnetic Field (No Applied Current)

In a bulk superconductor London's equations indicate that an applied magnetic field and the resultant shielding supercurrent are confined to a thin layer at the surface of

the specimen, as shown in Figure 3-1(a). However, the situation in a small superconductor may be quite different from that of the bulk material. For instance, in a film whose thickness is comparable with the penetration depth, the applied magnetic field is very imperfectly excluded, as shown in Figure 3-1(b). H. London[6] predicted that a very small superconductor should have a much higher magnetic threshold value than a bulky one. In order to investigate this prediction, the magnetic field is often applied parallel to the surface of the film because the demagnetization effects in this geometry are minimal. Following are discussions of London, Ginzburg-Landau, and BCS theories.

A. Formulations of H_{cf} Based on London Theory

The field distribution inside a thin film superconductor is obtained by applying the London differential equation.

$$\nabla^2 H = H/\lambda^2 \tag{1}$$

to a film having thickness, d, and infinite width in a uniform magnetic field H_a, parallel to the surface of the film. With this geometry, Eq. (1) is reduced to

$$\frac{d^2H(x)}{dx^2} = \frac{H(x)}{\lambda^2} \tag{2}$$

where x is the distance from the center of the film and H(x) must be equal to H_a for $x = \pm d/2$. With the boundary

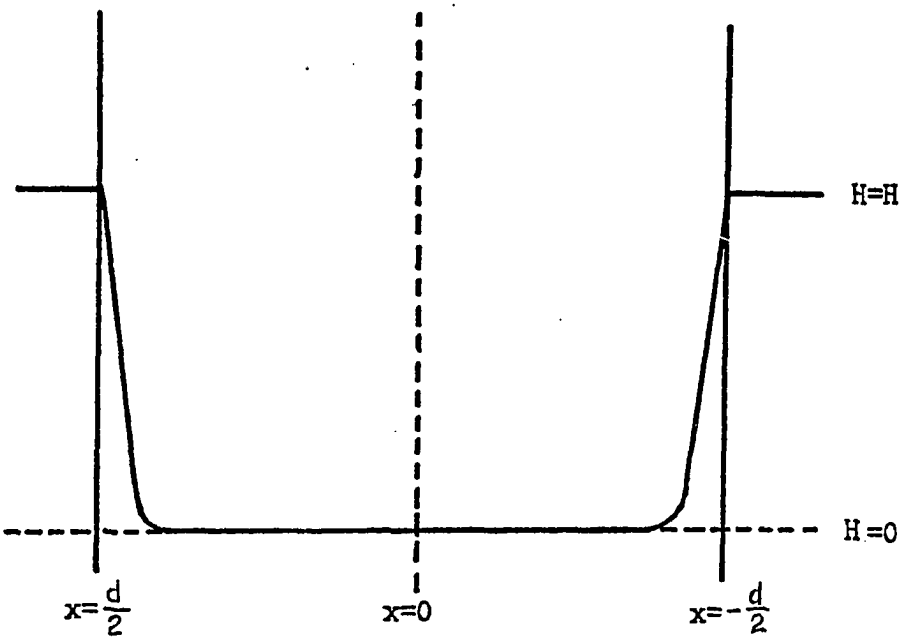

Figure 3 - 1 (a)

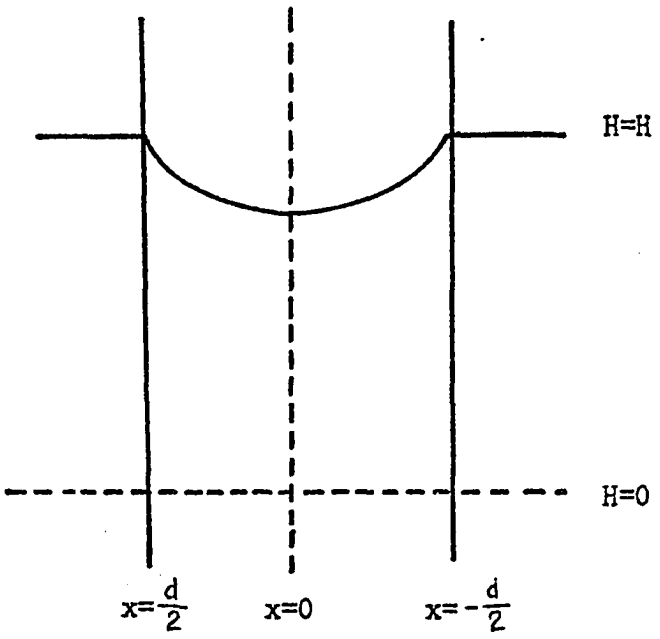

Figure 3 - 1(b)

Magnetic distribution in a superconducting plate placed in a magnetic field H parallel to its surface (a) $d \gg \lambda$; (b) $d \ll \lambda$.

conditions, the solution of Eq. (2) is given by

$$H(x) = H_a \frac{\cosh(\frac{x}{\lambda})}{\cosh(\frac{d}{2\lambda})} \qquad (3)$$

1) Calculation of H_{cf} using the free energy difference between normal and the superconducting states.

Gorter and Casimir[114] defined the critical magnetic field, H_c, in terms of the Gibbs free energy difference between the normal and the superconducting states in the absence of an applied magnetic field

$$G_n(0) - G_s(0) = -V \int_0^{H_c} M dH = VS \qquad (4)$$

where V is the volume of specimen, M is magnetization per unit volume and S is the area under the magnetization curve and H_c is a field to destroy superconductivity. Since the slope of the magnetization curve is less for a small specimen than for a bulk specimen of the same shape, the magnetization curve for the smaller specimen must continue to a higher magnetic field to have the same area, i.e., the critical field will be higher (See Figure 3-2(a)). However, this qualitative argument is based on the assumption that the area S is independent of size. Because of Meissner effect, $M = -H/4\pi$, then Eq. (4) becomes

$$S = \frac{G_n - G_s}{V} = \frac{H_c^2}{8\pi} \qquad (5)$$

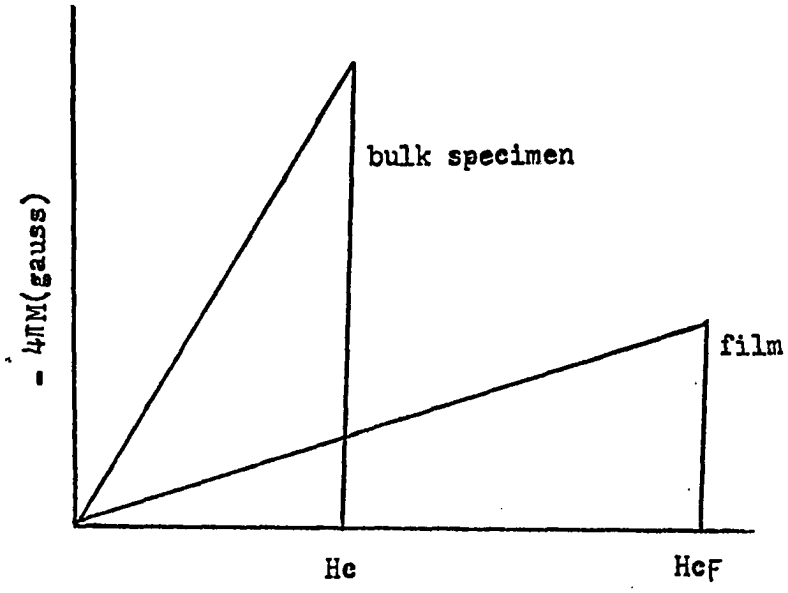

Figure 3 - 2 (a)

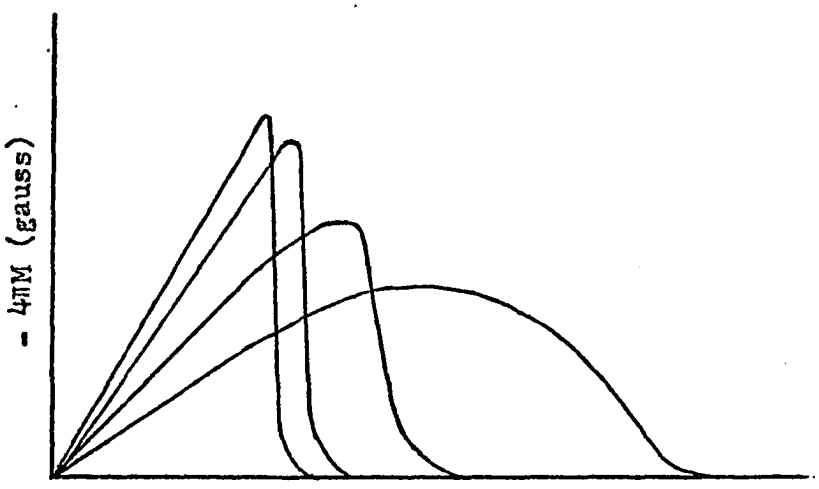

Figure 3 - 2 (b)

Magnetization curves of lead films at 4.2°K
(Reference 39)

where H_c is the critical magnetic field of the bulk specimen. According to Marcus,[115] it is convenient to write Eq. (5) in the form

$$\frac{G_n - G_s}{V} = \frac{H_c^2}{8\pi} = -\frac{MH_a}{2} \tag{6}$$

where M is the average magnetization per unit volume and is obtained by Ittner[116]

$$\overline{M} = \int_{-\frac{d}{2}}^{\frac{d}{2}} \frac{H(x) - H_a}{4\pi d}\, dx \tag{7}$$

Substituting Eq. (3) into Eq. (7) and integrating, yields

$$\overline{M} = -\frac{H_a}{4\pi}\left(1 - \frac{2\lambda}{d}\tanh\frac{d}{2\lambda}\right) \tag{8}$$

When the applied magnetic field at the film surface H_a becomes equal to the critical magnetic field of the film H_{cf}, i.e., $H_a = H_{cf}$ substituting Eq. (8) into Eq. (6) yields

$$H_{cf} = H_c\left(1 - \frac{2\lambda}{d}\tanh\frac{d}{2\lambda}\right)^{-1/2} \tag{9}$$

This is just the critical field predicted by F. London[117] with $d_n - d_s = 0$ (d_n and d_s are the surface energies of the normal and superconducting states, respectively)

When $d >> \lambda$

$$\tanh\left(\frac{d}{2\lambda}\right) \to 1$$

and (10)

$$H_{cf} \simeq H_c\left(1 + \frac{\lambda}{d}\right)$$

When $d<<\lambda$

$$1 - \frac{2\lambda}{d} \tanh \left(\frac{d}{2\lambda}\right) \rightarrow \frac{d^2}{12\lambda^2}$$

and (11)

$$H_{cf} \simeq \sqrt{12}\, \frac{\lambda}{d}\, H_c$$

2) Calculation of H_{cf} using the magnetic susceptibility.[40] If it is assumed that the magnetization curve is linear with the slope χ (susceptibility) right up to a critical field the area under the magnetization curve of the film S_F is given as

$$S_F = \frac{1}{2}\, \chi\, H_{cf}^2 \qquad (12)$$

The area under the magnetization curve of the bulk specimen S_o is given as

$$S_o = \frac{1}{2}\, \chi_o\, H_c^2 \qquad (13)$$

where χ_o is the susceptibility $-1/4\pi$ of a plate of infinite thickness. From the assumption that Eq. (5) is independent of the size of the specimen

$$S_F = S_o \qquad (14)$$

From Eq. (14)

$$\left(\frac{H_{cF}}{H_c}\right)^2 = \frac{\chi_o}{\chi} \qquad (15)$$

Schoenberg[40] assumed that the field distribution curve of Figure 3-1(b) is a parabola and is given as

$$H(\chi) = H_a\{1 - \frac{\gamma}{\lambda^2}[(\frac{d}{2})^2 - \chi^2]\} \qquad (16)$$

where γ is numerical constant depending on the nature of the theory of the penetration. For a large specimen the effect of penetration of the field is entirely equivalent to the removal of a layer of thickness λ from the specimen.

For $d>>\lambda$

$$\frac{\chi}{\chi_o} = 1 - \frac{\lambda}{d/2} \qquad \text{for a plate of thickness d} \qquad (17\text{-a})$$

$$\frac{\chi}{\chi_o} = 1 - \frac{2\lambda}{d/2} \qquad \text{for a wire of diameter d} \qquad (17\text{-b})$$

$$\frac{\chi}{\chi_o} = 1 - \frac{3\lambda}{d/2} \qquad \text{for a sphere of diameter d} \qquad (17\text{-c})$$

For a very small specimen the answer is less obvious. The average value of B is

$$\bar{B} = \frac{1}{d}\int_{-\frac{d}{2}}^{\frac{d}{2}} H(\chi)\, d\chi = H_o(1 - \frac{rd^2}{\gamma\lambda^2})$$

so that

$$\chi_o = \frac{1}{4\pi H_o}(\bar{B} - H_a) = -\frac{rd^2}{24\pi\lambda^2}$$

or

$$\frac{\chi}{\chi_o} = \beta\frac{d^2}{\lambda^2} \qquad (18)$$

where $\beta = \frac{\gamma}{\lambda}$. This relationship was obtained by Ginzburg[36] and by Pippard.[37]

When $d>>\lambda$, substituting Eq. (17-a) to Eq. (15) yields,

$$\frac{H_{cF}}{H_c} = 1 + \frac{\lambda}{d} \tag{19}$$

When $d<<\lambda$, substituting Eq. (18) to Eq. (15) yields,

$$\frac{H_{cF}}{H_c} = \beta^{-1/2} \frac{2\lambda}{d} \tag{20}$$

where β is a parameter determined by the actual field penetration law ($\beta = 1/3$ for an exponential penetration law).[40] Lock[39] obtained the susceptibility of a plate from Eq. (8), which is given as

$$\frac{\chi}{\chi_o} = 1 - \frac{2\lambda}{d} \tanh \left(\frac{d}{2\lambda}\right) \tag{21}$$

Applying the same approximation as Eq. (10) and Eq. (11), to Eq. (21), yields

$$\frac{\chi}{\chi_o} = 1 - \frac{2\lambda}{d} \quad \text{for } d>>\lambda \tag{22}$$

$$\frac{\chi}{\chi_o} = \frac{d^2}{12\lambda^2} \quad \text{for } d<<\lambda \tag{23}$$

Eq. (21) and Eq. (22) lead to the same results as Eq. (11) for H_{cF}. In his paper, Lock[39] criticized Ginzburg's introduction[36] of the surface free energy to Eq. (5) on the basis of the linearity of the magnetization curve up to the critical magnetic field because of Lock's observation of

its non-linearity of tin, lead and indium films. The discrepancy between the experimental and theoretical works of H_{cF}/H_c dependency on χ/χ_o was summarized by Shoenberg[40] that "the critical fields of thin films are higher than $(\chi/\chi_o)^{1/2}$ times H_c, simply because, for various possible reasons, the slope of the magnetization curve falls off from its initial value as the field is raised". Douglass[45] obtained the theoretical magnetization curve of a thin film ($d<<\lambda(T)$) as

$$M = -\frac{1}{48\pi}\left[\frac{d}{\lambda(T)}\right]^2 \left[1 - \left(\frac{H}{H_c}\right)^2\right] H$$

which predicts considerable rounding of the magnetization curve with a broad maximum at $H/H_c = 0.578$. However, this equation has not yet been applied to the development of any new theory of superconducting films, nor has it been used to modify existing theories.

B. Formulation H_{cF} based on Ginaburg-Landau theory[8]

Ginzburg and Landau[8] introduced a quantity called the "order parameter" $\psi(r)$ to characterize the degree of superconductivity at various points in the material. The order parameter, $\psi(r)$ is defined so as to be zero for a normal region and unity ($= \psi_o$) for a superconducting region in zero magnetic field at zero temperature. $\psi(r)$ is taken as a complex function and interpreted as analogous to a "wave function" for superconductivity, so that its absolute

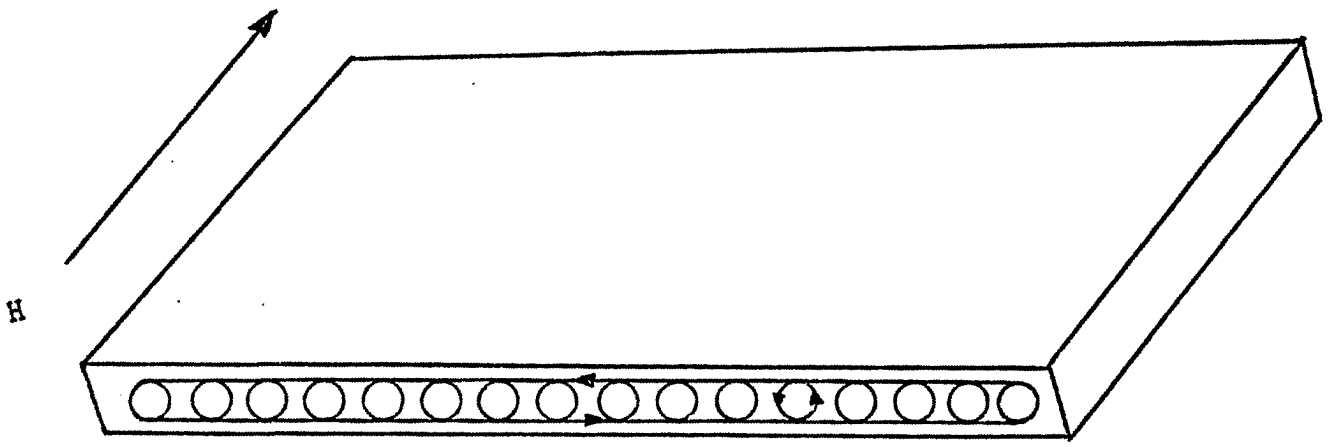

Figure 3 - 3

In parallel field geometry, vortices are limited by film thickness.

square $|\psi(r)|^2$ can be identified with the local superelectron density N_s. However, it should be noted that $\psi(r)$ is not the system wave function for the electrons in the material since it is defined as zero in the normal state. The order parameter is written as

$$\psi = \psi_o f$$

where f = 1 in the superconducting state and zero in the normal state, and is given as

$$f = f_o e^{i\phi}$$

where f_o is the modulus and ϕ is the phase of f. Then, the two Ginzburg-Landau equations can be written as

$$\begin{aligned} \left(i\frac{\nabla}{K} + a\right)^2 f_o &= f_o - f_o^3 \\ -\,\mathrm{curl}\cdot\mathrm{curl}\, a &= f_o^2\, a \end{aligned} \tag{24}$$

where K is the Ginzburg-Landau parameter and a is the normalized vector potential.

For thin films, Ginzburg[8] derived the following expressions for the critical magnetic field from Eq. (24). Ginaburg assumed that magnetization M is linear with the magnetic field H, i.e., M = constant x H.

$$\left(\frac{H_{cF}}{H_c}\right)^2 = \frac{4f_o^2(f_o^2 - 1)\cosh^2(n)}{1 - \sinh(2n)/n} \qquad (25\text{-a})$$

$$\left(\frac{H_{cF}}{H_c}\right)^2 = \frac{f_o^2(2 - f_o^2)}{1 - \tanh(n)/n} \qquad (25\text{-b})$$

where $n = \frac{f_o d}{2\lambda}$. f_o is of the order of unity and given as

$$|f_o|^2 = \left|\frac{\psi}{\psi_o}\right|^2$$

$|\psi_o|^2$ is the concentration of superelectrons, N_s. When $d/\lambda >> 1$, Eq. (25-a) and Eq. (25-b) are greatly simplified and give the expression for H_c as:

$$\frac{H_{cF}}{H_c} = 1 + \frac{\lambda}{d} \quad \text{for } d>d_c \qquad (26)$$

Expanding Eq. (24) and Eq. (25) into a series in terms of λ/d

$$\frac{H_{cF}}{H_c} = \sqrt{24}\,\frac{\lambda}{d} \quad \text{for } d<d_c \qquad (27)$$

where $d_c \sqrt{5}\lambda(t,d)$ and $t = T/T_c$. When $d>d_c$, the transition is the first-order one and when $d<d_c$, the second-order one. Combining Eq. (27) with Eq. (23), yields

$$\frac{H_{cF}}{H_c} = \left(\frac{2\chi_o}{\chi}\right)^{1/2} \qquad (28)$$

Schreiffer,[118] assuming specular reflection of electrons at the film surface, obtained the susceptibility of a thin film.

$$\left(\frac{\chi}{\chi_o}\right)_{spec} \simeq 0.194 \left(\frac{d^3}{\pi \xi_o \lambda_L^2}\right) \qquad (29)$$

Roger[119] calculated the susceptibility for random scattering,

$$\left(\frac{\chi}{\chi_o}\right)_{rand} \simeq \left(\frac{3}{64}\right)\left(\frac{d^3}{\pi \xi_o \lambda_L^2}\right) \qquad (30)$$

Toxen[55] used the results of Schreiffer and Roger and obtained H_c for cases of specular and random scattering

$$\left(\frac{H_{cF}}{H_c}\right)_{spec} \simeq 16.1 \left(\frac{\xi_o \lambda_L}{d^3}\right)^{1/2} \quad \text{for } d \ll \lambda \qquad (31)$$

$$\left(\frac{H_{cF}}{H_c}\right)_{rand} \simeq 18.5 \left(\frac{\xi_o \lambda_L}{d^3}\right)^{1/2} \quad \text{for } d \ll \lambda \qquad (32)$$

By comparing Eq. (31) to Eq. (32), Toxen[55] pointed out that the non-local calculation is not too sensitive to the type of surface scattering. Tinkham[120] concluded that specular reflection seldom plays an important role in films, either in the normal or the superconducting states. The Ginzburg and Landau equation, Eq. (24) and Eq. (25) are valid only for temperature very close to the critical temperature ($t \simeq 1$). To extend the temperature range, Ginzburg[121]

derived the following expression for thin films ($d<<\lambda$)

$$\left(\frac{H_{cF}}{H_c}\right)^2 = 24\delta \frac{\lambda(T\cdot d)^2}{d} \quad \text{for } d<<\lambda \tag{33}$$

where $\delta = \frac{1}{2}(1 + t^2)$, Eq. (33) gives

$$\left(\frac{H_{cF}}{H_c}\right)^2 = 24 \left(\frac{\lambda}{d}\right)^2 \quad \text{for } t\simeq 1 \tag{34}$$

$$\left(\frac{H_{cF}}{H_c}\right)^2 = 12 \left(\frac{\lambda}{d}\right)^2 \quad \text{for } t\simeq 0. \tag{35}$$

Eq. (35) is identical to Eq. (11) which is based on the London theory.

C. Formulations of H_{cF} Based on Microscopic Theories

Hauser and Helfand[49] used a modification of the BCS Kernel introduced by Miller[50] which takes into account the mean free path (the BCS-Miller Kernel), and obtained an expression for H_{cF} for very thin films

$$\frac{H_{cF}}{H_c} = \frac{\lambda_L}{d}\left(\frac{2\xi_o}{d}\right)^{1/2}\left[1 + 0.0825\left(\frac{d}{\xi_o}\right) + 0.2\left(\frac{d}{\ell}\right)\right] \tag{36}$$

where ξ_o is the coherence length at T=0 and related to the mean free path ℓ and the coherence length ξ at T by

$$\frac{1}{\xi} = \frac{1}{\xi_o} + \frac{1}{\ell} \tag{37}$$

The BCS theory takes into account only the lowest excitations, i.e., it applies only for 0°K (t≈0). Bardeen extended the temperature range and obtained the expression for H_{cF} with t≈1 and t≈0.

$$\frac{H_{cF}}{H_c} = \sqrt{24}\,\frac{\lambda}{d} \quad \text{for } t \approx 1 \tag{38}$$

$$\frac{H_{cF}}{H_c} = \sqrt{0.68}\;\; 24\,\frac{\lambda}{d} \quad \text{for } t\ 0 \tag{39}$$

D. Temperature Dependence of H_{cF}

Since H_c and λ depend on the temperature, H_{cF} must be dependent of the temperature. Empirically, the temperature dependence of the H_c is given as

$$H_c(T) = H_c(0)\left[1 - \left(\frac{T}{T_c}\right)^2\right] \tag{40}$$

where $H_c(0)$ is the bulk critical magnetic field at T=0. When $T \to T_c$.

$$H_c(T) = 2H_c(0)\left[1 - \left(\frac{T}{T_c}\right)\right] \tag{41}$$

The theoretical derivation of Eq. (40) was tried by Kok.[122] He assumed that the specific heat of the normal phase is to vary as $aT + bT^3$. However, the linear term comes from an electron gas model, which is only a crude description of a metal, and cannot account for superconductivity. Gorter and Casimir[34] derived Eq. (4) in the two fluid model by

assuming that the specific heat of the superconductor is proportional to T^3. Bardeen, Cooper and Schrieffer[5] obtained

$$H_c(T) = H_c(0)\left[1 - 1.07\left(\frac{T}{T_c}\right)^2\right] \qquad (42)$$

Experimental values generally lie between Eq. (40) and the curve by the BCS theory and Eq. (40) is used in the discussion below.

The penetration depth was obtained by F. and H. London as

$$\lambda_L = \left(\frac{mc^2}{4\pi N_s e^2}\right)^{1/2} \qquad (43)$$

and λ_L is called the London penetration depth. With the free-electron values, the value of λ_L is the order of 10^{-6} cm. The obtained value of the penetration depth of a pure bulk specimen is called the empirical λ, (generally about 5×10^{-6} i.e., several times larger than λ_L). According to the two-fluid model,[94] the temperature dependence of the empirical λ is given by

$$\lambda(T) = \lambda(0)\left(1 - t^4\right)^{-1/2} \qquad (44)$$

where $t = T/T_c$ and $\lambda(0)$ is λ at $T = 0°K$. As $T \to T_c$.

$$\lambda(T) \approx \frac{\lambda(0)}{2}\left(1 - t\right)^{-1/2} \qquad (45)$$

As mentioned in Chapter II, the marked dependence of the observed on the impurities in a superconductor led Pippard[42]

to introduce the coherence length ξ_o and to assume that an effective coherence length ξ is related to ξ_o of a pure metal by

$$\frac{1}{\xi(\ell)} = \frac{1}{\xi_o} + \frac{1}{\ell} \qquad (46)$$

$\lambda(0)$ is expressed in terms of the coherence length as

$$\lambda(0) = \lambda_L \left(\frac{\xi_o}{\xi(\ell)}\right)^{1/2} \quad \text{for } \lambda >> \xi. \qquad (47)$$

Thus we see that (0) is a function of the mean free path ℓ. The condition $\lambda >> \xi$ holds for pure metals at temperatures close to T_c (where $\lambda \to \infty$) and also for alloys and impure thin films where ℓ and ξ are reduced or limited by electron scattering at imperfections, impurities, or the film boundary so that as $\ell \to 0$, $\xi \to \ell$. By substituting Eq. (46) into Eq. (47), Tinkham[123] obtained explicitly the ℓ dependence for $\lambda(0)$ as

$$\lambda(0) \simeq \lambda_L \left(1 + \frac{\xi_o}{\ell}\right)^{1/2} \qquad (48)$$

For the limit $\lambda << \xi$, which holds for most pure bulk metals ($\ell \to \infty$) and temperature not too close to T_c, Faber and Pippard[124] obtained

$$\lambda(0)_{\ell \to \infty} = \left(\frac{\sqrt{3}}{2\pi} \xi_o \lambda_L^2\right)^{1/3} \quad \text{for } \xi >> \lambda \qquad (49)$$

Ittner[116] found that $\lambda(T)$ increases as the thickness decreases. $\xi(\ell)$ approaches ξ_o for the thick films. Tinkham assumed that ℓ is equal to d for the very thin limit since evaporated films are inherently quite "dirty", and derived

from Eq. (48)

$$\lambda(0) = \lambda_B \left(1 + \frac{\xi_o}{d}\right)^{1/2} \tag{50}$$

where λ_B is the observed λ of a pure specimen. That is, he pointed out that experimental data fit Eq. (48) better if λ_L is replaced by λ_B. However, both λ_L and λ_B are often used. Douglass and Blumberg[46] pointed out that λ of "dirty" thin film is limited by the thickness, not by the mean free path, i.e., $\ell \sim d$ and $\xi << \xi_o$, then $\xi \sim \ell$ from Eq. (46), and

$$\lambda(0) \simeq \lambda_L \left(\frac{\xi_o}{d}\right)^{1/2} \tag{51}$$

Therefore, $\lambda(t,d)$ can be written from Eq. (44) and Eq. (47) as

$$\lambda(t,d) = \lambda_L \left(\frac{\xi_o}{\xi(\ell)}\right)^{1/2} (1 - t^4)^{1/2} \tag{52}$$

For thin films near T_c, Eq. (52) becomes

$$\lambda(t,d) \simeq \frac{\lambda_L}{2} \left(\frac{\xi_o}{d}\right)^{1/2} (1 - t)^{-1/2} \tag{53}$$

Eq. (53) is almost identical to the equation which was obtained from the BCS theory together with the Ginzburg-Landau equations by Burger et.al.[125] For $\ell << \xi_o$ and $t \to 1$,

$$\lambda(t,d) \simeq 0.62\lambda_L \left(\frac{\xi_o}{\ell}\right)^{1/2} (1 - t)^{-1/2} \tag{54}$$

1) Type I superconducting films. For the thick films ($d > \sqrt{5}\,\lambda(t,d)$), substituting Eq. (40) in Eq. (10),

yields

$$H_{cF}(t,d) = H_c(0)(1 - t^2)(1 + \frac{\lambda(t,d)}{d}) \qquad (55)$$

For the thin films ($d \lesssim 5\lambda$), substituting Eqs. (40), (44), and (51) in Eq. (11), yields

$$H_{cF}(t,d) = \frac{\sqrt{24}\, H_c(0)\lambda_L^2 \xi_o^{1/2}}{d^{3/2}} \left(\frac{1 - t^2}{1 + t^2}\right)^{1/2} \qquad (56)$$

For the films $d = \sqrt{5}\,\lambda(t,d)$ from Eq. (11)

$$H_{cF}(t,d) = \sqrt{\frac{24}{5}}\, H_c(t) = 2.2\, H_c(t) \qquad (57\text{-a})$$

From Eq. (10)

$$H_{cF}(t,d) = H_c(t)(1 + \frac{1}{\sqrt{5}}) = 1.45\, H_c(t) \qquad (57\text{-b})$$

From Ginzburg-Landau theory, the square of H_c near T_c is given by

$$H_{cF}(t,d) = 12\, \frac{\lambda^2(0,d)}{d}\, T_c \left(\frac{dH_c}{dT}\right)_{T_c} (T_c - T) \qquad (58)$$

2) Type II superconducting films. The critical magnetic field of the thick film ($d \gg \lambda$) is defined as the upper critical field H_{c_2} for bulk superconductor.

$$H_{cF}(t) = H_{c_2}(t) = \sqrt{2}\, K\, H_c(0) \qquad (59)$$

Using the Gorkov[44] relation $K \simeq \frac{\lambda}{\xi_o}$ and $\sqrt{8\pi}\lambda\xi_o H_c = \phi_o$, Eq. (59) becomes

$$H_{cF}(t) \simeq \frac{\sqrt{8\pi} H_c^2(0)}{\phi_o} \lambda_L^2 (1 + \frac{\xi_o}{\ell})(1 - t) \qquad (60)$$

For the thin film ($d<<\lambda$), $H_{cF}(T)$ is given as

$$H_{cF}(t) = \sqrt{24}\, H_c(t) \frac{\lambda(t,d)}{d} \tag{61}$$

which is the same as Eq. (56). By equating Eq. (60) and Eq. (61) a simple relation for the critical thickness at which the switch of the thick to thin-film behavior takes place can be obtained as

$$H_{cF}(t) = \frac{\sqrt{12}\, \lambda(t,d)}{K} \tag{62}$$

Physically, this value corresponds to the distance between two Abrikosov vortices.[61] d_c can be written as

$$d_c \simeq \left(\frac{\phi_o}{H_{cF}}\right)^{1/2} \tag{63}$$

where $\phi_o = \frac{hc}{2e} = 2 \times 10^{-7}$ G-cm^2. Tinkham[123] and White[126] implied that the changeover to thick-film behavior occurs when the Abrikosov vortices containing one quantum of flux ϕ_o would just fit the cross section of the film. (See Figure 3-3).

III. Critical Current (No Applied Magnetic Field)

The current flowing in a bulk superconductor is confined to a surface layer having a thickness on the order of the penetration depth λ_L.[127] In general there can be two contributions to the current flowing on the surface of the superconductor. One is the transport current from external sources. Another is the screening current which

circulates to cancel the magnetic flux inside the superconductor. The current density $\vec{J}$ can be considered to be the sum of a component $\vec{J}_t$ due to the transport current and a component $\vec{J}_s$ which arises from the screening currents.

$$\vec{J} = \vec{J}_t + \vec{J}_s \tag{65}$$

The superconductivity breaks down in the magnitude of the total current density at any point exceeds the current J_c. The Maxwell equation curl $\vec{H} = \frac{4\pi}{c} \vec{J}$ relates the supercurrent density at any point and the magnetic field at that point. This relation holds whether the supercurrent is a screening current, a transport current or a combination of both. If the total current flowing on the superconductor is sufficiently large, the current density at the surface will reach the critical value J_c and the associated magnetic field at the surface have a value H_c. Conversely, a magnetic field H_c at the surface is always associated with surface supercurrent density J_c. This leads to the following general hypothesis: that a superconductor loses its zero resistance when, at any point on the surface, the total magnetic field, due to transport current and applied magnetic field, exceeds the critical field H_c. The critical current of that specimen is the maximum amount of transport current which can be passed through the superconductor without resistance. The stronger the applied magnetic field, the smaller is this

critical current. If there is no applied magnetic field the only magnetic field will be that generated by any transport current. So in this case, the critical current is that current which generates the critical magnetic field H_c at the surface of the specimen. This is Silsbee's hypothesis[85] and the special case of the general hypothesis mentioned above. Below, the example of the cylindrical film is given. This is because cylindrical films are symmetric and therefore easier to do calculations with.

A. Application of Silsbee's Hypothesis[85]

(Applied Current Only, No Applied Field)

1) Calculation of critical current for a film with the thickness $d>>\lambda$, deposited on a cylinder with radius a.

The current flows in an outer region of approximate thickness λ. Using Ampere's law, and assuming the distribution of the current density within is constant,

$$2\pi a H_c = \frac{4\pi}{c} 2\pi a \lambda_L J_c \tag{66}$$

Then

$$J_c = \frac{cH_c}{4\pi\lambda_L}$$

The total current is given as

$$I_c = 2\pi a \lambda_L J_c = \frac{acH_c}{2} \tag{67}$$

2) Calculation of critical current for a film with the thickness $d<<\lambda$, deposited on a cylinder with radius a. The current distribution is approximately uniform throughout the film thickness d. If the current is uniform around the cylindrical film, the field on the inner surface of the film is zero, and at the outer surface, using Ampere's law,

$$2\pi a H_c = \frac{4\pi}{c} 2\pi a \, dJ_c$$
$$J_c = \frac{cH_c}{4\pi d} \tag{68}$$

The total critical current is

$$I_c = 2\pi a \, dJ_c = \frac{acH_c}{2} \tag{69}$$

This is the same as Eq. (67). Therefore, according to Silsbee's hypothesis, I_c is independent of the film thickness d.

B) Application of H. London's Method[86]

(Applied Current Only, No Applied Field)

In the presence of a transport current supplied by an external source, the transition is irreversible due to the fact that energy is continuously dissipated in the normal state.[91] Therefore, the simple thermodynamic approach of equating the free energies of the superconducting and normal phases, i.e., Eq. (5), can not be applied in the presence of a transport current. This difficulty was solved by H. London,

who considered a much thinner layer of thickness λ_L, containing a boundary between the superconducting and normal states and discussed the free-energy balance during a reversible isothermal displacement of this boundary. He concluded that in a small specimen the kinetic energy of the critical current equals the difference in the free energy of the normal and superconducting states.

$$g_n - g_s = \frac{1}{2} \left(4\pi\frac{\lambda^2}{c^2}\right) J^2 \tag{70}$$

where g_s and g_n are the free energy per unit volume of the superconducting and normal phases, and J is the current density at the superconducting boundary.

$$J = \frac{cH_c}{4\pi\lambda_L} \tag{71}$$

According to this argument, the criterion for destruction of superconductivity is that there is a critical current density given by Eq. (71) rather than a critical magnetic field. Therefore, the current given by Eq. (71) is the critical current density

$$J_c = \frac{cH_c}{4\pi\lambda_L} \tag{72}$$

Critical current for cylindrical films for two cases are calculated by H. London's method as follows:

1) Calculation of critical current I_c for a film with the thickness $d>>\lambda$, deposited on a cylinder with radius a.

Using Eq. (72),

$$I_c = 2\pi a \lambda_L J_c = \frac{acH_c}{2} \tag{73}$$

2) Calculation of critical current I_c for a film with the thickness $d<<\lambda$, deposited on cylinder with radius a.

$$I_c = 2\pi a d J_c = \frac{acH_c}{2}\left(\frac{d}{\lambda_L}\right) \tag{74}$$

Eq. (74) is smaller than Eq. (73) by the factor of d/λ_L. Therefore, the London's method predicts that the critical current, I_c, decreases as the film thickness decreases.

The cases of wires and flat films are calculated in Appendix 1. The results of these calculations show the same conclusions stated above.

Pippard[37] suggested that the kinetic energy of the normal electrons $\frac{1}{2} \Lambda_n J^2$ should be added to Eq. (70) for a thin film.

$$\frac{G_n - G_s}{V} = \frac{1}{2}\left(4\pi\frac{\lambda^2}{c^2}\right)J^2 + \frac{1}{2}\Lambda_n J^2 \tag{75}$$

where Λ_n is τ/σ. τ is the relaxation time and σ is the conductivity in the normal state of the metal.

From Eq. (75), J_c is modified as

$$J_c = \frac{cH_c}{4\pi\lambda'} \tag{76}$$

where

$$\lambda' = (\lambda^2 - c^2 \Lambda_n/4\pi)^{1/2} \qquad (77)$$

If Eq. (76) is used for J_c, I_c for thin wires and films are a little bigger than ones obtained by H. London's method. Bardeen[128] confirmed London's method on the basis of the BSC theory.

At this point the critical magnetic field produced by the critical current is discussed briefly. The relationship between the critical magnetic field produced by the critical current, H_{cI}, the critical magnetic field for a thin film with no current H_{cF}, and the bulk critical magnetic field H_c is derived. To calculate the surface field H_{cI} present outside a film of thickness d carrying a current density J_c, a film deposited on a cylinder of radius a>>d is considered. Using Ampere's law and intergrating H_{cI} around the circumference,

$$2\pi a H_{cI} = \frac{4\pi}{c} 2\pi a d J_c$$

thus,

$$H_{cI} = \frac{4\pi}{c} J_c d \qquad (78)$$

Substituting Eq. (72) in Eq. (78) yields

$$H_{cI} = \frac{d}{\lambda} H_c \qquad d<<\lambda \qquad (79)$$

Since Eq. (79) is independent of a, Eq. (79) can be applied to a geometry such as that of a film deposited on a

superconducting shielded plane, where the field produced by current is present on one side of the film only. If the field is present on both sides without edge effects,

$$H_{cI} = \frac{d}{2\lambda} H_c \qquad d<<\lambda \tag{80}$$

Using Eqs. (11) and (79), for a cylindrical film or shielded planar film

$$H_{cI}\, H_{cF} = \sqrt{12}\, H_c^2 \tag{81}$$

Using Eqs. (12) and (80), for an unshielded planar film

$$H_{cI}\, H_{cF} = \sqrt{3}\, H_c^2 \tag{82}$$

Eqs. (81) and (82) are useful because they contain only directly measurable parameters.

Now, the temperature dependence of critical current density, J_c is discussed.

From Eq. (72),

$$\frac{J_c(t)}{J_c(0)} = \frac{H_c(t)}{H_c(0)} \Big/ \frac{\lambda_L(t)}{\lambda_L(0)} \tag{83}$$

Substituting Eqs. (40) and (44) in Eq. (83) yields

$$\frac{J_c(t)}{J_c(0)} = (1 - t^2)^{3/2} (1 + t^2)^{1/2}$$

or

$$J_c(t) = \frac{cH_c(0)}{4\pi\lambda_L(0)} (1 - t^2)^{3/2} (1 + t^2)^{1/2} \tag{84}$$

At the temperature near T_c, substituting Eqs. (41) and (45) in Eq. (83) yields

$$J_c(t) = \frac{cH_c(0)}{4\pi\lambda_L(0)}(1 - t)^{3/2} \qquad (85)$$

C. Calculation of Critical Current Using Bardeen's Theory[105]

Bardeen's derivation of the relationship between J_c and H_c is based on H. London's theory. He considered the total free energy of superconducting state as

$$(g_s)_{total} = g_s + \frac{1}{2} n_s m V_s^2 + \frac{1}{2}|\chi|H_a^2 \qquad (86)$$

where g_s is the free energy of the superconducting state, is the kinetic energy of n_s superelectrons with the velocity V_s and $\frac{1}{2}|\chi|H_a^2$ is the free energy of the external magnetic field H_a, where χ is the susceptibility. At the transition, $(g_s)_{total} = g_n$. Using Eq. (5),

$$\frac{H_c^2}{8\pi} = \frac{1}{2} n_s m V_s^2 + \frac{1}{2}|\chi|H_a^2 \qquad (87)$$

The critical current density is given as

$$J_s = (\frac{e}{m})\, n_s m V_s \qquad (88)$$

For no external magnetic field, substituting Eq. (87) with in Eq. (88) yield,

$$J_s = (\frac{e}{m})(\frac{n_s m}{4\pi})^{1/2} H_c \qquad (89)$$

Using Eq. (43),

$$J_c = \frac{cH_c}{4\pi\lambda_L} \tag{90}$$

Bardeen[105] pointed out that λ_L in Eq. (66) should be interpreted as the nonlocal value given by Eq. (47) and that Eq. (66) should be multiplied by $(2/3)^{3/2}$ for the limit $T \sim T_c$ and by (2/3) for $T \sim 0$ and $\ell << \xi_o$.

$$J_c = \left(\frac{2}{3}\right)^{3/2} \frac{cH_c}{4\pi\lambda_L} \left(\frac{\xi}{\xi_o}\right)^{1/2} \qquad \text{for } t \sim 1 \tag{91}$$

$$J_c = \left(\frac{2}{3}\right) \frac{cH_c}{4\pi\lambda_L} \left(\frac{\xi}{\xi_o}\right)^{1/2} \qquad \text{for } t \sim 0 \tag{92}$$

Substituting Eq. (43) in Eq. (47) with $\xi \sim \ell$, yields

$$\lambda(0) = \lambda_L \left(\frac{\xi_o}{\xi}\right)^{1/2} = \left(\frac{c^2 m^2 \xi_o}{4\pi \hbar n_s e^2 \ell}\right)^{1/2} \tag{93}$$

The coherence length ξ_o is based on the BCS theory given as

$$\xi_o = \frac{\hbar V_f}{\pi \Delta(0)} \tag{94}$$

where V_f is the velocity of superelectrons at the Fermi surface and $\Delta(0)$ is one-half the energy gap at 0°K. Substituting the normal conductivity $J_n = ne^2\ell/mV_f$, Eq. (93) and Eq. (94) in Eq. (84) yields the temperature dependence of J_c as

$$J_c(t) = \frac{H_c(0)}{3} \left(\frac{\sigma_n \Delta(0)}{\hbar}\right)^{1/2} (1 - t^2)^{3/2} (1 + t^2)^{1/2} \tag{95}$$

The magnitude of J_c at t=0 is given by Eq. (92) and Eq. (95) as

$$J_c(0) = \frac{H_c(0)}{3} \left(\frac{\sigma_n \Delta(0)}{\hbar}\right)^{1/2} \qquad (96)$$

D. Calculation of Critical Current Using Ginzburg-Landau[7] Theory

Ginzburg obtained the following equation for a film deposited on a cylinder.

$$(\psi_o^2 - 1)\psi_o^2 = \frac{(\frac{H_{cI}}{H})\{1 + \frac{\sinh(2n)}{2n}\}}{4\sinh^2(n)} + \frac{(\frac{H_{cI}}{H})\{1 - \frac{\sinh(2n)}{n}\}}{4\cosh(n/2)}$$

where $n = \frac{\psi_o d}{\lambda_L}$ and H_a is applied magnetic field parallel to the current. From Eq. (97).

1) When $d << \lambda_L$

$$\frac{H_{cI}}{H_c} = \underbrace{\frac{2}{3}\sqrt{\frac{2}{3}}}_{0.544} \frac{d}{\lambda_L}\left[1 - \left(\frac{H_a}{H_c}\right)^2 \frac{d^2}{24\lambda_L^2}\right]^{3/2} \qquad (98)$$

The critical current density is

$$J_c = 0.544 \frac{cH_c}{4\pi\lambda_L}\left[1 - \left(\frac{H_a}{H_c}\right)^2 \frac{d^2}{24\lambda_L^2}\right]^{3/2} \qquad (99)$$

The temperature dependence of J_c is given by

$$J_c(t) = 0.544 \frac{cH_c(0)}{4\pi\lambda_L(0)}(1 + t^2)^{1/2}\left[1 - t^2 - \frac{H_a^2 d^2 (1 + t^2)}{H_c^2(0)\,24\lambda_L(0)^2}\right]^{3/2} \qquad (100)$$

When no magnetic field is applied, i.e., $H_a = 0$, from Eq. (98)

$$H_{cI} = 0.544 \frac{d}{\lambda_L} H_c \tag{101}$$

2) When $d >> \lambda_L$

$$\frac{H_{cI}}{H_c} = \left[\frac{8}{5}\sqrt{\left(\frac{3}{5}\right)^3}\frac{d}{\lambda_L} - \left(\frac{H_a}{H_c}\right)^2\right]^{1/2} \tag{102}$$

The critical current density is given in the limit $T << T_c$ by

$$J_c(t) = \frac{c\sqrt{2}}{6\sqrt{3}} \frac{H_c(t)}{\lambda(t)}$$

$$= \frac{2c}{27} \frac{H_c(0)}{\lambda_L(0)(1 + \xi_o/\ell)^{1/2}} (1 - t)^{3/2} \tag{103}$$

The dependence of J_c on film thickness does not appear explicitly, but it enters through ℓ, so that J_c decreases slowly with decreasing film thickness. The ratio $J_c(T)/J_c(0)$ is, however, independent of ξ_o and ℓ and gives the same results as Eq. (85).

When $H_a = 0$, Eq. (102) becomes

$$H_{cI} = 0.86 \left(\frac{d}{\lambda_L}\right)^{1/2} H_c \tag{104}$$

For $d << \lambda$, Ginzburg obtained for a single side film (a cylindrical film or shielded planar film),

$$H_{cI} H_{cF} = \frac{8}{3} H_c^2 \tag{105}$$

For a two sided film (unshielded planar film)

$$H_{cI}H_{cF} = \frac{3}{4} H_c^2 \qquad (106)$$

The foregoing discussions were confined to type I superconductors. Unfortunately, no satisfactory theory exists for the critical current density of type II superconductors since the critical current is limited by the occurence of a complicated mixed state consisting of flux threads or vortices.

E. Calculations of Critical Current Using Non-Uniform Current Distributions

The foregoing discussions assumed that the current distributions within the penetration depth are uniform. However, several authors[40,100,104,106,117,130,131] pointed out experimentally or theoretically that this assumption is not true. Some[40,130,131] of them mentioned that in a current-carrying thin film, the current is concentrated in the edge and the current and field distribution corresponding to the London equation has not yet been solved for the general case of a thin strip with a rectangular cross-section. One way to solve this difficulty is to use the compensated geometry mentioned in Chapter II. Another is to describe the distribution of current and field by other methods instead of solving the London equations for a film with a rectangular cross-section. The following section is a discussion of the latter.

1) The case of an infinitely wide film with thickness d.

a) A film with applied current, but no applied field

Although the London equations can not be applied to a film with a rectangular cross-section, they can be solved for the case of an infinitely wide film. The current is in the y-direction, the thickness is measured in the x-direction and I_w is the magnitude of the current per unit width in the z-direction. Solving the London equation with boundary conditions.

$$H(\chi) = -H(-\chi) \quad , \quad J(\chi) = J(-\chi) \tag{107}$$

yields

$$J(\chi) = J(\frac{d}{2}) \frac{\cosh(\frac{\chi}{\lambda})}{\cosh(\frac{d}{2\lambda})} \tag{108}$$

The current per unit width

$$I_w = \int_{-\frac{d}{2}}^{\frac{d}{2}} J(\chi) d\chi = 2\lambda J(\frac{d}{2}) \tanh(\frac{d}{2\lambda}) \tag{109}$$

$$J(\frac{d}{2}) = \frac{I_w}{2\lambda} \coth(\frac{d}{2\lambda}) \tag{110}$$

From Maxwell's equations

$$H(\chi) = \frac{4\pi\lambda}{c} J(\frac{d}{2}) \frac{\sinh(\frac{\chi}{\lambda})}{\cosh(\frac{d}{2})} \tag{111}$$

$$H(\frac{d}{2}) = \frac{2\pi}{c} I_w \tag{112}$$

b) A film with applied field, but no applied current

The solution of the London equation is given from Eq. (3) as

$$H(\chi) = H_a \frac{\cosh(\frac{\chi}{\lambda})}{\cosh(\frac{d}{2\lambda})} \qquad (3)$$

$$H(\frac{d}{2}) = H_a$$

From Maxwell's equations

$$J(\chi) = \frac{cH_a}{4\pi\lambda} \frac{\sinh(\frac{\chi}{\lambda})}{\cosh(\frac{d}{2\lambda})} \qquad (113)$$

$$J(\frac{d}{2}) = \frac{cH_a}{4\pi\lambda} \tanh(\frac{d}{2\lambda}) \qquad (114)$$

the case of a) and b) are shown in Figure 3-4(a) and 3-4(b).

2) The case of film with rectangular cross-section

a) Bower's method[100]

It is assumed that the current density is constant through the film thickness $d \sim \lambda$ and that $wd >> \lambda^2$, where w is the film width.

1) In all but the edge regions

The current density is given by

$$J(X) = \frac{J(X=0)}{[1 - (\frac{2X}{w})^2]^{1/2}} \qquad (115)$$

where X is the distance from the center of the film. Although Eq. (115) gives an infinite density at X = w/2, it does not give an infinite magnetic field outside the film.

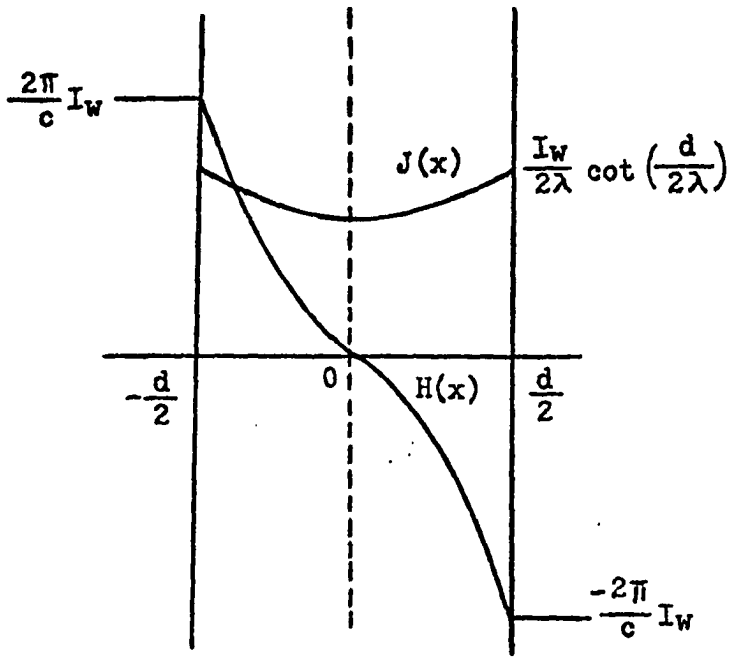

Figure 3 - 4(a)

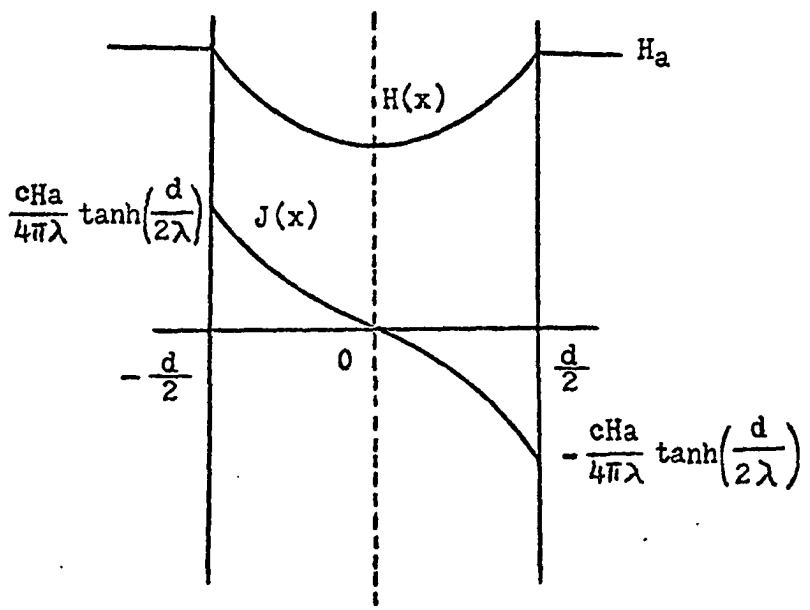

Figure 3 - 4(b)

Figure 3-4. The case of an infinitely wide film with thickness d.

ii) For the edge regions

$$J(X) = J(\frac{w}{2}) \exp\left[X - (\frac{w}{2} - X)\frac{d}{b\lambda^2}\right] \qquad (116)$$

where b is constant on the order of unity.

The method which Newhouse[132] used was derived by Edwards. Edwards carried out a conformal transformation of the magnetic field around a superconducting cylinder and obtained the magnetic field and current distribution of a flat film (See the Edwards' derivation in Appendix 2). The result of the current distribution is the same as that of Bowers except for constants. Since Bowers' work was unpublished and quoted by Glover[100] in Seventh International Conference (1961), it is not known whether Edward's work was related to Bowers' or not. Edwards' results are

$$H(X) = \frac{4I}{cw}\left[1 - (\frac{2X}{w})^2\right]^{-1/2} \qquad (117)$$

$$J(X) = \frac{I}{w}\left[1 - (\frac{2X}{w})^2\right]^{-1/2} \qquad (118)$$

b) Glover and Coffey's method[104]

Matching Eq. (11) and Eq. (116) at the point for which slope and magnetic field are equal, yields

$$J(\frac{w}{2}) = \exp(\frac{1}{2})\,(\frac{wd}{2b})^{1/2}\,\frac{J(X=0)}{\lambda} \qquad (119)$$

Total current I is given as

$$I = \int_{-\frac{w}{2}}^{\frac{w}{2}} J(X)dX = \frac{\pi wd}{2} J(0) \qquad (120)$$

The ratio of the current at the center to that of the edge is given from Eq. (119) by

$$\frac{J(\text{center})}{J(\text{edge})} = \frac{J(x=0)}{J(\frac{w}{2})} = \exp(\frac{1}{2})^{-1} (\frac{2b}{wd})^{1/2} \lambda \qquad (121)$$

By eliminating J(0) from Eq. (120) and Eq. (121), the current density at the edge is obtained as

$$J(\text{edge}) = J(\frac{w}{2}) = \exp(\frac{1}{2}) (\frac{2}{wd})^{1/2} \frac{I}{\pi\lambda} \qquad (122\text{-a})$$

When the total current I is the critical current, the current density at the edge is the critical current density.

$$J_c = \exp(\frac{1}{2}) (\frac{2}{bwd})^{1/2} \frac{I_c}{\pi\lambda} \qquad (122\text{-b})$$

The temperature dependence of J_c is given from Eq. (44) and Eq. (122-b) as

$$J_c(t) = \exp(\frac{1}{2}) (\frac{2}{bwd})^{1/2} \frac{I_c}{\pi\lambda(0)} (1 - t^4)^{1/2} \qquad (123)$$

Dividing Eq. (121) by the value at 0 K, yields

$$\frac{J_c(t)}{J_c(0)} = \frac{I_c(t)}{I_c(0)} (1 - t^4)^{1/2} \qquad (124)$$

Eq. (124) takes into account the nonuniform current distribution in a plane rectangular film. From Eq. (95), it can be seen that the temperature dependence of J_c essentially governed by the $(1 - t^2)^{3/2}$ term, and is not affected by edge build-up. It remains the same at the $(1 - t^2)^{3/2}$ approximation. Therefore,

$$\frac{J_c(t)}{J_c(0)} = (1 - t^2)^{3/2} \tag{125}$$

Substituting Eq. (125) in Eq. (124) yields

$$\frac{I_c(t)}{I_c(0)} = \frac{1 - t^2}{(1 + t^2)^{1/2}} \tag{126}$$

Eq. (125) is compared with Eq. (95) by Bardeen.

c) Marcus' method[100]

Marcus derived the equation from the London and the Maxwell equations for a cylindrical superconductor

$$J(\vec{r}) = c + \frac{\beta}{2\pi} \int_S J(\vec{r}') \ln|\vec{r}' - \vec{r}'| dS \tag{127}$$

where $\beta = \frac{1}{\lambda} \cdot \vec{r}$ is a general point and S is cross-section area of the specimen. He solved (127) for S of a rectangular film with width w and thickness d by a computer. The results are shown in Figure 3-5. As shown in Figures 3-5 (c) and (d), J peaks at the edge and is nearly uniform in the region several penetration lengths away from the edges.

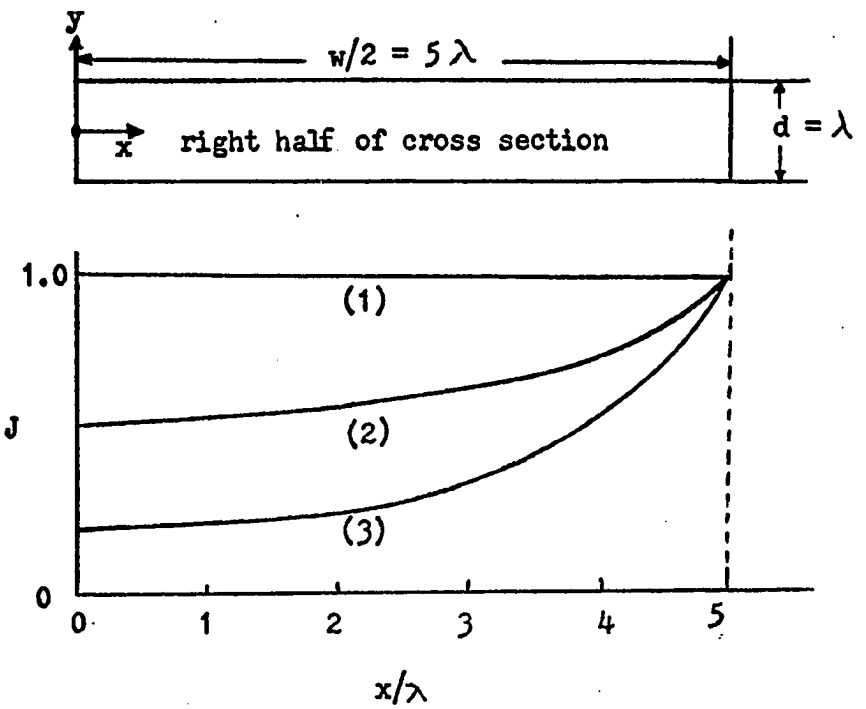

Figure 3 - 5 (a)

Current densities, J(x), vs. distance from center of film measured in penetration depths, λ in superconducting films rectangular cross-section, width w, thickness d, carrying steady current. (1):$d = \lambda$, $w = 10\lambda$ (2):$d = \lambda$, $w = 10\lambda$ (3):$d = 3.81\lambda$, $w = 38.1\lambda$. (1) is the case of uniform current distribution.

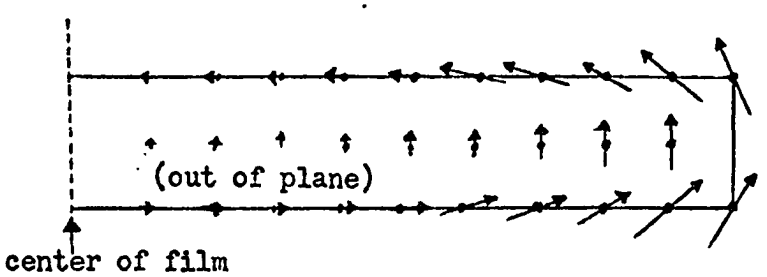

Figure 3 - 5 (b)

Direction and magnitude (proportional to lengths of arrows) of field in and around superconducting film.

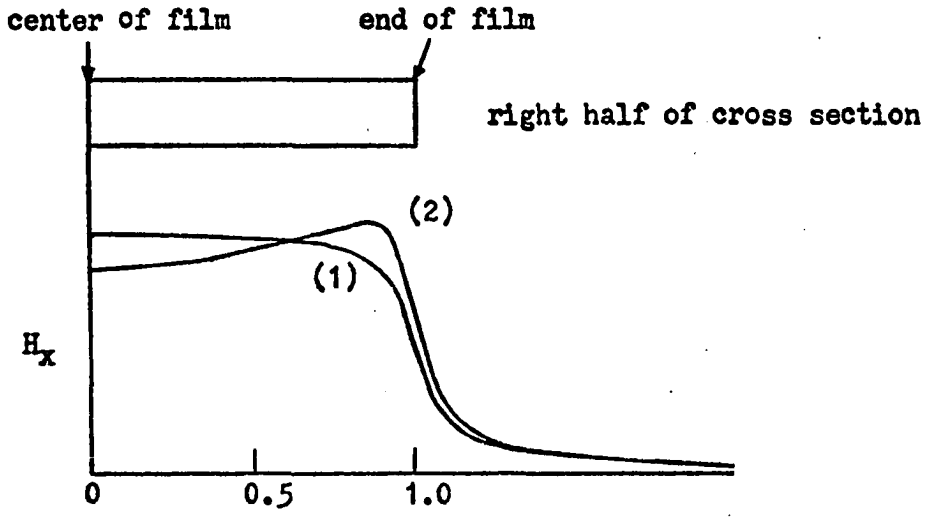

Figure 3 - 5 (c)

Horizontal component of magnetic field, $H_x(x,d/2)$ in plane of top surface of film vs. distance from center of film.

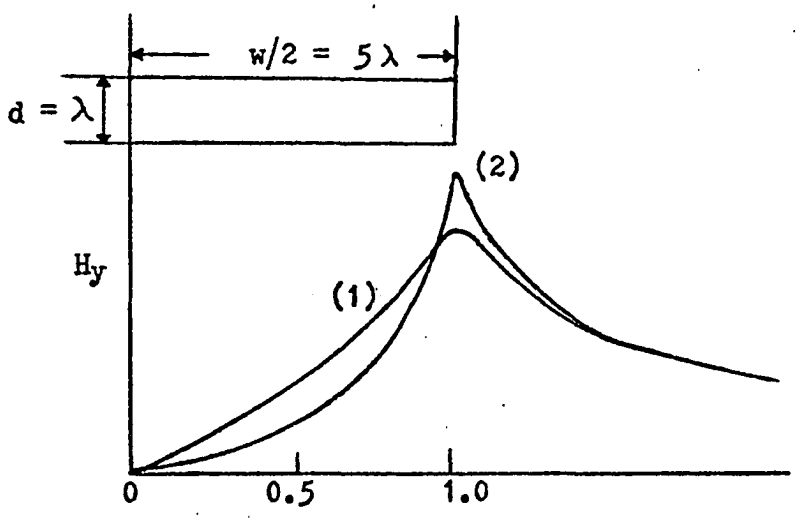

Figure 3 - 5 (d)

Normal component of magnetic field, $H_y(y,d/2)$, in plane of top surface of film vs. distance from center of film.

Marcus gave the ratio of the current at the center to that at the edge as

$$\frac{J(\text{center})}{J(\text{edge})} = \frac{1.65\lambda}{(wd)^{1/2}} \qquad (128)$$

Cohen and Abeles[133] pointed out that J(center) can be approximately equal to the average current density I_c/wd since w/λ is very large and obtained J(edge) as

$$J(\text{edge}) = \frac{I_c}{1.65(wd)^{1/2}} \qquad (129)$$

which is very similar to Eq. (122-b) obtained by Glover and Coffey.[104]

d) Meservey and Tedrow's method[130]

They combined the current and field distributions of both the infinitely wide film of thickness d and the finite width film in which current distribution is constant through thickness d. To remove the singularity at w/2 in Eq. (115) or Eq. (118), they introduce the small distance δ and modified Eq. (117) as

$$H(X) = \frac{I}{2\pi\left[\left(\frac{w}{2} + \delta\right)^2 - X^2\right]^{1/2}} = I_f(X) \qquad (130)$$

They obtained

$$\delta = \frac{d}{4} \quad \text{for} \quad d<\lambda$$

$$\delta = \frac{\lambda}{2} \quad \text{for} \quad d>\lambda$$

By combining $f(\chi)$ with the results of the infinitely wide film, they obtained

$$H(x,y) = If(x)\frac{\sinh(\frac{y}{\lambda})}{\sinh(\frac{d}{2\lambda})} \tag{131}$$

$$J(x,y) = If(x)\frac{\cosh(\frac{y}{\lambda})}{\sinh(\frac{d}{2\lambda})} \tag{132}$$

where x is the distance from the center of the width w, and y is the distance from the center of the thickness d. The current distribution of Eq. (132) is shown in Figure 3-6.

IV. The Relationship Between the Applied Current and Applied Magnetic Field

Ginzburg-Landau equations are used for the type I superconducting film and a laminar model similar to London and Goodman's is used for the type II superconducting film.

1) Alphonse and Bergstein's Method for the Type I Superconducting Film

Alphonse and Bergstein solve the Ginzburg-Landau equations[7] Eq. (24) for a current-carrying thin film in the presence of applied magnetic field parallel to the surface of a film. The cross section of a film to a parallel external magnetic field and transport current is shown in Figure 3-7. The transport current is in the z-direction, the applied magnetic field H_J, is in the y-direction and the field due to the transport current H_a, is in the y-direction. Ginzburg-Landau equations Eq. (24) then involve

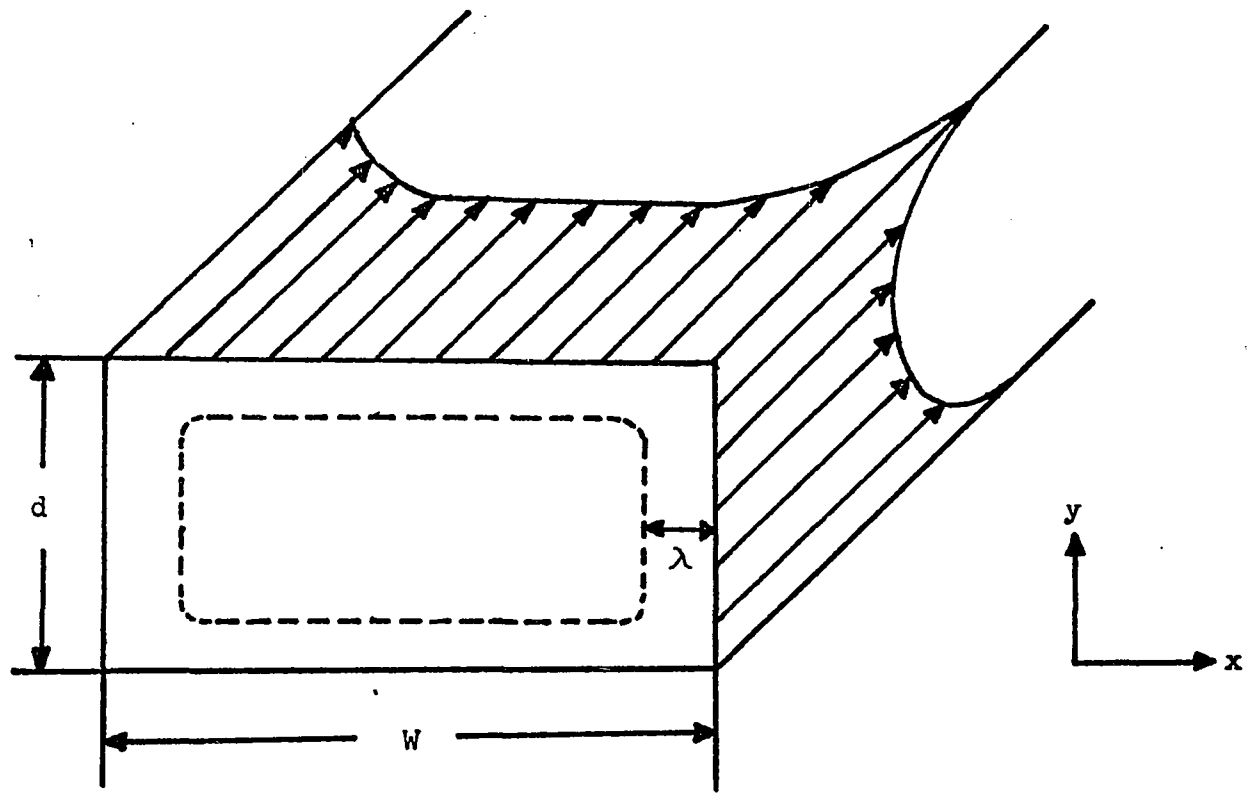

Figure 3 -6 . Current distribution in a superconducting film with rectangular cross-section. The origin is taken at the ceter of the eross-section.

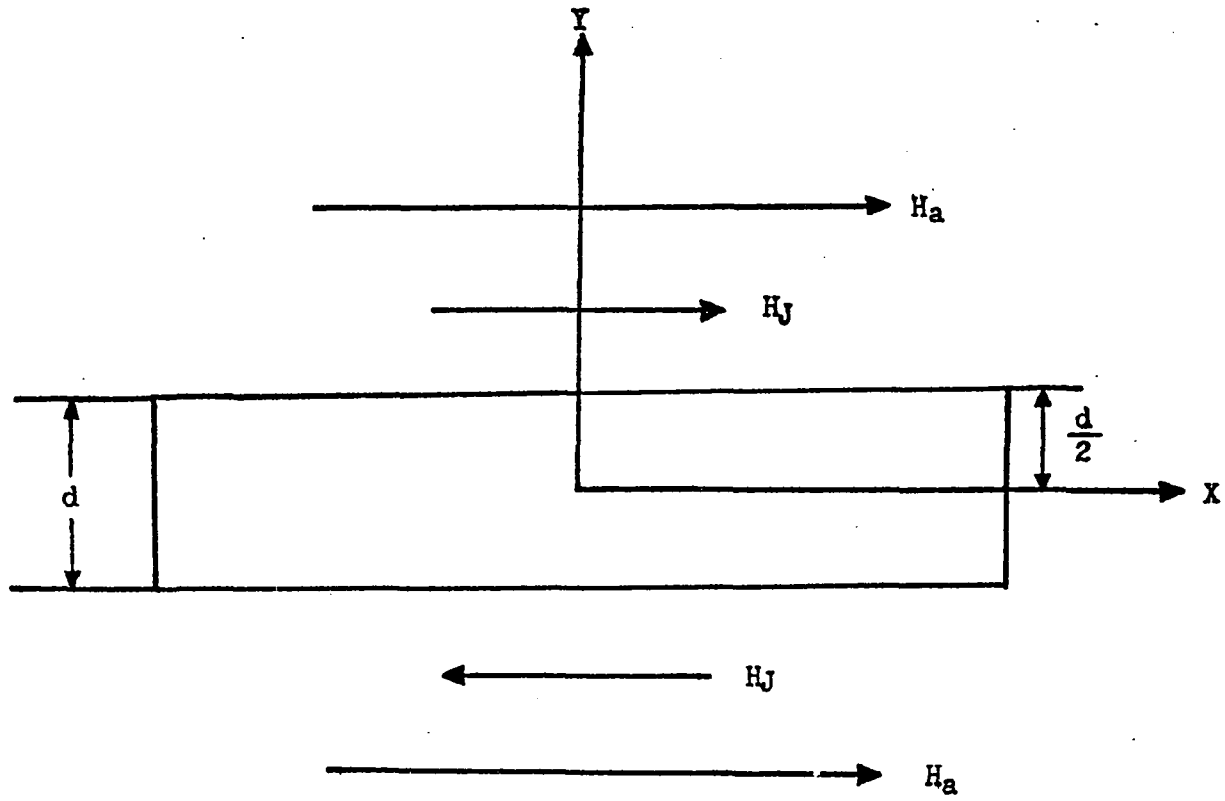

Figure 3 - 7

Cross section of film in tangential external field and carrying transport current.

the x coordinate given as

$$\lambda^2 \frac{d^2 f_o}{dx^2} = K^2[(a^2 - 1)f_o + f_o^3]$$

and (133)

$$\lambda^2 \frac{d^2 a}{dx^2} = f_o^2 a$$

where a is the normalized vector potential, and is given as

$$a = \frac{A}{\sqrt{2}\, U_o H_c \lambda}$$

where A is the vector potential.

The boundary conditions are at $\pm \frac{d}{2}$

$$\frac{df_o}{dx} = 0 \quad , \quad H(\pm \frac{d}{2}) = H_a + H_J \tag{134}$$

where H_e is the applied magnetic field and H_J is the magnetic field due to the applied current. The critical field at the surface of the specimen H can be reduced by various combinations of H_a and H_J. The value of f_o at the top surface of the specimen is the critical order parameter f_{oc}. The values of H_J range from 0 to H_{Jc}, where H_{Jc} is the critical current density in the absence of external field ($H_a = 0$). The values of H_a go from 0 to H_{ac} where H_{ac} is the critical external field in the absence of current ($H_J = 0$). From Ginzburg-Landau equations,

$$(1 - f_o^2) f_o^4 = (\frac{H_a}{H_{ac}})^2 f_o^4 + (\frac{4}{27})(\frac{H_J}{H_{Jc}})^2 \tag{135}$$

At the top surface of the film

$$f_{oc}^{\ 2} = \frac{2}{3}\left(\frac{H_J}{H_{Jc}}\right)^{2/3} \tag{136}$$

Substituting Eq. (136) to Eq. (135) yields

$$\frac{H_a}{H_{ac}} = \left[1 - \left(\frac{H_J}{H_{Jc}}\right)^{2/3}\right]^{1/2} \tag{137}$$

From Eqs. (72), (119) and (120), it can be seen that the applied current I is linearly proportional to the magnetic field due to I. Then, the term of $(H_J/H_{Jc})^{2/3}$ in Eq. (137) can be replaced by (I/I_c), where I_c is the critical current without the applied field. H_{ac} in this case is H_{cF} and H_a is H. Therefore, Eq. (137) can be rewritten as

$$\frac{H}{H_{cI}} = \left[1 - \left(\frac{I}{I_c}\right)^{2/3}\right]^{1/2}$$

or

$$\left(\frac{I}{I_c}\right) = \left[1 - \left(\frac{H}{H_{cI}}\right)^{2}\right]^{3/2} \tag{138}$$

2) El Bindari and Litvak's Method for the Case of the type II Superconducting Film

El Bindari and Litvak derived the relationship between current I and external field H by their laminar model. Magnetic field and current profiles for a cross section near the center of the film is shown in Figure 3-8.

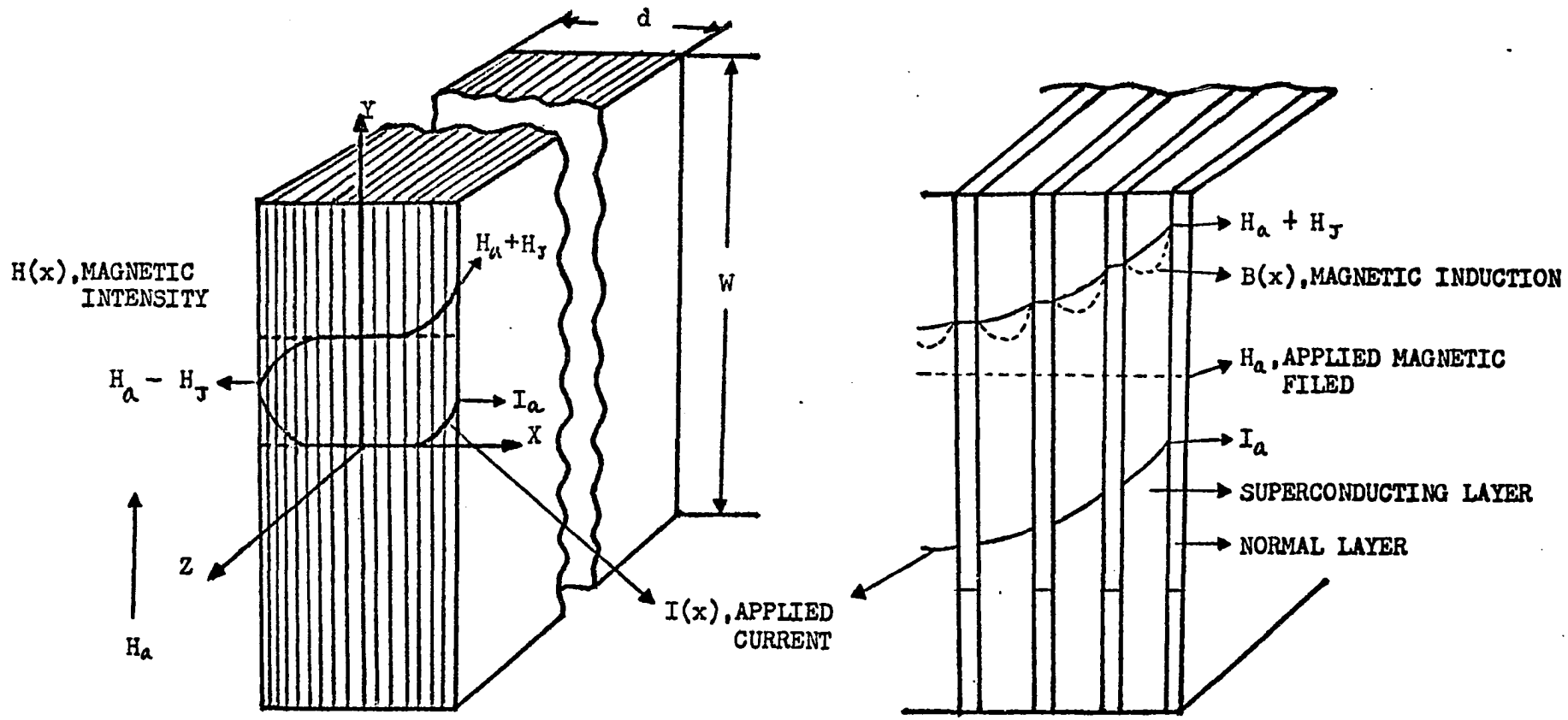

Figure 3 - 8

Magnetic field and applied current profiles for a cross section near the center of the sample. The layers of suprtconducting and normal states of the sample are shown.

They assumed the following for their model:

(a) The alternating layers of normal and superconducting specimen are parallel to the external field.

(b) The applied field has its full value in each of the normal layers. Negligible current flows in them.

(c) The aspect ratio of a film is sufficiently small to neglect end effects.

(d) The magnetic induction B and the applied current density J in the superconducting specimen obey the London equation, that is,

$$\nabla^2 B = \frac{B}{\lambda^2}$$

$$\nabla^2 J = \frac{J}{\lambda^2}$$

(e) The interfacial free energy is given by $g\frac{H_c\lambda}{8\pi}$ where g is Googman's nondimensional surface energy parameters.

The relation between current I and external magnetic field H is given as:

$$\frac{I}{I_c} = 1 - \left(\frac{H}{H_c}\right)^{1/3} \qquad (139)$$

V. Equations Used in This Work

When the thickness of a film becomes comparable to the electron mean free path, it is necessary to consider the influence of the surface of the film on the electromagnetic properties of the film. However, it is still not well understood how the surface conditions, for instance, surface texture, adsorption of gases on the surface and reflection of electrons from the surface affect the mean free path. Although observed magnetization curves of films deviate from ones of the bulk specimen, none of the theories take this deviation into account. Most equations for films derived from the London, BCS and Ginzburg-Landau theories can be applied to only limited conditions such that the temperature is near T_c, the thickness is much smaller than λ, the current density distribution in the film is uniform, etc. No comprehensive theory is yet established. In sections I - IV a survey of existing theories was presented. Results of these theories which are used in the analysis of this work are summarized below.

The critical magnetic field for thick films for type I superconductors:

$$H_{cF}(t,d) = H_c(0)(1 - t^2)\left(1 + \frac{\lambda(t,d)}{d}\right) \qquad (55)$$

$$H_{cF}(t,d_c) = 1.45\ H_c(t) \qquad (57\text{-}b)$$

The critical magnetic field for thin films for type I

$$H_{cF}(t,d) = \frac{\sqrt{24}\, H_c(0) \lambda_L^2 \xi_o^{1/2}}{d^{3/2}} \tag{56}$$

$$H_{cF}(t,d_c) = 2.2\, H_c(t) \tag{57-a}$$

For the calculation of the value of ξ_o,

$$\lambda(0) \approx \lambda_L \left(1 + \frac{\xi_o}{\ell}\right)^{1/2} \tag{48}$$

$$\lambda(0) = \lambda_L \left(\frac{\xi_o}{d}\right)^{1/2} \tag{51}$$

The temperature dependence of the current density and the current

$$J_c(t) = \frac{cH_c(t)}{4\pi\lambda_L(t)} = \frac{cH_c(t)}{4\pi\lambda_L(0)} (1 - t^2)^{3/2} (1 + t^2)^{1/2} \tag{84}$$

$$\frac{J_c(t)}{J_c(0)} = (1 - t^2)^{3/2} \tag{125}$$

$$\frac{I_c(t)}{I_c(0)} = \frac{(1 - t^2)}{(1 + t^2)^{1/2}} \tag{126}$$

where Eqs. (125) and (126) take into account the nonuniform current distribution in plane rectangular film. The relationship between the applied current and the critical magnetic field for type I superconductors:

$$\frac{I}{I_c} = \left[1 - \left(\frac{H}{H_{cF}}\right)^2\right]^{3/2} \tag{138}$$

The relationship between the applied current and the critical magnetic field for the type II superconductor:

$$\frac{I}{I_c} = 1 - \left(\frac{H}{H_c}\right)^{1/3} \tag{139}$$

CHAPTER IV

ULTRA-HIGH-VACUUM (UHV) SYSTEM

The components of the experimental system are listed below. A detailed description of each component follows this list.

1) Vacuum Chamber
2) Auger Electron Spectrometer (AES)
3) Sputter Deposition Gun
4) Residual Gas Analyzer (RGA)
5) Specimen Manipulator
6) Gas Manifold
7) Automatic Pressure Controller (APC)

The system as a whole will be referred to as the UHV system (Ultra-High-Vacuum System).

1) Vacuum Chamber

A vacuum of less than 10^{-8} torr was required to avoid contamination of film surfaces. Before evacuation of the experimental system, all internal surfaces were

carefully cleaned to avoid outgassing problems, since the pressure necessary for sputtering was less than 10^{-8} torr. Any substances present which vaporizes upon lowering of pressure, such as fingerprints and residual lubricants from machining processes, prevent the attainment of a sufficient vacuum and may cause film contamination as well. One means of reducing this problem was to use an all-clean system with a vacuum pump which did not require oil or mercury for its operation. The level of undesired contaminants was continuously monitored by a residual gas analyzer. The vacuum chamber has an ion pump for high vacuum and contains an AES and a RGA. It has demountable UHV seals made from OFHC copper gaskets.

2) Auger Electron Spectrometer (AEC)

The Auger Electron Spectrometer which was used is the PHI Model 5000, manufactured by physical Electronic Industries, Inc. It consists of the PHI Model 10-150 cylindrical-Auger electron optics system, the electronic analysis system and the recording system. The cylindrical-Auger electron optics system consists of an electron velocity analyzer of cylindrical geometry with a coaxial electron gun and an electron multiplier. The electron gun produced a focused high current beam of electrons directed along the axis of the analyzer. The electron beam incident on the target excites Auger electrons which are emitted from

the target and separated in energy by the velocity analyzer. The output signal of the analyzer is amplified by the electron multiplier. For a point source, the limiting resolution is slightly less than 0.3 percent. The magnetic shield in the cylindrical analyzer minimizes the unshielded portion of the Auger electron trajectories, while reducing the magnetic field inside the analyzer to a negligible value. However, because of finite source size and residual magnetic fields in the immediate target vicinity, the observed resolution ranges from 0.5 to 1.0 percent. Since the natural half width of most Auger peaks is about 5 eV, an experimental resolution of one percent is adequate for detection of 0-1500 eV Auger electron peaks. The schematic diagram of this optics system and associated electronics is shown in Figure 4-1. The electronics analysis system consists of PHI 11-010 Electron Gun Control, PHI 11-500 Auger System Control, PAR 122 Lock-in Amplifier, Keithley 246 Electron Multiplier Supply and a Fluke 432A 3KV Power Supply. The recording apparatus includes an HP 1206B Oscilloscope for system setup and dynamic monitoring and an HP 7035B X-Y Recorder.

3) Sputter Gun

The sputter gun consists of a replaceable target cathode in a hollow sleeve, a passive, disk-shaped anode and a cylindrical permanent magnet, cooling-water manifold and fittings, and high-voltage connectors. All of the former

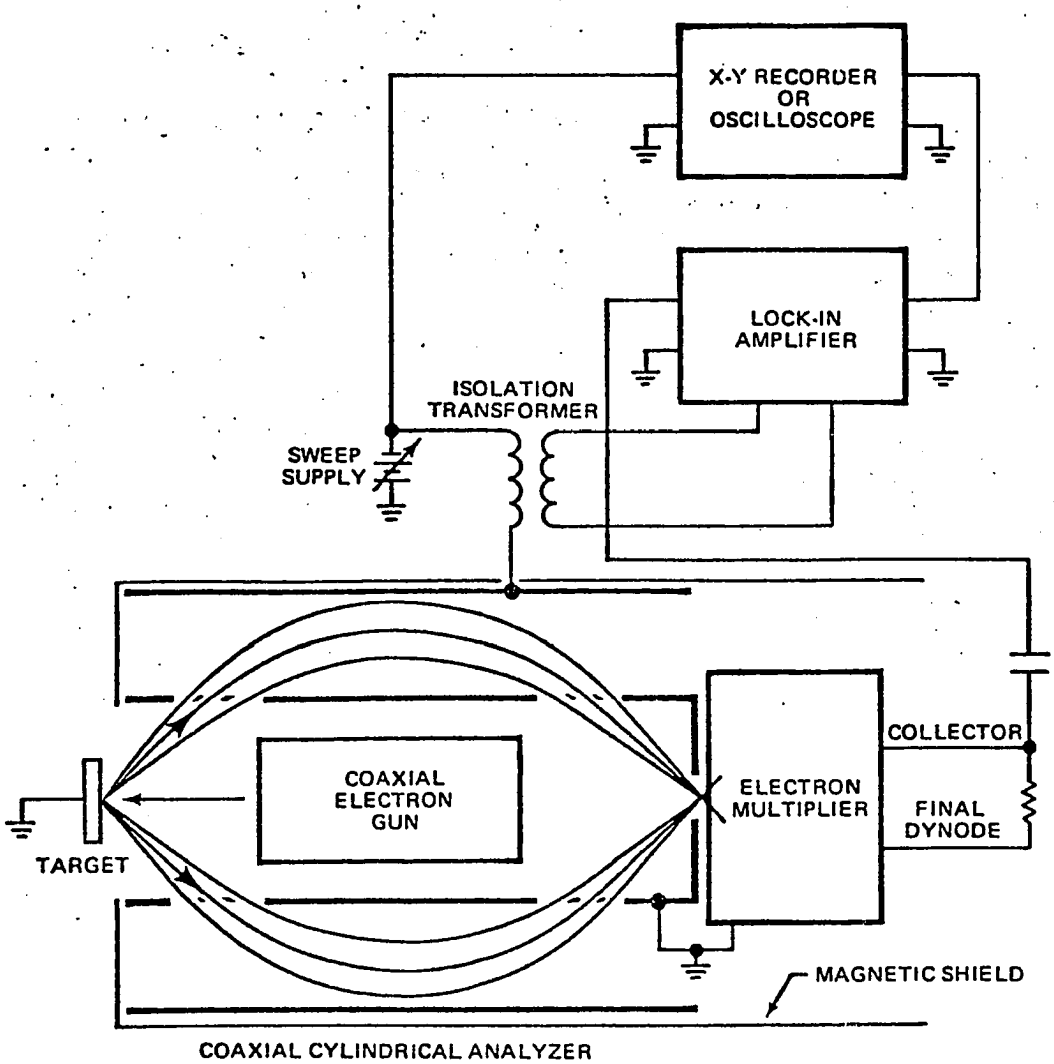

Figure 4 - 1

PHI Cylindrical-Auger Electron Optics System and associated electronics.

PHI MODEL 10-150

Cylindrical-Auger Electron Optics

Analyzer Energy Resolution -------	0.5% to 1.0%
Beam Diameter----------	25 m at specimen with 1 amp beam current
Beam Current ----------	Greater 100 amp
Beam Voltage ----------	0 volt to 5,000 volts
Signale-to-noise ----------	100:1, 2024 ev Au peak 600:1, 920 ev Cu peak with 5 Kev, 50 amp beam, 300 msec. time constant, 8 ev peak-to-peak modulation
Electron Gun Cathode ----------	Replaceable tungsten ribbon
Shielding ----------	Magnetic shield of UHV material encloses entire instrument
Apertures ----------	Cylinder aperaures covered with 100 line per inch mesh
Electron Multiplier ----------	Type: 14 stage BeCu
Dimensions	
Magnetic Shield ----------	8.9 cm (3.5") O.D.
Specimen to Flange Distance ----	22.8 cm (9")
Specimen to Analyzer Distance --	6.5 mm (0.261")
Mounting ----------	Complete units is mounted on a 10 cm (4") I.D. UHV flange
Electrical Connections ----------	Bakeable MHV Coaxial connectors on a separate connector plate, stress isolated from the vacuum feedthroughs

are contained in a dome-shaped aluminum housing. The interior unit is made of stainless steel, copper, and aluminum, is bakeable to 350°C, and mounted on a standard UHV flange.

Only the anode and the target holder are exposed to the vacuum chamber, all other components are isolated by UHV seals. The anode is removable.

Power Input	5.0 Kw maximum
Operating Voltage	-300 to -800 volts, depending on cathode materials
Current Density	Variable over range of 100 to 3000 mA/sq. inch
Operating Pressure	5 x 10^{-3} torr
Cooling Water Required	1/2 g per minute minimum
Body Construction	Machined OFHC copper, 304 stainless steel
Electrical Isolation	Alumina ceramic-metal cable termination
Vacuum Seals	ConFlat^{R} 8 inches Flange
Dimensions	8 inches in diameter, 8 inches high
Manufactor	Sputtered Films, Incorporated
Model	UHV-3

Sputter Deposition Cathode (the target)

Manufactor	Haselden Co.
Materials	Lead and Niobium 99.99%
Shape	Ring
Size	3.126" + 0.001" O.D. 2.876" + 0.030" I.D. 0.900" +).030" Height

4) Residual Gas Analyzer (RGA)

Gas molecules enter the source region of the analyzer tube and are ionized by high energy electrons emitted by a heated filament. The ions thus produced are then accelerated into the analyzing region. This region consists of a "V" shaped rail and a solid cylindrical rod positioned parallel

to each other a precise distance apart. The red is supplied with a high frequency (RF) as voltage superimposed on a regulated supply of DC voltage, while the rail is at ground potential. Ions are injected down the length of the analyzer tube between the rod and rail but at a slight angle to the center axis. The AC and DC fields acting on the ion cause it to oscillate in a complex transverse fashion as it travels at a constant velocity along the length of the tube. For particular electrical conditions only ions of a specific mass-to-charge ratio will move in such a path as to allow the ion to complete its travel and impinge upon the collector. This is the "tuned" ion. All other ions will somewhere strike the rail or rod and thus be prevented from reaching the collector. Other ionic masses can be "tuned" by varying the potentials applied to the rod. This is done automatically and uniformly in the SPI-10 by the sweep generator and results in an oscilloscope presentation of the mass spectra. The mass spectra will be linear with respect to the positions of the mass peaks. This means that mass peak identification becomes a simple matter of sealing.

Manufacturer ---------- Veeco Instruments, Inc.
Model ---------- SPI-10

5) Specimen Manipulator

The manipulator permits precision positioning of the multiple specimen mount in the UHV system. The X and Y translations employ micrometer controls for precise and measurable lateral adjustments.

Manufactor	Physical Electronics Industries, Inc.
Model	PHI 10-501M
Rotation	360°
X and Y Translations	± 6.3 mm (0.25")
Z Translation	± 15.0 mm (0.60")
Tilt	± 5 about two orthogonal axes
Electrical Feed throughs	two 5 Kv, 15 A two 5 KV, 150 A
Bakeout	250°C
Mounting	10 cm (4") I.D. UHV flange

6) Gas Manifold

An isolated gas manifold was constructed, permitting the introduction of ultra-pure gas into the sputtering system without contamination. Figure 4-2 shows a schematic diagram of the system which operates as follows. The valve above each gas bottle is opened and the entire gas manifold is evacuated with a sorption pump. After the pressure measured by the thermocouple gauge, has reduced to less than 1×10^{-5} torr, the valve is closed. Then the bellows valve which leads to an 8 liter per second ion pump is opened and the system is further evacuated to a pressure of 1×10^{-8} torr. The manifold is held at this pressure with the ion pump until introduction of the desired gas. The gases argon, nitrogen and xenon are supplied by AIRCO INDUSTRIAL CO. with a purity of better than one part million in a liter glass bottle. For example, if it is necessary to admit argon into the system, the valve above the argon bottle is closed and the magnetic breaker is pulled into

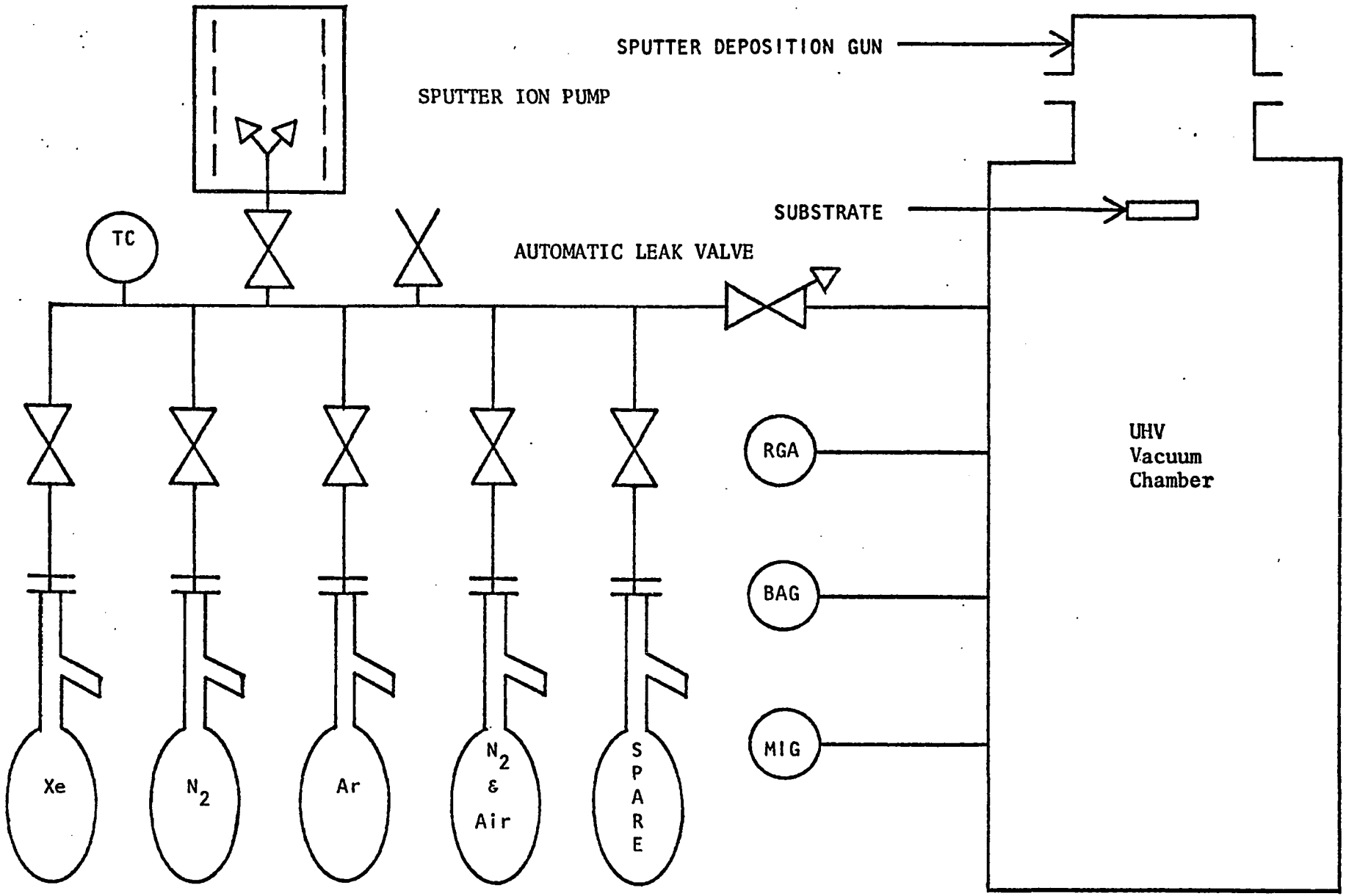

Figure 4 - 2 Gas Manifold Schematic.

the cylinder above the bottle and dropped upon the nipple. This breaks the nipple and fills the region behind the valve with a pure argon atmosphere. The valve to the remaining four bottles is then closed as is the valve to the ion pump, and then the valve above the argon bottle is opened until the pressure in the manifold rises to approximately 1×10^{-1} torr. The gas manifold is now filled with argon gas at pressure of approximately 1×10^{-1} torr with an impurity level of less than 1 part per million. This pure gas can now be admitted to the UHV system by using the automatic control unit.

7) Automatic Pressure Controller (APC)

The automatic pressure controller is an electro-mechanical instrument designed to automatically regulate the gas pressure in a system. When combined with a suitable pressure transducer or transducer which is influenced by pressure or flow, the APC will accurately maintain any desired pressure or partial pressure in a system from one atmosphere to less than 10^{-11} torr. Pressure control is accomplished by automatically and continuously admitting the correct gas flow to a dynamic system to compensate for gas being removed at constant or rapidly varying rates by pumps, adsorption or other means. Backfilling in a static system is also readily accomplished. The control unit is designed to continually compare the signal furnished by the transducer

with a reference signal which is internally generated in the control unit. The reference signal is processed by the user to correspond to the output voltage of the transducer at the control unit. If the output is not at this value, there will exist a difference between the reference voltage and the transducer output voltage. This difference voltage signal is chopped, amplified, phase detected and used to control the servo-driver which opens or closes the leak value, thus decreasing the difference signal.

Manufactor	Granville-Phillips Co.
Model	Series 213
Sensitivity	± 0.2% full scale with full gain a and maximum motor velocity
Accuracy	± 1% full scale of the input voltage
Response Time	30 seconds from fully open to fully closed for the servo valve

The Method of Preparation of Films

The methods commonly used to prepare thin films of solids may be classified as

(A) Electrolytic deposition, which includes cathodic and anodic deposition.

(B) Sputtering deposition, including the more recently developed method of reactive sputtering.

(C) Deposition in vacuum from a heated source (thermal evaporation or vapor evaporation)

(D) Deposition from vapor reactants.

(E) Diffusion.

Two methods, B and C, were examined for possible use. The former, the sputtering method, was chosen because of its advantages in producing niobium carbonitride and lead films. A primary advantage of sputtering deposition is the capability to deposit such materials as refractory metals (e.g. molybdenum, tungsten, niobium, etc.) and dielectrics. A second advantage is the ability to simultaneously deposit binary or more complex films using only a single source. Vapor evaporation usually requires multiple sources with attendant difficulties and problems in maintaining predetermined parameters (e.g. deposition rate, composition of the films, etc.). Another advantage of using sputter deposition is that sample purity can be more easily maintained. A previous objection to sputter deposition was the inability to isolate physically and electrically the substrate from the sputtering function. This caused substrate heating and contamination of films due to adsorption of foreign particles. This objection has been negated by the new development which this unit has adopted, i.e., isolating the substrate from the sputtering source.

In operation, the hollow cathode is energized with a negative d-c potential in an atmosphere consisting of a gas such as argon at a pressure of 1 to 2 x 10^{-3} torr. The field from the permanent magnet constrains emitted electrons

to a tight, spiral pattern near the surface of the cathode. By this means, the electrons are forced to travel a comparatively long path, and the probability of an ionizing collision with an argon atom in the vicinity of the cathode is raised to a high level. The glow discharge resulting from ionization of the gas is maintained as long as the appropriate potential is applied to the cathode. When an argon atom is ionized, it acquires a positive charge and is attracted to the negative cathode with a force sufficient to dislodge an atom of the cathode material. These sputtered particles are ejected from the cathode in random directions and the material leaves the sputter gun cavity in a pattern that encompases virtually all angles of impact on the substrates. (See Figure 4-3) The process results in a deposition of sputtered material that becomes a film with excellent uniformity and step coverage. Neither the substrate holder nor the substrates themselves are part of the sputter gun electrical circuit. Secondary electrons are trapped by the magnetic field, preventing electron bombardment of the substrates. This enables the sputter gun to avoid a major cause of substrate heating and provides cool sputtering. The sputter gun is operated at potentials of 600 volts or less. The power density of the sputter gun is 2 kilowatts over approximately four square inches of cathode surface. The supply of the sputter gun which was used is Model 1 KW

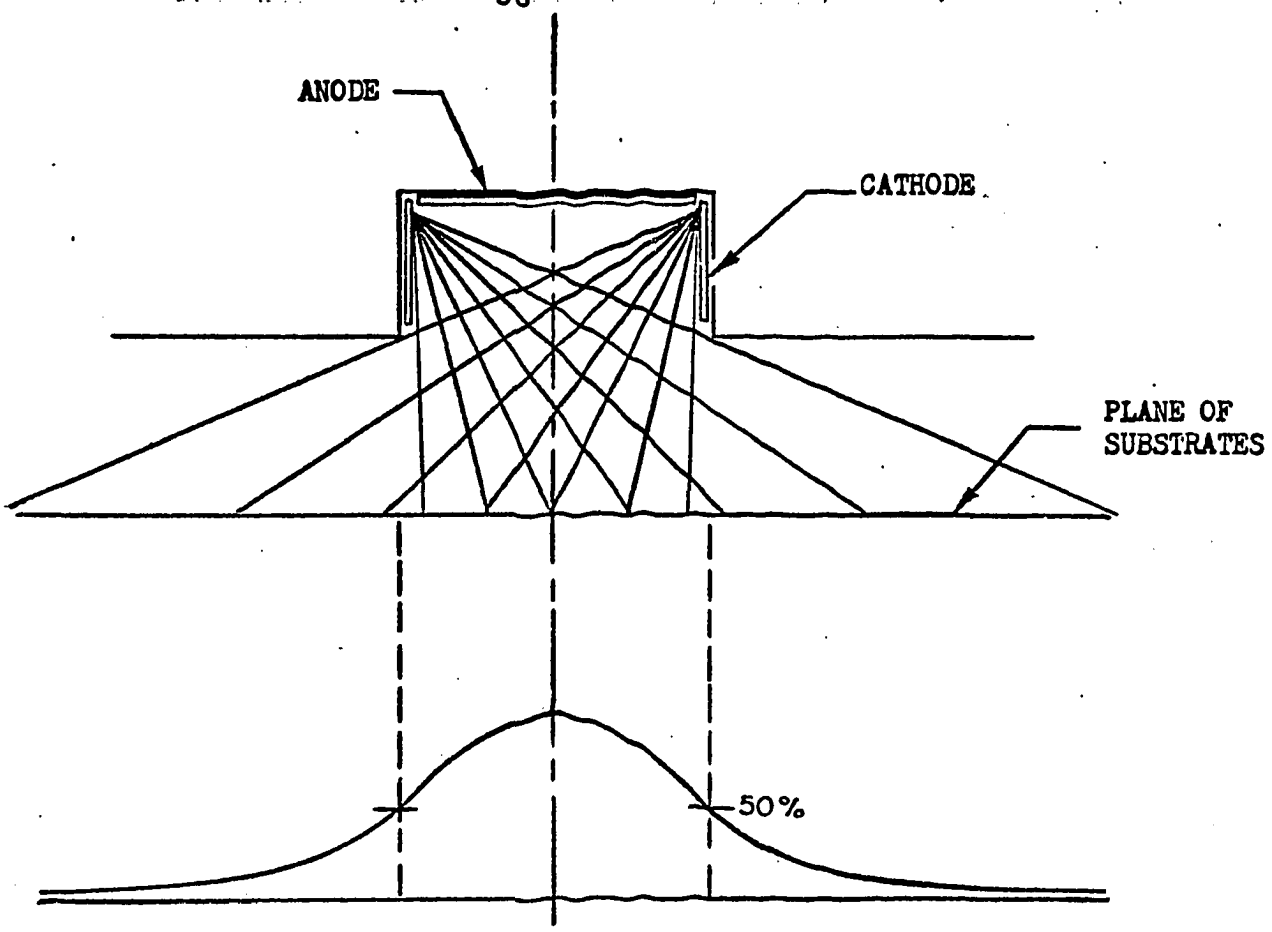

Figure 4 - 3

Distribution of Sputtered Materials. Curve shown applies only when top of substrate material is 2.125 inches from bottom of target holder.

Power Supply of the same company, which delivers a 1.0 kilowatt current-controlled output up to a maximum of 2 amperes. With the vacuum evaporation method, heating of the hearth is unavoidable and often leads to source contamination by migration of hearth impurities. Such contamination occurs whether heating is accomplished through electrical resistance or by electron beam. Another advantage of sputter deposition is that the deposition rate remains constant with time, provided the current density and voltage do not vary. The constant current density and voltage are easily attained by using an automatic pressure controller and a regulated power supply.

Sputtering Deposition

When atoms or ions having energies in excess of about 30 electron volts strike a surface of materials, the ejection is due to positive ion bombardment, it is referred to as "Cathodic Sputtering". The number of atoms of material ejected per arriving particle is referred to as the sputtering yield. It varies from about 10^{-4} atoms/ion near the minimum threshold to about 10 atoms/ion at optimum bombardment energies of a few thousand volts. In practice, it is much easier to accelerate ions in a controlled manner rather than to provide a beam of energetic neutral particles. Thus sputtering is almost always performed using ions.

Preparation for the Deposition of Films

The UHV system is always maintained at a pressure less than 1×10^{-5} torr where the 200 liter per second ion pump starts to operate, avoiding contamination from the air when it is not used. The sorption pump is baked overnight by a heater before it is used. The gate valve to the 200 liter per second ion pump is closed. Through the gas inlet valve, the nitrogen gas is introduced to the UHV system at atmospheric pressure in order to avoid the direct exposure of the interior of the UHV system to the air. The sorption pump is cooled by liquid nitrogen until its pressure reaches 1 micron (1×10^{-3} torr) on the thermocouple gauge. After removing the sputter gun unit from the UHV system, the substrates which have been cleaned are placed in the specimen holder through the hole where the sputter gun is located, using surgical gloves. The distance between the carrousel disk and the substrate should be 2.125 inches. After all substrates are placed on the holder, the sputter gun is mounted to the UHV system with a new chemically cleaned copper gasket, thereby resealing the UHV system. The valve to the sorption pump is now opened. After the pressure of UHV system reaches 1 micron on the thermocouple gauge, a millitorr ionization gauge is used. When the pressure reaches 5×10^{-5} torr, the valve to the sorption pump is closed and the gate valve to the ion pump is opened. If at this pressure, the ion pump is not ready to operate,

a titanium-sublimation pump is used to bridge the pressure gap until the ion pump comes into full operation.

The partial pressures of different gases are constantly checked by the residual gas analyzer. If too much water vapor or carbon dioxide are in the UHV system after 2-3 hours, the UHV system should be baked by heating tapes. The UHV system is covered by aluminum foils to prevent unnecessary heat loss. The temperature of the heating tapes is controlled by a variac in order to maintain the pressure in the UHV system to less than 5×10^{-5} torr, where the ion pump can safely operate. During the heating of the UHV system, the residual gas analyzer is used to check residual gases in the system. Depending on the degree of contamination, the UHV system is baked for a day to a week. After baking, it takes 3-20 hours for the UHV system to be put into equilibrium with the ion pump. When the ionization gauge shows less than 1×10^{-8} torr and the most sensitive scale in the residual gas analyzer shows that the peak of mass spectrum of residual gases is roughly the same height as the one of helium, the pressure of the UHV system is ready for the deposition of films. If the pressure of less than 1×10^{-9} torr is necessary, the UHV system is cooled by dry ice with alcohol. This process freezes most residual gas molecules to the walls of the system.

Deposition of Films

The automatic pressure controller (APC) responds only to the system pressure dropping below a preset level. The ancillary pump is required to correct any pressure overshot by the sluggish feedback response of the APC. The sorption pump which functions as the ancillary pump is cooled to a pressure less than 1×10^{-5} torr. (See Figure 4-4) A pressure of approximately 10 times less than that desired can be obtained rather easily by using the APC. The adjustment of the valve to the sorption pump must be maintained within a critical range in order to avoid hunting behavior. Then using manual control of the APC, the desired pressure is obtained by gradually opening the automatic leak valve to the gas manifold. After the desired pressure is obtained, the mode of operation is changed from manual to automatic. The APC constantly monitors the pressure of the UHV system and adds gas as necessary. The proper current for sputter gun is chosen and power is applied. A glow discharge color can be seen through the window of the UHV system. The discharge color varies with different gases and pressures. For instance, argon gas yields a reddish purple color and nitrogen a blue color. When the pressure decreases, the color becomes lighter. Without the APC, the pressure of the system decreases and reaches a point where the deposition stops. The pressure decrease occurs because the introduced gas is buried into the film during the deposition.

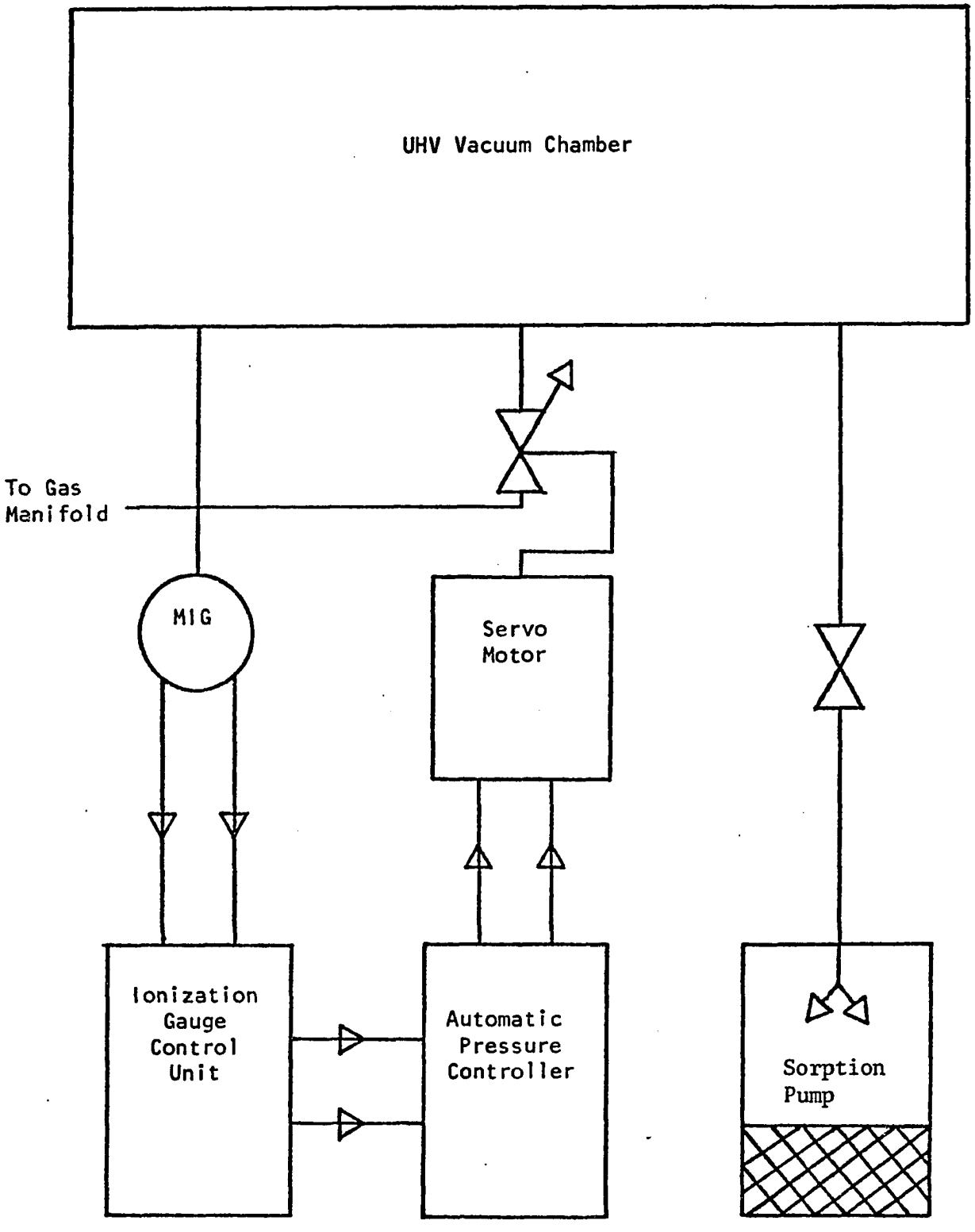

Figure 4 - 4a

Automatic Pressure Control Schematic

Film purity depends upon deposition gas purity which is maintained by the titanium sublimation pump. The film thickness is controlled by the time of deposition, which is measured by a stop watch. In the beginning of the deposition, occasionally there are erratic fluctuations of the sputter gun operating voltage and current levels. This is caused by the initial cleanup of the surface oxide layer of the target. In such a case, the current should be held below the desired level. The irregularity in the shape of the target ring and contamination of its surface cause local abnormally hot spot which result in melting. The opposite surfaces of a sapphire single-crystal plate have different texture. In order to investigate the effect of roughness of the surface of deposited films, two plates with opposite surface are mounted on the specimen holder side by side and are exposed to deposition for the same period of time. After the film is deposited, its Auger spectra can be taken by bringing them back the pressure of the UHV system to less than 5×10^{-5} torr without exposing the film to the air. From this Auger spectra, the contamination of the film or the composition of elements of the film (if it is alloy) can be found immediately. The influence of air on the film can be seen easily by comparing the Auger spectra of the film to one of the film exposed to air.

a) Lead Film Deposition

Lead was deposited on glass and sapphire single-crystal plates using argon gas at 1 to 2 x 10^{-2} torr at 0.5 amperes.

b) Niobium Film Deposition

Niobium was deposited on sapphire single-crystal plates using argon gas at 1.5 x 10^{-1} torr at 1 ampere.

The Deposition Parameters

Macroscopic film characteristics such as the thickness, purity and grain size influence the ultimate film superconducting parameters such as critical magnetic field, critical transition temperature and critical current. These macroscopic characteristics depend strongly upon the deposition rate, which is mainly a function of current and pressure. The substrate temperature and gas impurities also affect the deposition rate.

For a given amount of applied power, high sputtering rates will usually be obtained under conditions which favor high current and low voltage. This is because the number of ions striking the target is directly proportional to the current whereas the sputtering yield tends to increase at a less than linear rate with increasing applied voltage. With increasing pressure the current in the discharge increases while the voltage decreases so it is not surprising that the deposition rate will usually increase with pressure.

Certain impurities can have a significant effect on the deposition rate. The effect of hydrogen and helium is associated with the fact that these gases have high ionic mobility in the discharge but because of their low mass, have very low sputtering yield (effectively zero). The former property causes these atoms to carry more than their proportionate share of the discharge current but, since they cause virtually no sputtering, the net result is a decrease in deposition rate. The effect of oxygen stems from the fact that, before material can be sputtered, adsorbed oxygen on the target surface must first be removed. If the desorbed oxygen is continuously being replaced by oxygen out of the glow, a decrease in deposition rate occurs.

In materials such as gold, where an adsorbed layer of oxygen does not form, no decrease in rate is seen in the pressure of oxygen.

The change of deposition rate by the substrate temperature is due to the thermal re-emission of material which, after arrival at the substrate, returns to the vapor phase because it has not succeeded in finding a suitable bonding site within a certain time period. Because of this effect, it is important to maintain uniform temperature across the substrate surface during deposition. In the case of sputtering this presents something of a problem if the

substrate is constantly being heated through bombardment by high energy electrons which originate at the target.

The UHV system produces for a nearly constant deposition rate by controlling the pressure, impurities and the temperature during the deposition. The pressure can be kept constant by the automatic pressure control unit. The impurities can be monitored by the residual gas analyzer (see Figure 4-4b) and even though it is difficult to eliminate some impurities, the amount of impurities in the gas can be kept constant. As mentioned the sputter gun can do cool sputtering because the secondary electron emitted from the target is trapped in the magnetic field around the target and this prevents electron bombardment of the substrate. Therefore, the deposition rate for the UHV system is a well controlled parameter.

Deposition of Thin Film on a Substrate

In order to measure the superconducting parameters of the thin film, it was necessary to obtain values of voltage and current for various magnetic field intensities. The conventional "four-point" technique, as illustrated in Figure 4-5 was used. The generation of a geometrical pattern can be accomplished by two common methods. One is using a mechanical mask during the film deposition to permit only selected substrate areas to receive the film. One advantage of this method is that it saves time since the

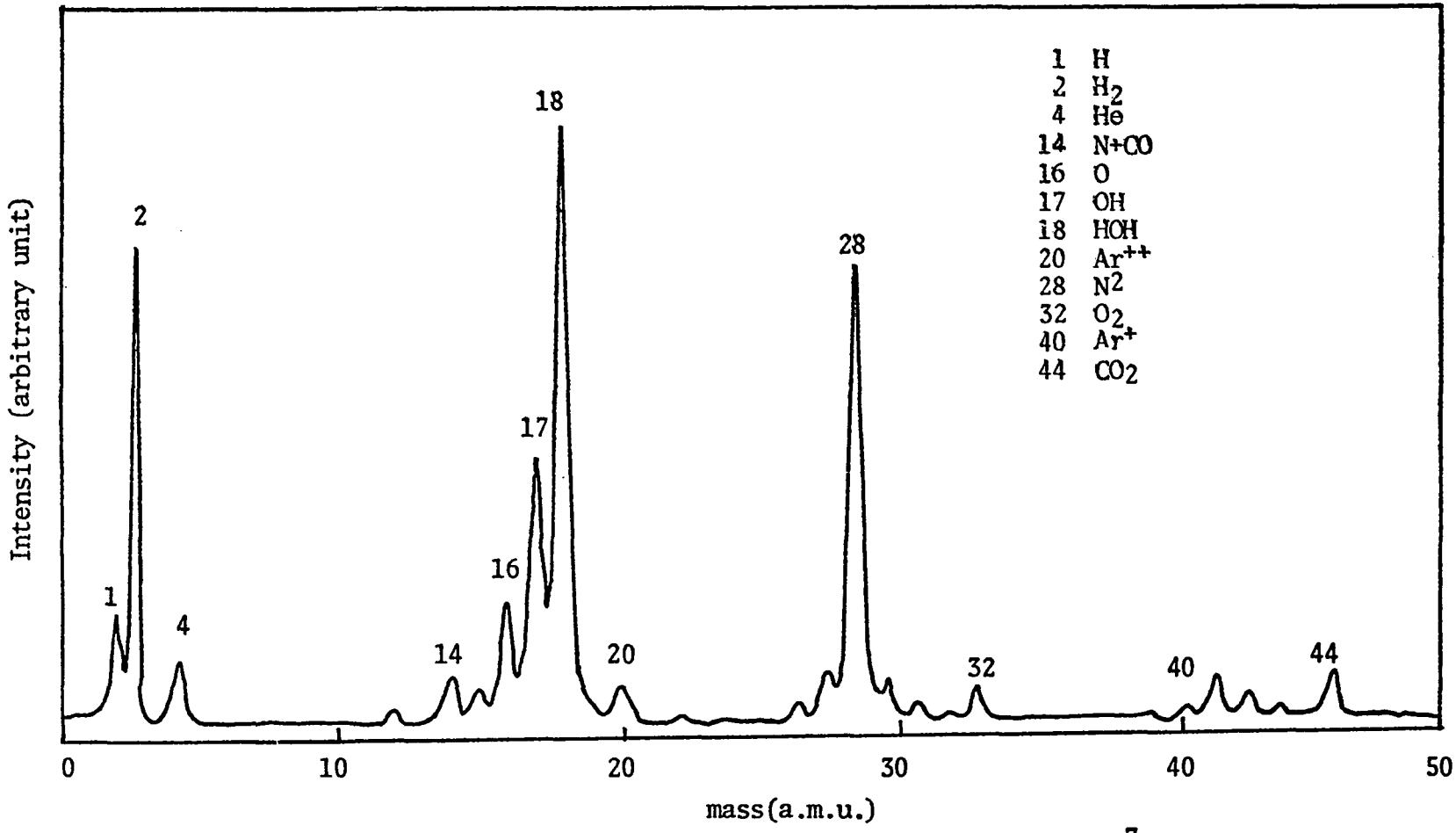

Figure 4 - 4b. Residual gases of the ultra high vacuum system at 3 x 10^{-7} torr.

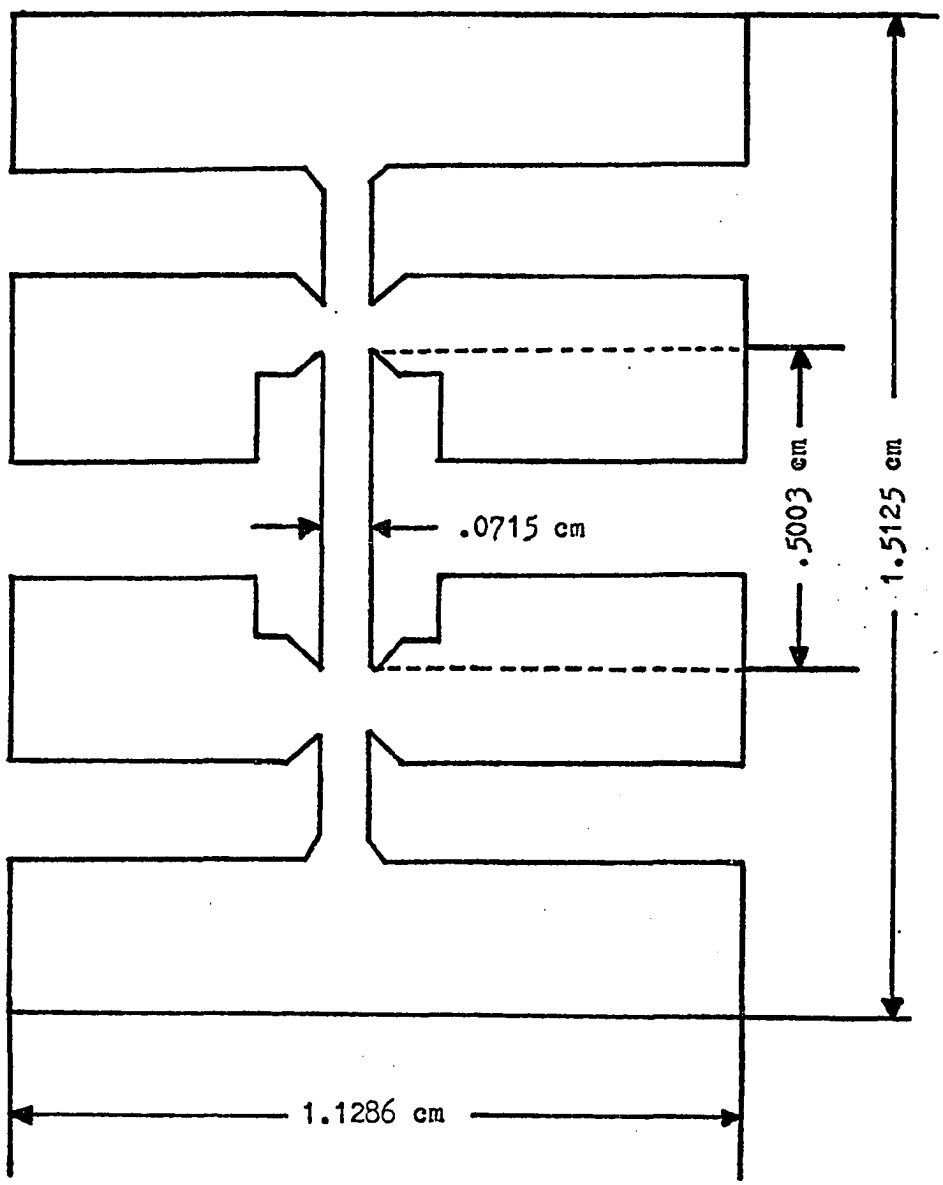

Figure 4 - 5

Thin film pattern used to make electrical measurment.

pattern is produced at the same time the film is deposited on the substrate. Also, the possibility of the film pattern being destroyed or defective is negligible. Yet another advantage is that the film is less contaminated because no chemical etching substance are involved in the process. The disadvantage of this method is difficulty in producing a mechanically precise mask which must meet critical mechanical tolerances. The film edge precision obtained depends on mask and substrate flatness. The mask with more open structure is less likely to remain flat in use. Sputtering imposes another requirement on the mask and substrate flatness. The mask with more open structure is less likely to remain flat in use. Sputtering imposes another requirement on the mask since the mask is bombarded by atoms from the target and tends to warp. This warping effect occurs even with cool sputtering because the effect is not entirely thermal.

Although a thick mask can avoid these problems, it yields a less sharp edge definition. Thus in either extreme of the thickness of the mask problems will arise. The only way to avoid them would perhaps be to have a precision sputtering mask manufactured.

The other method of generating the necessary pattern is photoetching. After the film is deposited on the substrate, it is coated uniformly by photoresist, and then exposed to the image of a mask under ultraviolet light in a contact printing

procedure. The desired film pattern is obtained by etching away those parts of the film which were exposed to the light. One advantage of this method is that complex pattern can be produced rather easily and economically by a relatively simple photographic technique. Also the definition of the film edge is good, which prevents "the edge effect" in the superconducting measurement. The disadvantage is that this process is time-consuming and has a high probability of film destruction. Also contamination of the film may result from exposure to the chemical etchants. In comparing the two methods, the former was preferable in this experiment; however, the cost of manufacturing a mechanical mask was beyond the budget of this experiment, so the latter method was chosen.

Ionization Gauge Calibration

In order to reproduce films repetitively, the calibration of sputtering gas pressure is necessary. For any particular temperature, the vapor pressure of the gases is known. By a choice of gas and temperature, the vapor pressure in the UHV system can be selected. Thereby, any gas, if it is of the correct magnitude, can be used to calibrate a millitor ionization gauge, or other ionization gauges. Usually nitrogen gas is used as a reference to calibrate ionization gauges. Because of different ionization cross section or different ionization

probabilities of different gases, corrections must be made for each gas. The nitrogen equivalent pressure can then be calculated by multiplying the vapor pressure of the gas by the ratio of its ionization cross section (or ionization probability).

$$\text{pressure(equivalent to } N_2) = \frac{P(N_2)}{P(\text{gas})} \text{ pressure(gas)} \qquad \text{(A)}$$

For example, xenon gas is selected to calibrate a millitorr ionization gauge. The UHV system for this calibration is shown schematically in Figure 4-6. While this is a specific arrangement, any components will work. The sorption pump could be replaced by a mechanical pump or diffusion pump, the ionization gauge by a thermocouple gauge, and so forth. The UHV system is evacuated to a pressure less than 1×10^{-8} torr, the xenon reservoir is chilled with liquid nitrogen, and the gate valve to the ion pump is closed. Then, the titanium sublimation pump is activated and the valve to the xenon reservoir is opened. The pressure in the UHV system is monitored with the ionization gauge until equilibrium is reached. Using equation (A) the ionization gauge should read 6.64×10^{-3} torr since the vapor pressure of xenon at 77.2 K (the temperature of liquid nitrogen) is 2.45×10^{-3} torr and $P(N_2)$ and $P(X_e)$ are 1.0 and 0.37 respectively. If the ionization gauge does not show this value, the emission

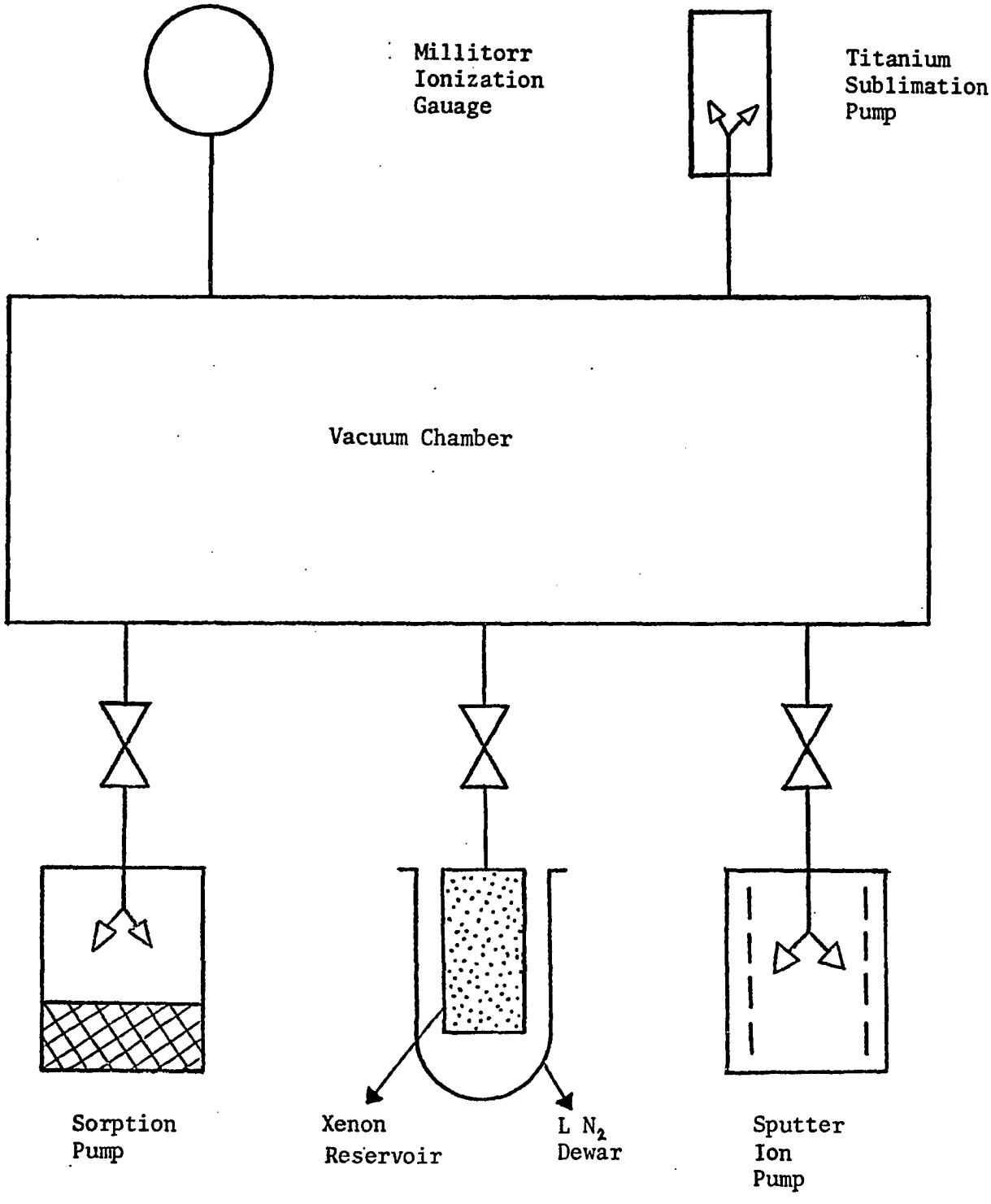

Figure 4 - 6

Vacuum System used in the calbration of Millitorr Ionization Gauge

current should be adjusted until the correct value is shown. Using this process the millitorr ionization gauge is calibrated.

Photoetching of Thin Film Patterns

Various photoresists are necessary to the process of photoetching. There is a great deal of flexibility in the choice of an appropriate photoresistive compound. Photoresists are film-forming materials which undergo marked change in solubility under the influence of ultraviolet light. Two types of photoresists exist, negative and positive resist systems, differentiated by the nature of their photochemical change in solubility. Negative photoresists, on exposure to ultraviolet light, undergo cross-linking reactions which decrease their solubility in certain solvent systems. Positive photoresists undergo photochemical decomposition reactions which affect their dipole moments, and increase their solubility in aqueous solvent systems. The photoresist used in this experiment was a negative photoresist.

There are two distinct families of Kodak resists within the negative photoresist classification. These are the cross-linkage poly-vinyl cinnamate resins specifically KPR, KPR-3 and KOR, and the poly-isoprene plus the diazido cross-linking agent systems KMER and KTFR. KMER was chosen because of its readily available documentation concerning extensive application research.

Contact Production

Attaching electrical leads to the film in order to make superconducting measurements posed a difficult problem, especially in the case of niobium. This difficulty was solved by sputter depositing copper through a mask onto the niobium film. This gave a bond with excellent adhesion, good wetability, and made a good contact. The lead film electrical contacts were produced rather easily by heating the sample on a hot plate and using a low wattage soldering gun to connect a copper wire to the film.

Cryogenic Apparatus

The equipment needed for the required measurements of thin film superconductors is relatively simple. It may be classified in two ways, cryogenics and electronics. The cryogenic apparatus consists of a set of insulated Pyrex dewars, mounted to a brass header, into which a non-magnetic stainless steel sample holder is inserted. The dewars and header assembly are installed in a movable cart which also houses the manometer, a 5 KW magnet of Magnion Inc., a fluorescent light used to examine the liquid helium level, a gaussmeter and a vacuum pump. The sample holder is actually made of a copper tail attached to a long stainless tube for thermal resistance to the outside environment. A brass block, to which the four samples are affixed, is mounted to the copper tail which extends into the liquid helium. This block

provides the heat conductance and a small thermal inertia, which guarantees that all four samples mounted to the block are at the same temperature. A Cryo-Resistor (a germanium thermometer) from Cryo Cal, Inc. is inserted into the block to measure sample temperature. The electronics instruments consist of the following components:

AM1 - Cohu, Electronic Galvanometer, Model 204 A.R.

AM2 - Cohu, Electronic Galvanometer, Model 204 A.R.

VM1 - Hewlett-Packard D.C. Micro-Volt-Ammeter 425 A.R.

VM2 - Hewlett-Packard D.C. Micro-Volt-Ammeter 425 A.R.

PS1 - Hewlett-Packard-Harrison 6433 B Power Supply

PS2 - Heathkit Low Voltage Power Supply, Model 1P-27

PS3 - Heathkit Low Voltage Power Supply, Model 1P-18

PS4 - Magnion 5 KW Magnet Power Supply, HS-1050B

SG1 - Hewlett-Packard, Low-frequency Function Generator, Model 202A

GM - RFL Industries Gaussmeter, Model 750

REC - Hewlett-Packard, Moseley Autograf, X-Y recorder, Model S6

Figure 4-7 is a block diagram of the experimental arrangement of this equipment which functions as follows.

AM2, VM2 and PS2 are used to measure the resistance of a resistor placed within the brass block holding the samples which indicates the block temperature. AM1, VM1 and PS1 are used to measure the sample resistance. PS3 delivers power to the brass block heating coil, while PS4

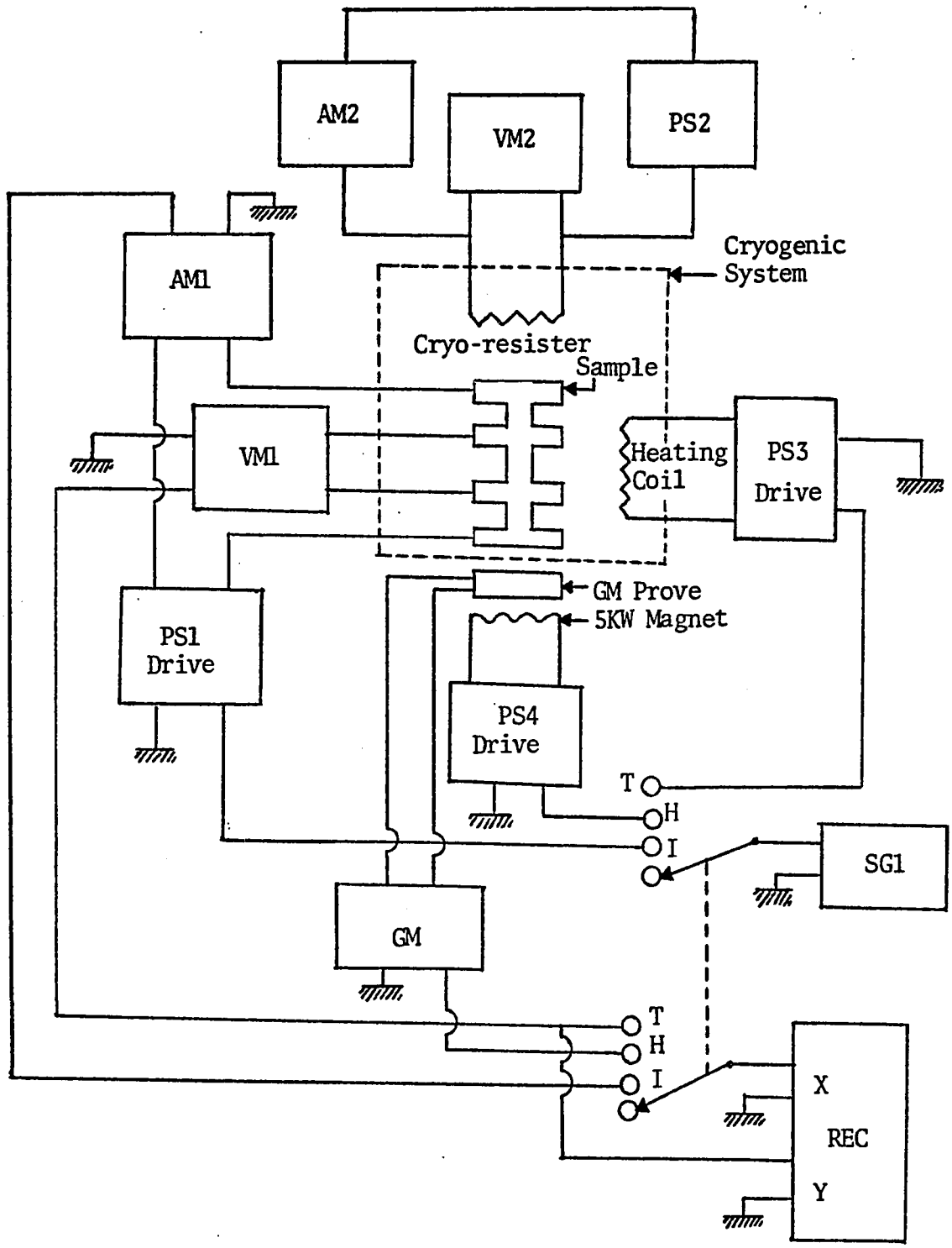

Figure 4 - 7

A block diagram of the experimental arrangement of the cryogenic apparatus.

drives the magnet whose field is measured by GM. The magnet has a maximum field of 6 kilogauss at a pole gap of 3". SG1 is used to sweep the outputs of PS1, PS3 and PS4 to generate critical current, critical temperature, and critical magnetic field curve, respectively. The period of the sweep can be adjusted to a maximum of 130 seconds, while the change in the variable swept over the period can be made as small as desired. The output of VM1 (as a measure of sample resistance) is the Y input of REC. Am1, VM1 and GM can be fed to the X input to produce critical current, critical temperature, and critical magnetic field curves, respectively. To facilitate measurements, a control panel was constructed which contains the following: a sample selection switch which connects six leads from any one of four samples (or the cryoresistor) to be connected to the sample resistance measuring network; a test selection switch, while simultaneously connects the sweep (SG1) and the inputs of REC for various measurements; a sample current reversing and null switch which also lifts the recorder (REC) pen when in the null position; sweep controls, line voltage monitoring meter; recorder quadrant selector; a 0-1 volt output for remote monitoring of any one of significant system parameters.

Cryogenic Measurement

Four samples are mounted on a block. The electrical isolation between the film contacts, and the block should be

checked before the holder is assembled into the dewar. The jacket of the inner dewar is evacuated by a mechanical pump before the liquid nitrogen is poured into the outer dewar. The inner dewar is pumped out and is filled by helium gas to eliminate any water vapor which would freeze during cooling of the dewars. Any ice present would cause heating of the liquid helium. The temperature of the inner dewar is monitored by a thermo-couple until it reaches the temperature of liquid nitrogen. This takes from six to eight hours. The liquid helium is then transferred to the inner dewar through a transfer tube. The electrical isolation of the films from the block should be checked again. If a short circuit between the film and the block is found in any sample, it is eliminated from the measurement procedure. Small diameter copper wires pass through the stainless steel and copper tube comprising the shaft of the sample holder and are attached to an instrument panel, which provides connections to the various measuring instruments. Sample heating is done through this panel as well.

Sample heating is provided by a coil of heater wire, wrapped around the copper tail just below the samples. The cryoresistor thermometer was calibrated at 45 points from 1.5"K to 40"K traceable to the National Bureau Standards, and a computer generated interpolation table was supplied for the range from 1.5°K to 20°K. The range from 20°K to 40°K was calibrated only every 2°K and an interpolation

table was not supplied for this range. To remove this deficiency, a set of tables was computer generated to cover this region in steps of 0.01°K. The magnetic field is changed by changing the current through the magnetic coil and the applied current through the sample can also be varied.

Creation of Rough Surface of Films

In order to investigate the influence of surface roughness on the superconducting properties of thin films, various degrees of roughness are required. However, because of the minute thickness of thin films, it is almost impossible to make the surface of these films rough by direct grinding or by impression of an optical grating on the film. After several different methods were attempted, it was found that depositing films on substrates which have different surface roughness is much easier than making the surface of the films rough directly. Modification of the surface texture of the substrate was very difficult because of its extreme hardness. In view of this, a commercially produced sapphire single crystal plate with a rough and a smooth side was selected for use. In order to measure the roughness of the two surfaces, the stylus technique was used.

Stylus Technique

In the stylus method, a stylus is lightly drawn across the surface of material and small changes of the

vertical movement of stylus are magnified and recorded. The stylus is a pyramidal, conical or hemispherical diamond with a flat or round tip. There are two ways for magnification of change of this vertical movement of the stylus. One way is by picking up the change in vertical movement electrically and amplifying the signal electronically. The instrument which was used was of the latter type and is called "Dektak". It is manufactured by Sloan Instruments Corporation. The Dektak stylus is hemispherical and 0.001 inch in diameter. The stylus tracking force is approximately 15 milligrams (0.00053 ounce) and can be increased for different applications. The fundamental structure of the Dektak is shown in Figure 4-8. The stylus arm with the stylus at the forward end swings on jeweled pivots and is suspended by a single coil spring used for tracking force adjustments. The sensor in the head is a differential transformer that can sense electrically the position of a core attached to the stylus arm. The whole sensing head assembly is mounted on a vertical sample and the core is centered in the transformer. The differential transformer reads the differences in elevation as the sample is moved horizontally under the stylus. These differences in elevation are displayed in visual form by the chart recorder. The differential transformer drives a precision amplifier whose gain is set by switches which consist of seven levels ranging from 1,000 to 1,000,000 Å full scale. The output of the amplifier is a

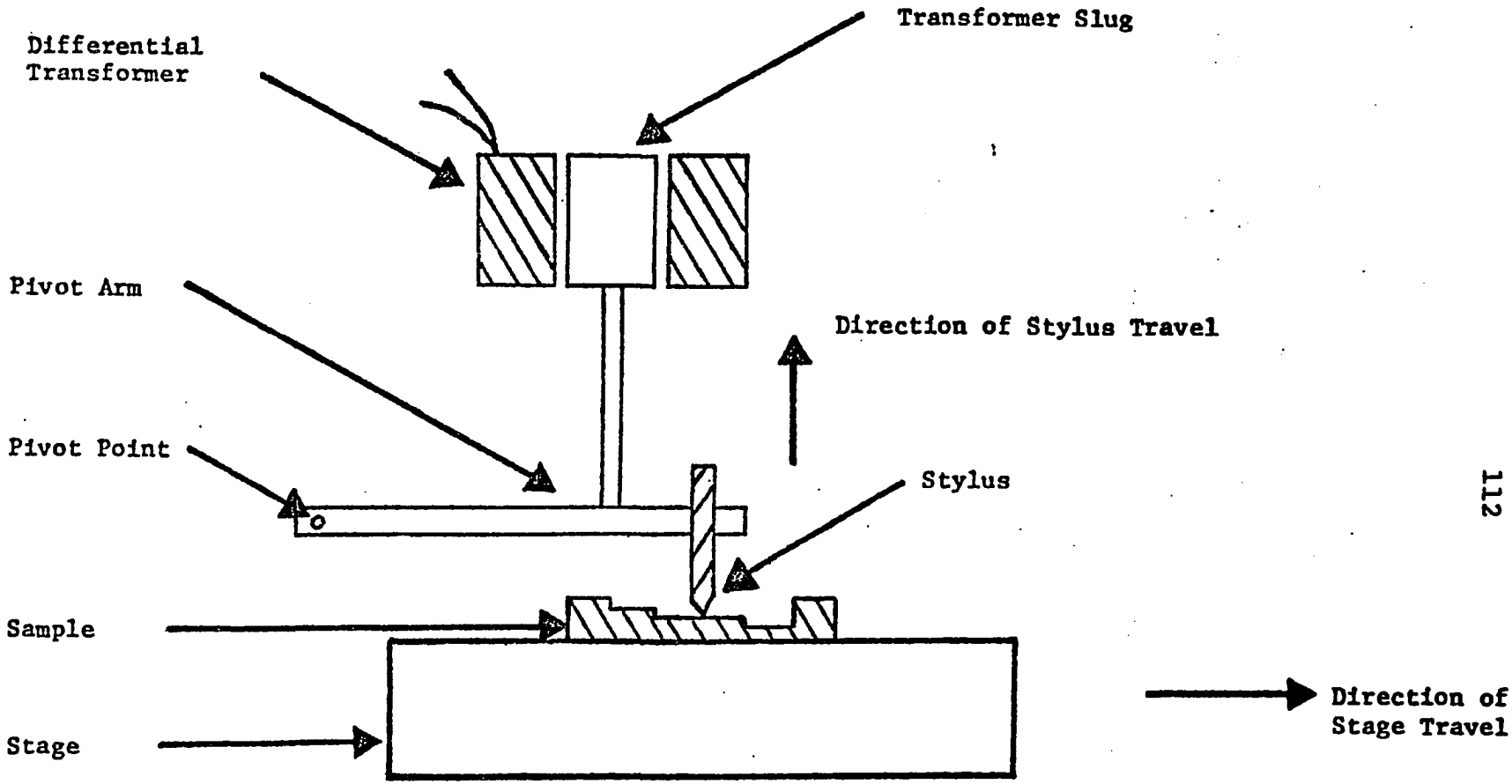

Figure 4 - 8

The fundamental structure of the Dektak stylus.

bipolar signal correlated with the position of the core in the transformer. This electrical signal may be used to drive an X-Y chart recorder or alternatively, it may be sampled and recorded by a computer in a digital format for future analysis and processing. In this experiment a PDP 8/o minicomputer was interfaced with the Dektak. The stage can be leveled manually to accomodate a sample with a surface that is not parallel to the reference plane of the measuring instrument. If the sample is not level, the recorder pen will veer off at an angle and thus indicate the need for an adjustment of the leveling thumbwheel. The drive for the horizontal stage traverse is provided by a permanent magnet D.C. motor with an integral tachometer. The speed is controlled by a servo-amplifier that compares the output of the servo-amplifier control motor power to maintain the speed within 1 percent of that selected. The profile scanning speed is regulated at 0.01, 0.1, and 1.0 centimeter (0.3937 inch) per minute. A manual override provides rapid traverse, both forward and reverse, to expedite preliminary scan, rescan and sample positioning.

A typical surface profile of a sapphire substrate is shown in Figure 4-9. Figure 4-10 is a surface profile of a lead film. A typical surface profile of photoetched film is shown in Figure 4-11.

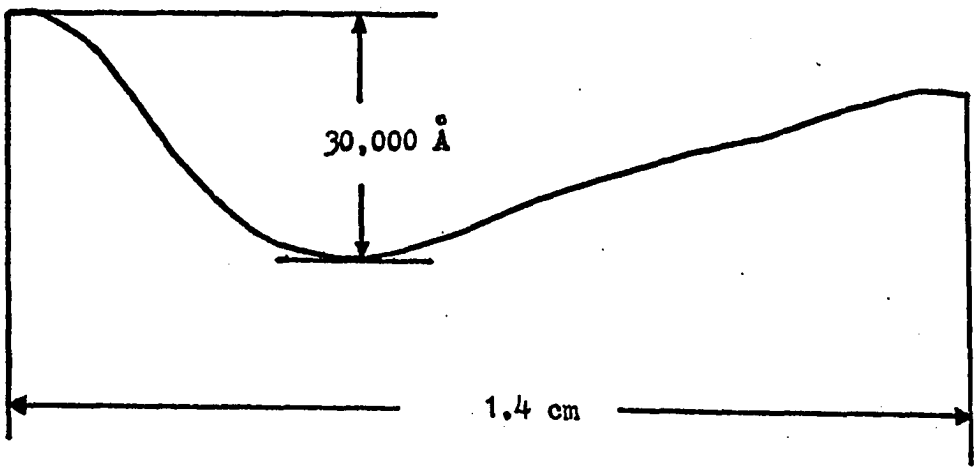

Figure 4 - 9

A typical surface profile of a sapphire substrate



Figure 4 - 11

Profile of a typical film, showing the lead, compare with Figure 4 - 6 , where this profile is just above the the label ".0715 cm".

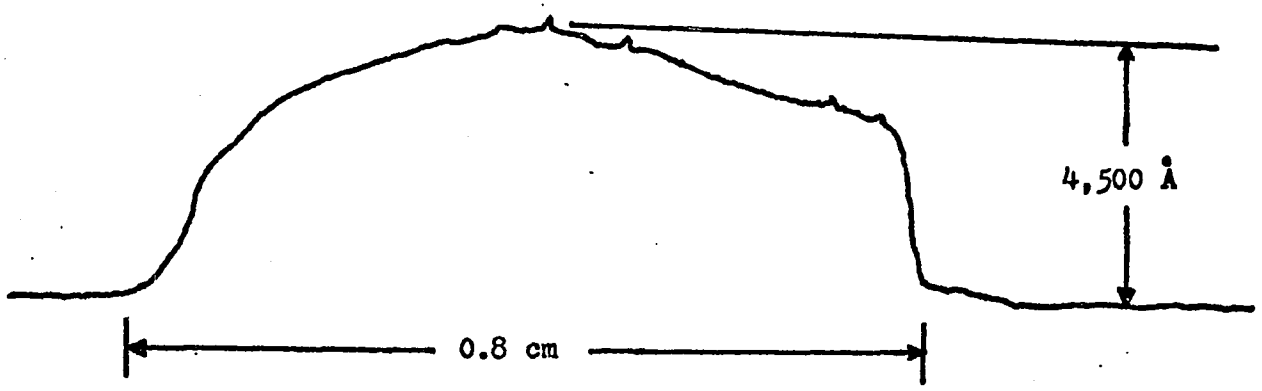

Figure 4 - 10

A typical surface profile of a lead film.

Minimum detectable step	25 Å
Rapid traverse, forward and reverse	0 to 5 cm/minute
Stylus diameter	0.001 inch
Stylus tracking force	15 mg
Scan limit stops	0 to 6 cm
Maximum sample thickness accommodated	1 inch
Manufactor	Sloan Instruments Co.
Model	Dektak

Definition of Surface Roughness

The surface profile is defined as the curve on the cross section which is perpendicular to the nominal surface of the specimen. In practice, this profile is that which is recorded by the stylus. The nominal surface is defined as the surface which includes a mean line. A mean line is such that the sum of the square of the distance between the line and the profile becomes the minimum. The roughness curve is the curve from which the waviness is eliminated from the surface profile. There are two ways to eliminate the waviness from the profile. One is mechanical: a large diameter stylus is used to measure the waviness and the roughness curves is obtained by subtracting the waviness from the surface profile. The alternative is electrical: the filter circuit is used to cut off the signal of peaks and valleys larger than certain heights or depth. The surface profile recorded by Dektak which is equipped with this filter circuit is the roughness curve itself. There are two ways to describe the roughness curve quantitatively: the arithmetic average and the root mean square. The roughness

by the arithmetic average, H_{AA} and the roughness by the root mean square, H_{RMS} are defined by the following formulae:

$$H_{AA} = \frac{1}{L} \int_0^L |y - h| dx$$

$$H_{RMS} = [\frac{1}{L} \int_0^L (y - h)^2 dx]^{1/2}$$

where L is the length, measured along the nominal surface, over which average is taken, and y is the vertical displacement and h is the position of the nominal surface (i.e., a mean line). Both of these equations can be solved graphically by dividing the profile into n increments, measuring discrete values y for each increment and performing the following summations:

$$H_{AA} = \frac{1}{n} \sum_{i=1}^{n} |y_i - h|$$

$$H_{RMS} = [\frac{1}{n} \sum_{i=1}^{n} (y_i - h)^2]^{1/2}$$

A histogram of $y_i - h$ versus frequency for the smooth side of the sapphire single crystal plate is shown in Figure 4-12. This histogram can be approximated by a Gaussian distribution. Then, H_{AA} and H_{RMS} can be considered as the mean deviation and standard deviation respectively.

Profile Resolution

The influence of the stylus diameter on profile resolution was considered. The stylus can not follow very

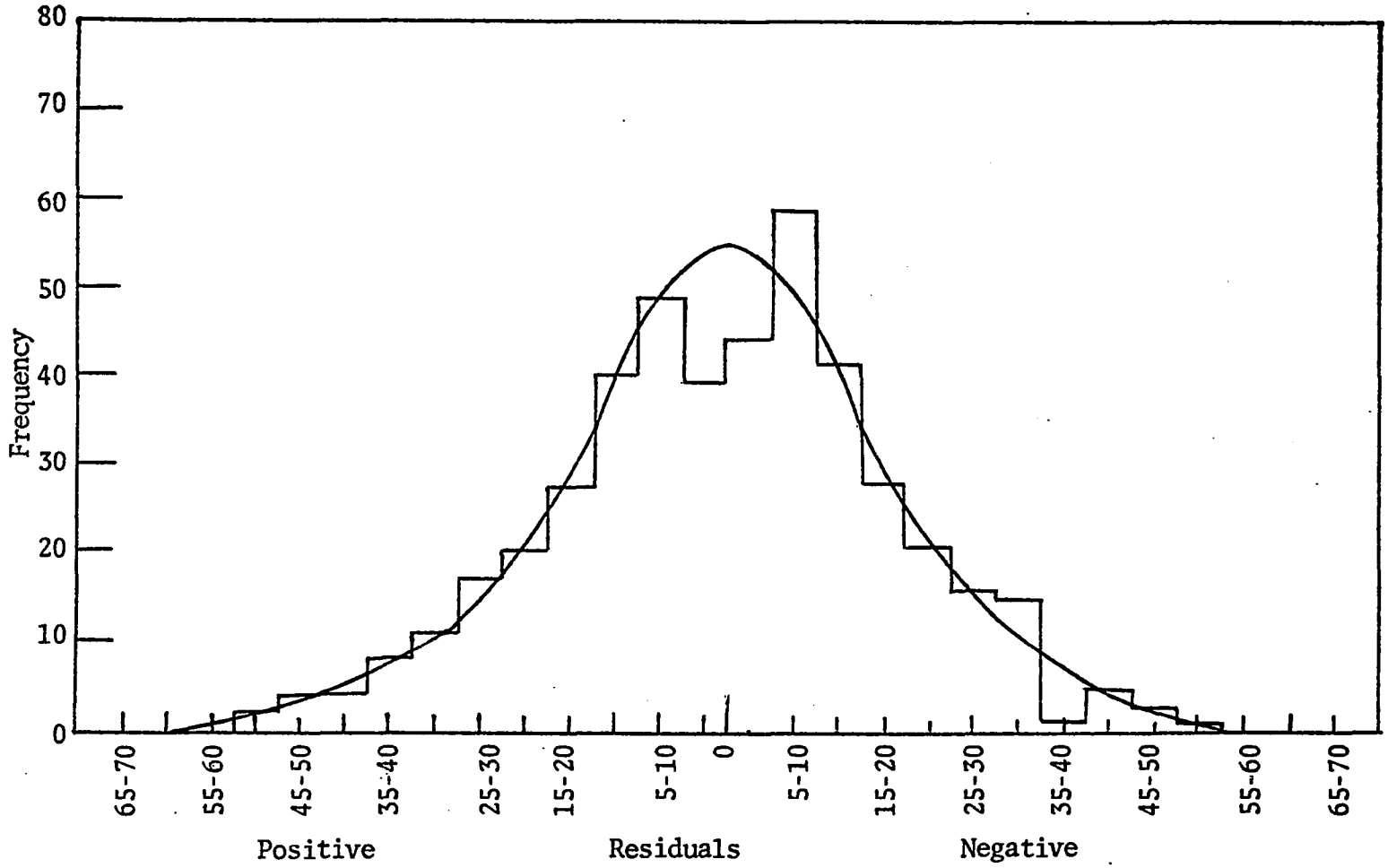

Figure 4 - 12

A histogram of y_i - h versus frequency for the smooth side of the sapphire single crystal plate.

narrow cracks and grooves to the bottom due to the stylus diameter. If the surface is simplified with triangle valleys and peak as shown in Figure 4-13, the profile of the bottom of a valley is sharp and the top of a peak is round with the same diameter as that of the stylus. The distance b between the bottom of valley and the center of spherical part of the stylus is an error caused by the size of diameter of the stylus. If the stylus diameter is d and the angle of the valley is 2θ, b is given by

$$b = \frac{d}{2} (\text{cosec } \theta - 1)$$

For instance, if the stylus diameter is 20 μ and 2θ is 150°, b becomes .35 μ. If the error is to be 1 percent, the minimum roughness that can be measured is 35 μ. To find the horizontal resolution, a 1000A step shown in Figure 4-14(a) was considered. The stylus climbs the step over a distance of 1.6 microns. Although the distance appears quite long at the magnification of 20,000X as in Figure 4-14(b), it is actually insignificant in a typical Dektak chart where the vertical magnification is much higher than the horizontal (See Figure 4-14(c)). At a horizontal magnification of 1,000X, the broadening of the step increases as the step height increases as in Figure 4-15. Hence, the 0.001 inch diameter stylus is well suited for making routine thickness measurements when definitive horizontal resolution is unimportant.

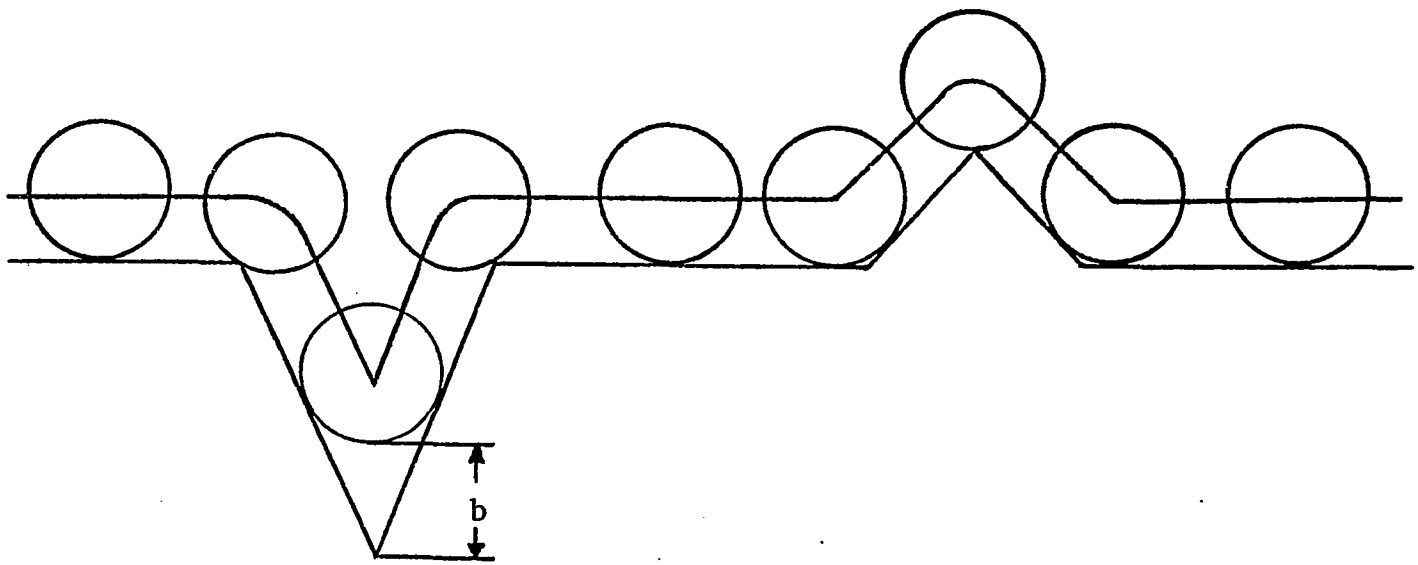

Figure 4 - 13

The surface simplified with triangle valleys and peaks, and the profile of the surface with the stylus as the round circle.

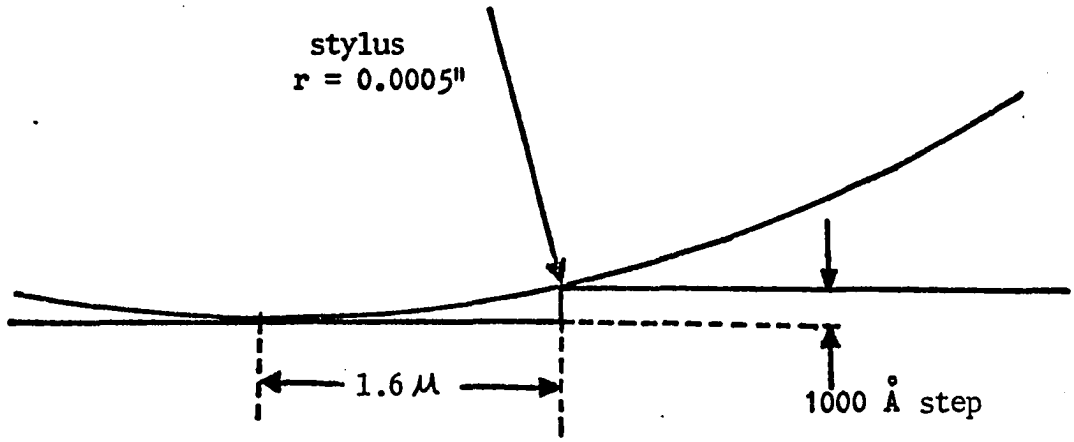

Figure 4 - 14 (a)

The stylus clims over a distance of 1.6 microns.

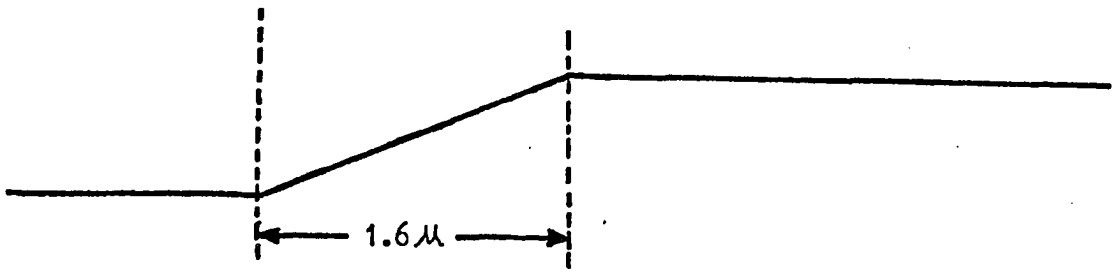

Figure 4 - 14 (b)

The distance of 1.6 microns at the magnification of 20,000X.

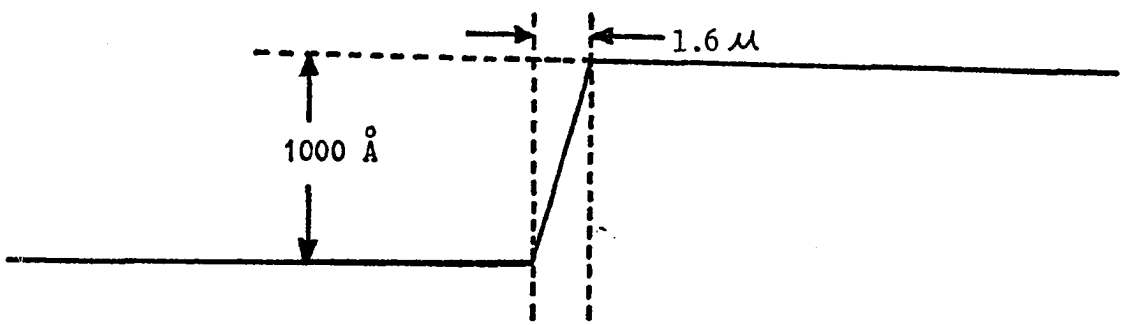

Figure 4 - 14 (c)

The vertical magnification is much higher than the horizontal.

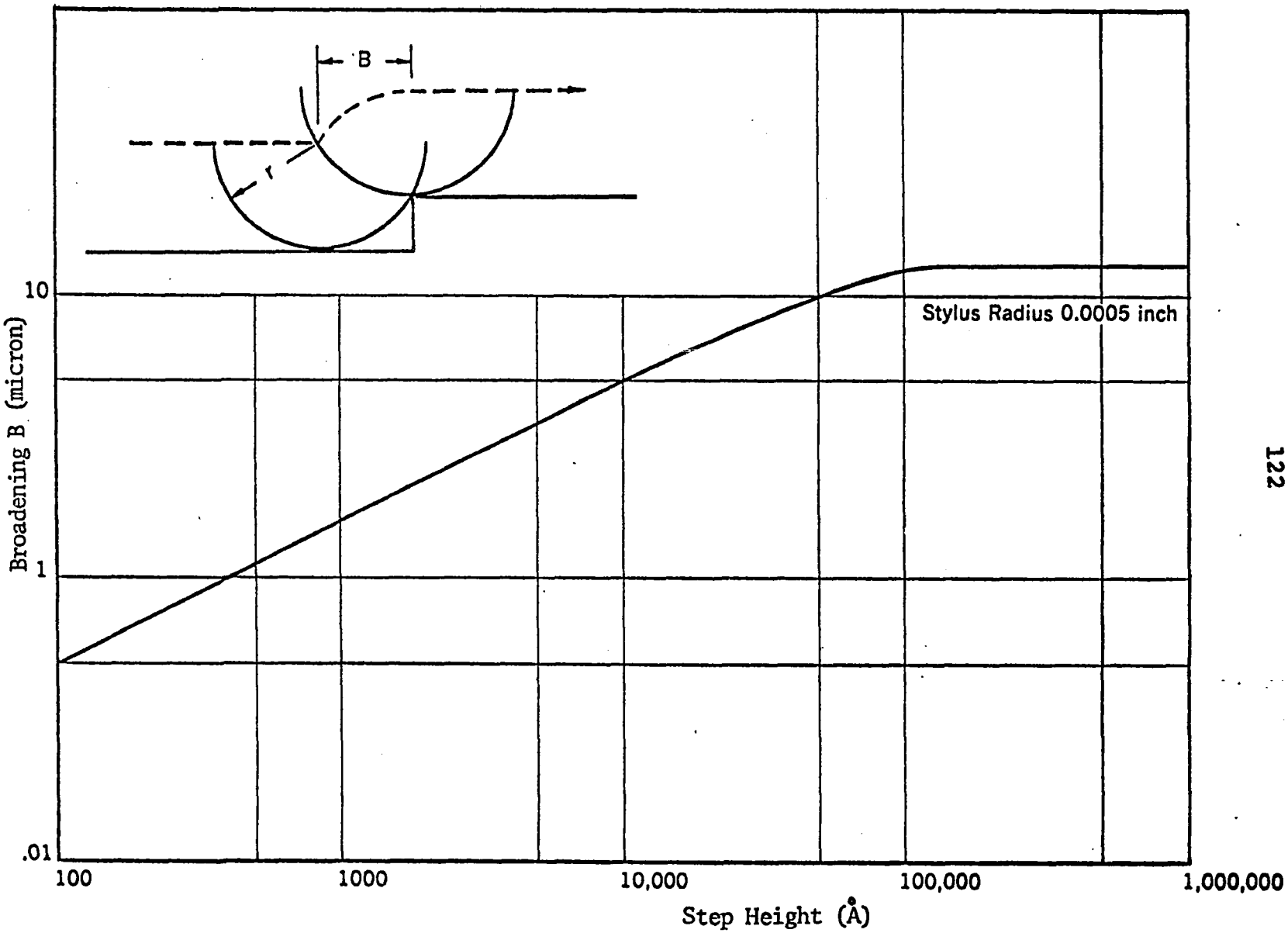

Figure 4 - 15 The broadening of the step of the profile of the surface by the horizontal magnification.

CHAPTER V

RESULTS AND DISCUSSION

A. Measurement of Critical Field and Temperature

To measure the transition, the resistance versus temperature curve at a constant magnetic field is used. The error of magnetic field measurement is 1%. The critical temperature at the transition, T_c, is defined by extrapolating the linear part of the resistance versus temperature curve back to zero resistance. (See Figure 5-1. T_c is nearly the same as the temperature where resistance is first observed in the film.) Because the transition occurs gradually as the field increases, it is not practical to adopt the conventional method that T_c is defined as $1/2(T_2 - T_1)$ where T_1 and T_2 are respectively the nominal temperature for the onset and completion of the transition. When a constant magnetic field is high, the transition curve is in the form of a hysteresis loop. In this case, T_c is defined by extrapolating the linear part of the rising

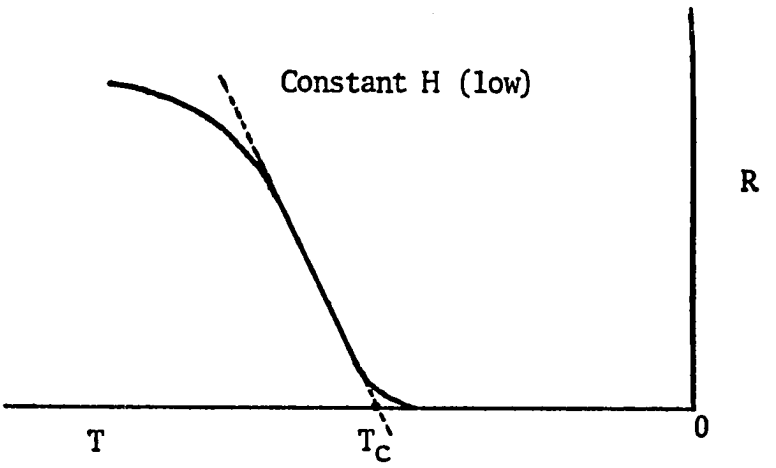

Figure 5 - 1. The definition of T_c for low H.

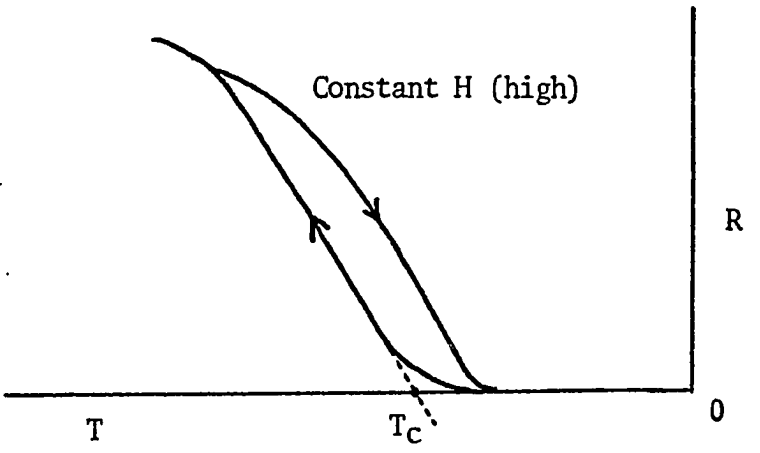

Figur 5 - 2. The definition of

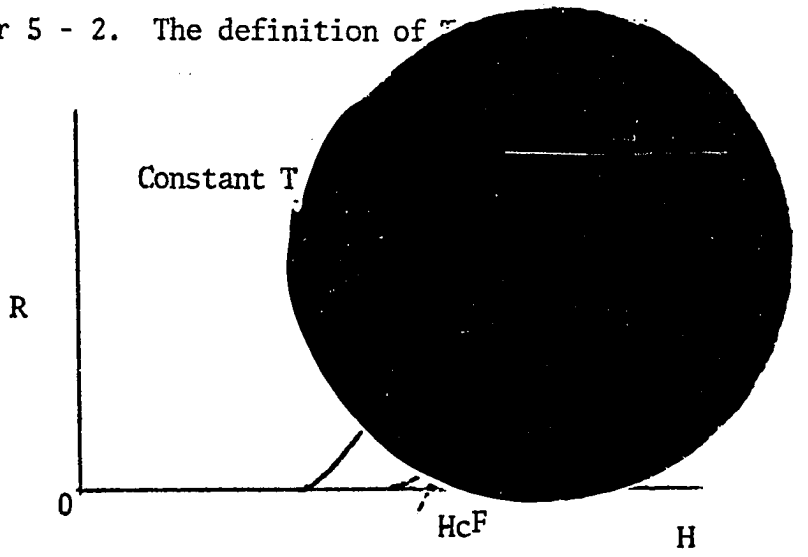

Figure 5 - 3. The definition of H_{cF}.

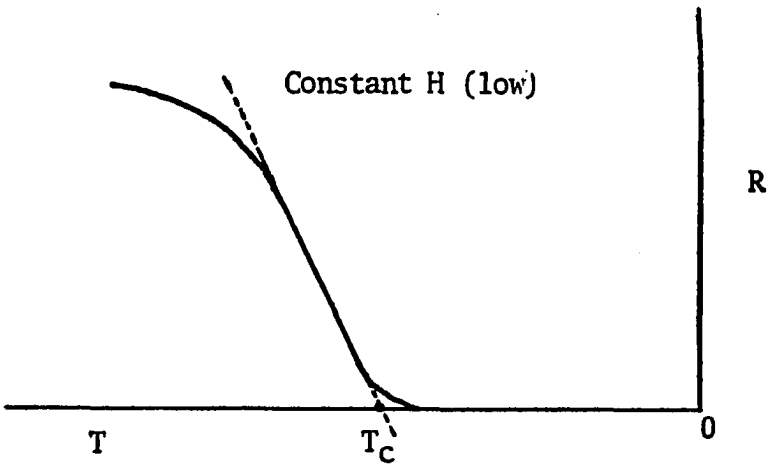

Figure 5 - 1. The definition of T_c for low H.

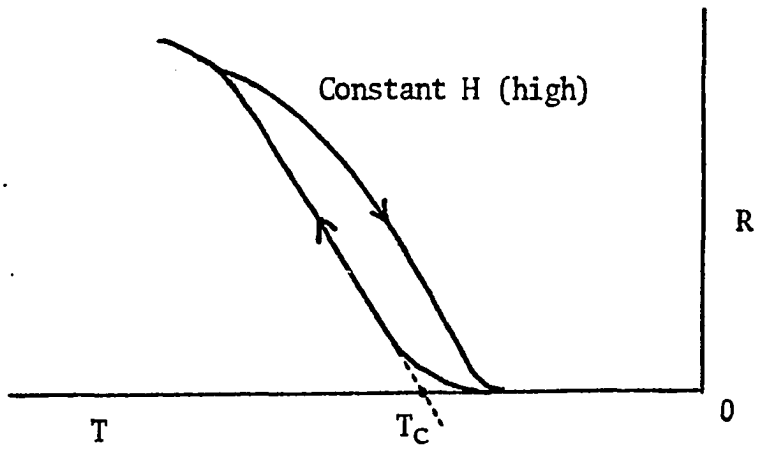

Figur 5 - 2. The definition of T_c for high H.

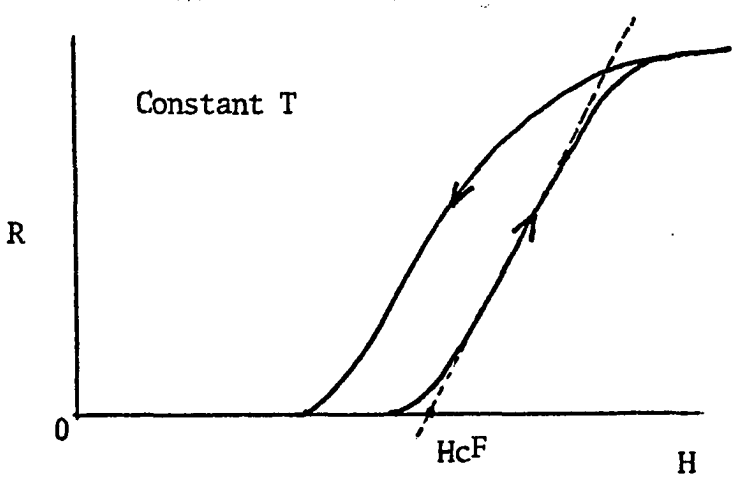

Figure 5 - 3. The definition of H_{cF}.

transition curve is in the form of a hysteresis loop. In this case, T_c is defined by extrapolating the linear part of the rising transition line of the loop (See Figure 5-2). The resistance versus magnetic field curve at a constant temperature was also attempted. It produced an unstable transition with a hysteresis loop. Only specimen R6 showed a reasonable result in this curve. ("S" or "R" attached in front of sample numbers means that a film is deposited on the smooth side or the rough side of a substrate, respectively.) The critical magnetic field H_{cF} of this curve is defined by extrapolating the linear part of the rising transition line (See Figure 5-3).

B. Critical Thickness, d_c

The thickness range of films used was from 300Å to 6000Å. According to the Ginaburg-Landau theory, the critical thickness d_c is given as $\sqrt{5}\,\lambda$. Substituting d_c in the equation for thick film approximation, Equation (26) gives the upper limit of critical magnetic field, $1.45H_c(0)$ where $H_c(0)$ is the critical field of bulk specimen at $T = 0$. Substituting d_c in the equation for thin film approximation, Equation (27) gives the lwer limit of the critical magnetic field, $2.2H_c(0)$. This means that neither Equation (26) nor Equation (27) can apply to films with intermediate thickness. Films are deposited on smooth or rough surfaces of a substrate. Data for sample S5, S6, R6, S7, and S8 is

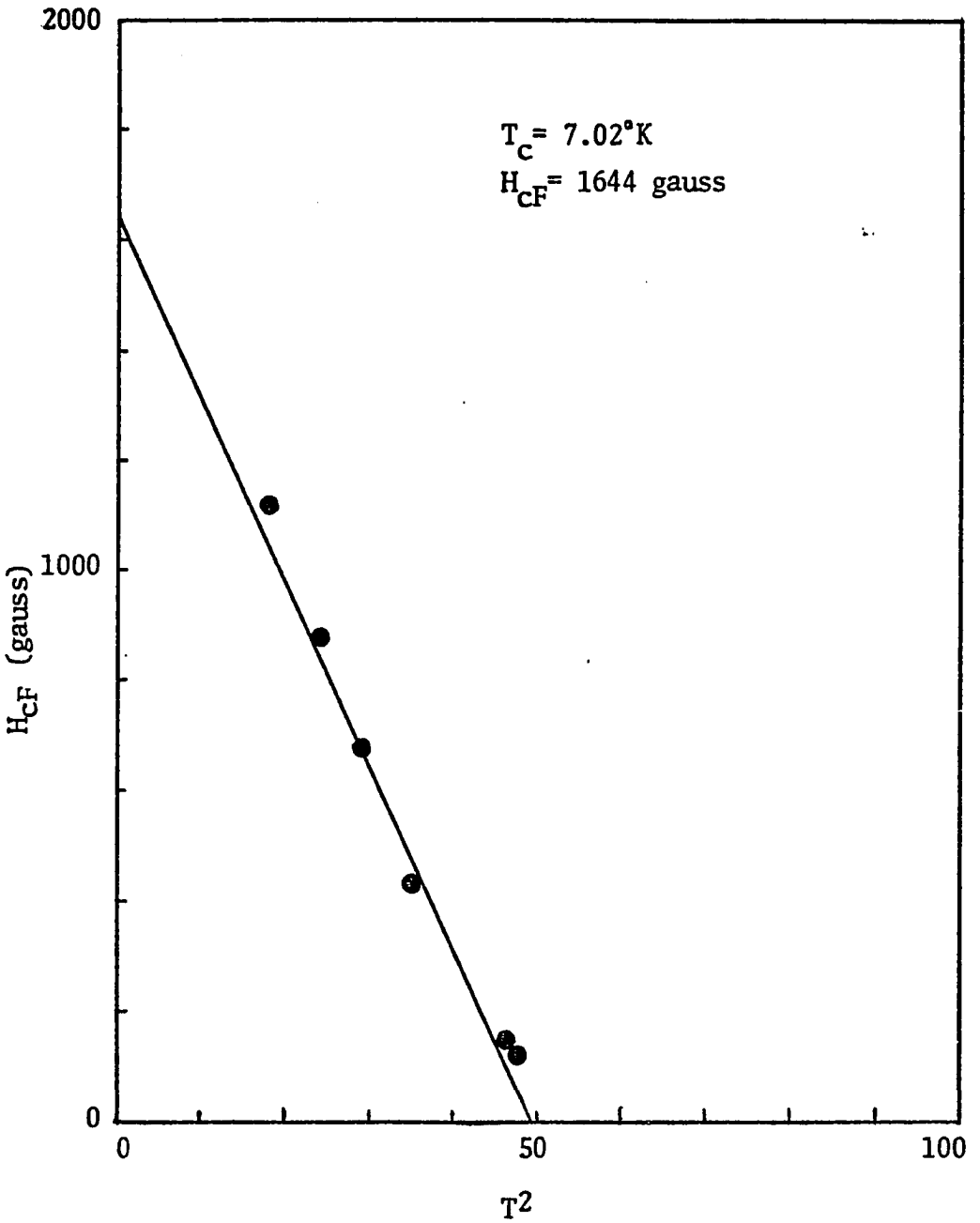

Figure 5 - 4(a) H versus T^2 for the lead film roughened by sand paper of #180.

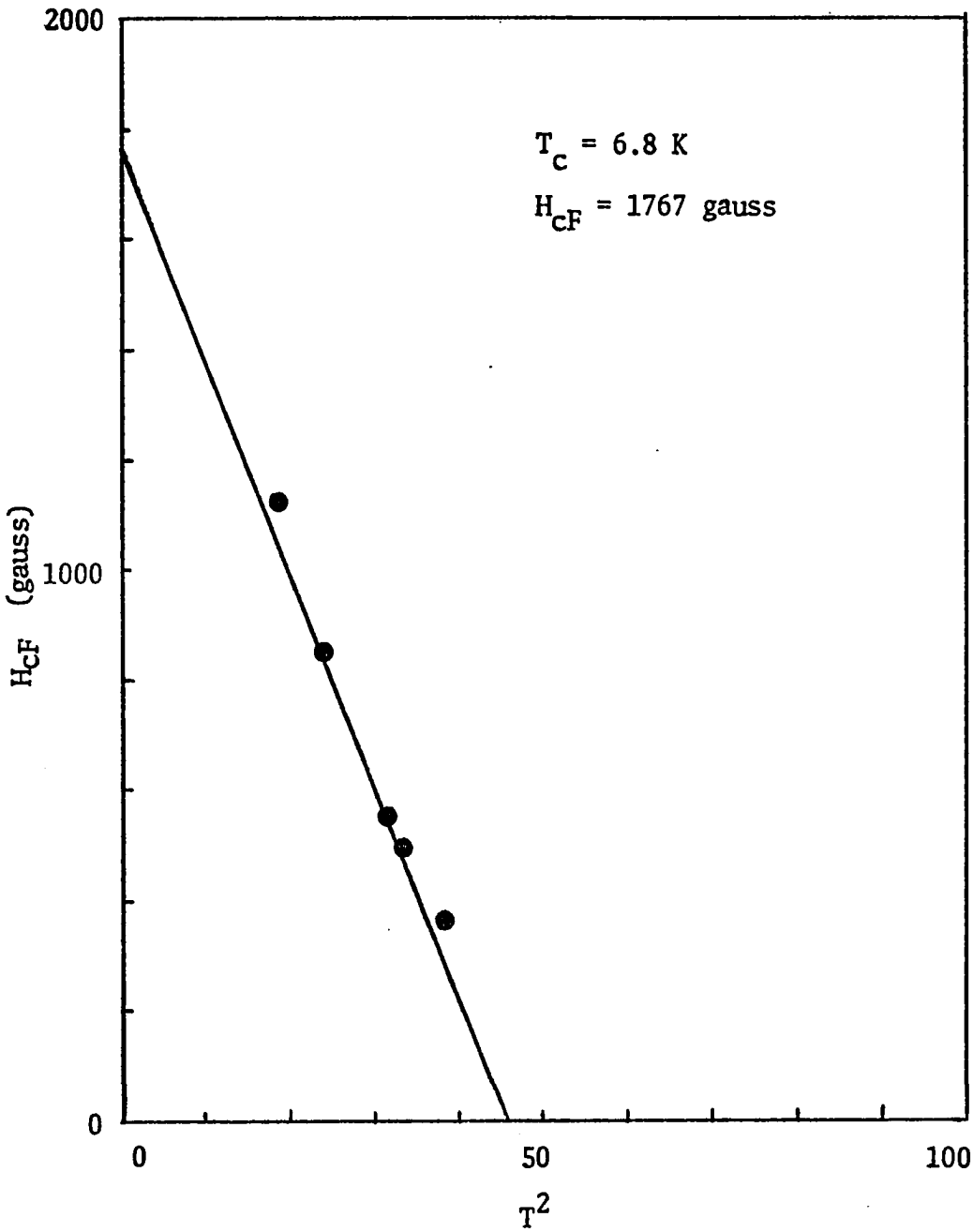

Figure 5 - 4(b) H versus T^2 for the lead film roughened by #320 sand paper.

PLEASE NOTE:

This page not included in material received from the Graduate School. Filmed as received.

UNIVERSITY MICROFILMS

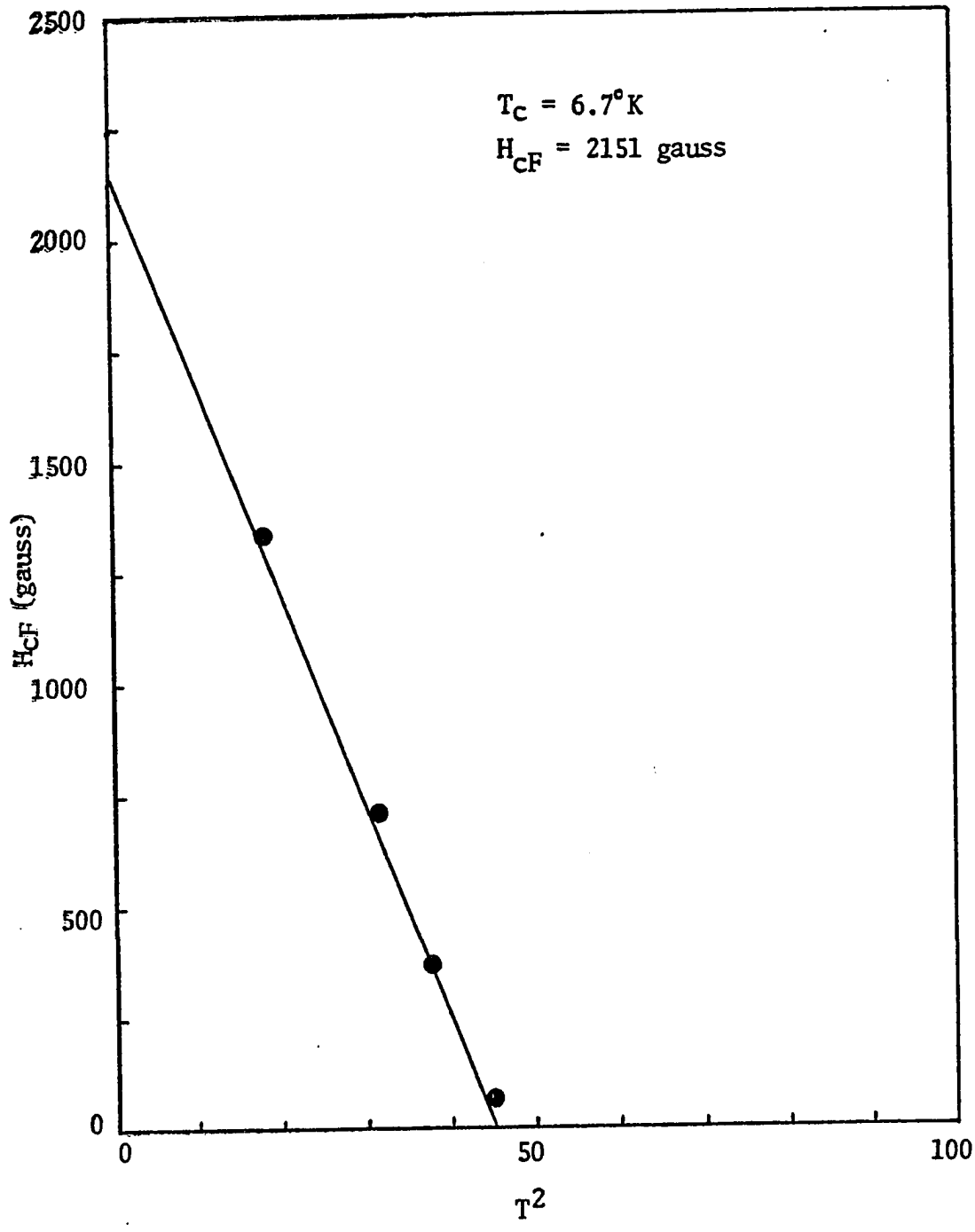

Figure 5 - 4(c) H versus T^2 for the lead film roughened vertically.

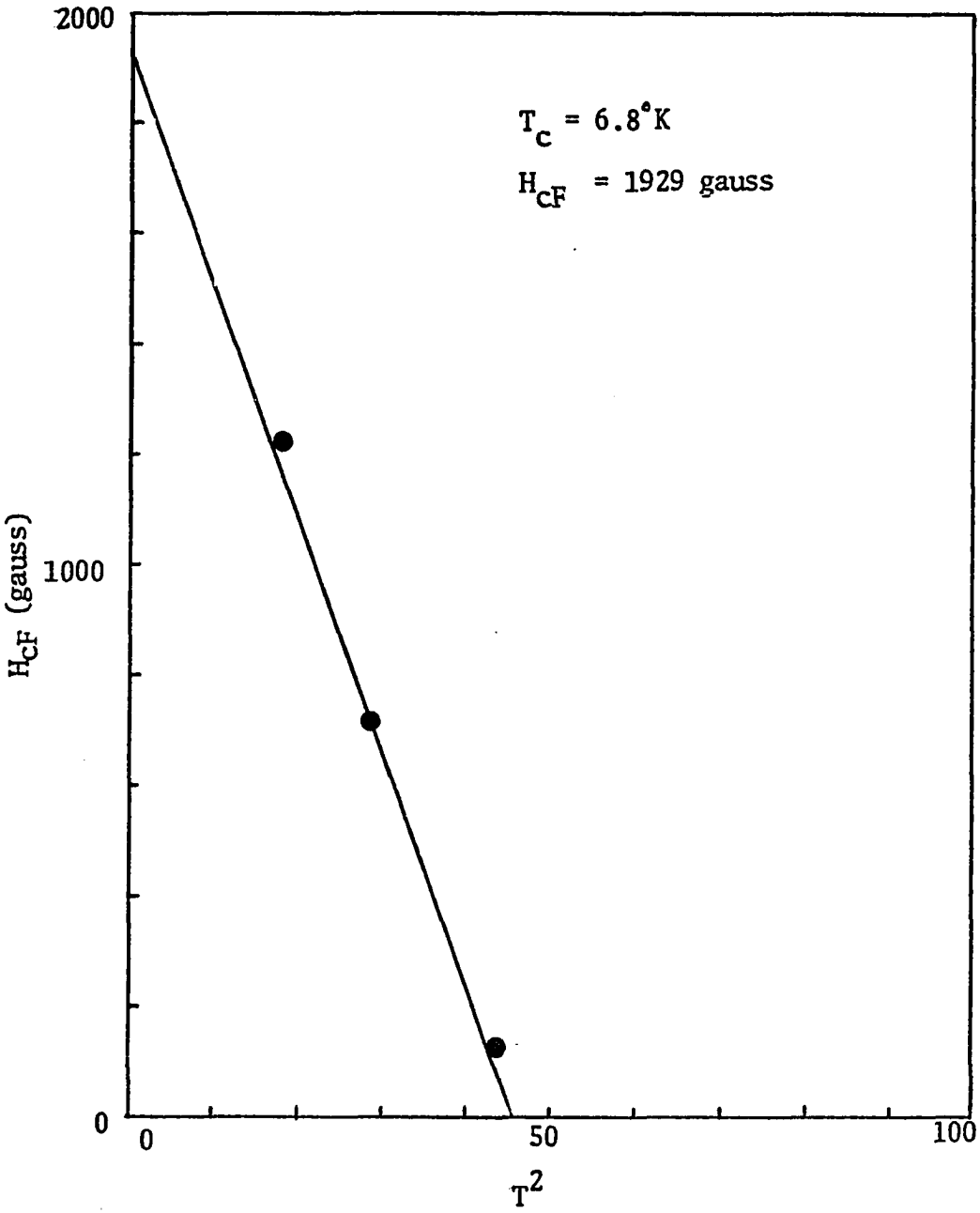

Figure 5 - 4(d) H versus T^2 for the film roughened horizontally.

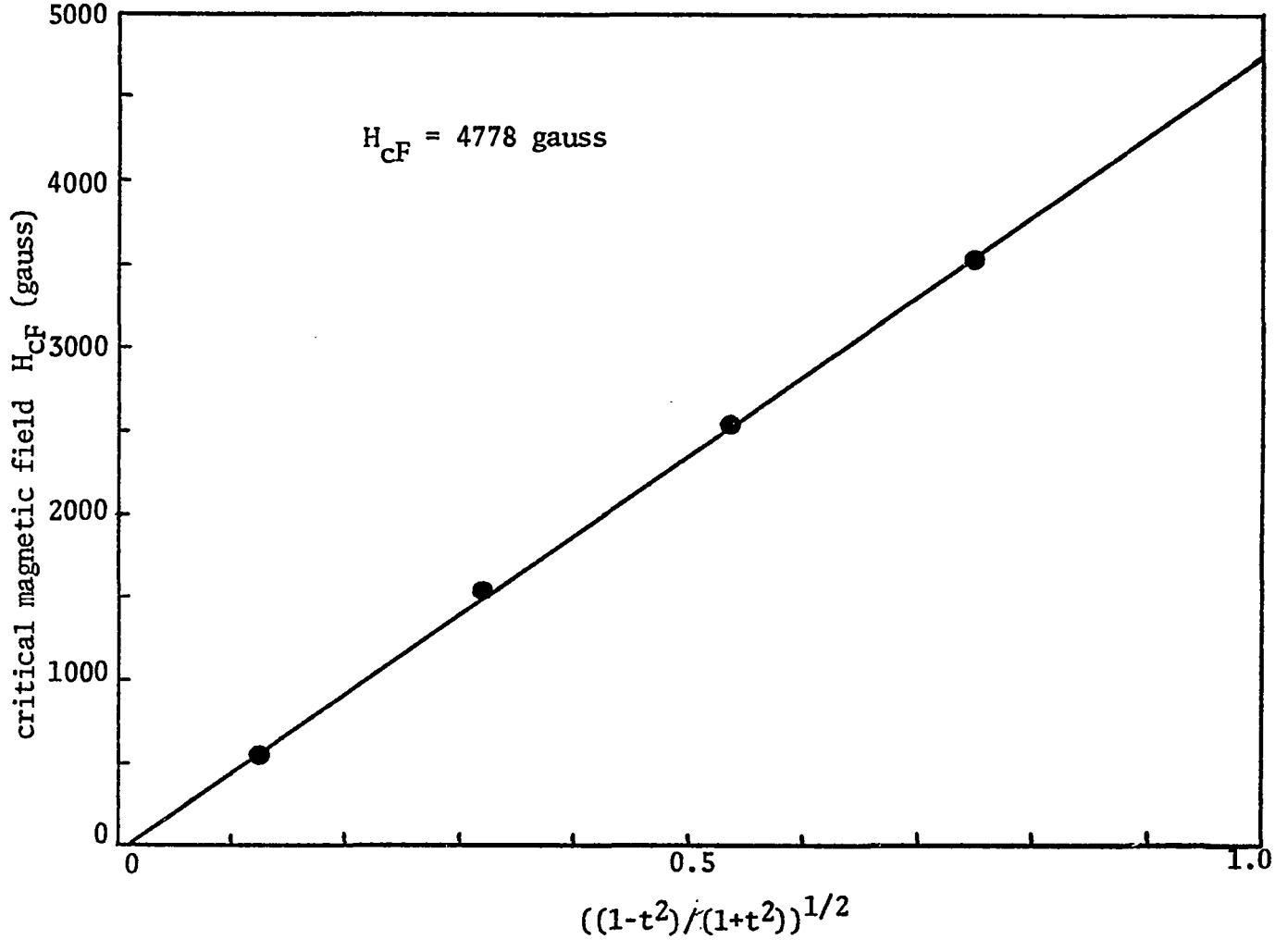

Figure 5 - 5. Data for sample S1 is plotted by Eq.(27) of the thin film approximation.

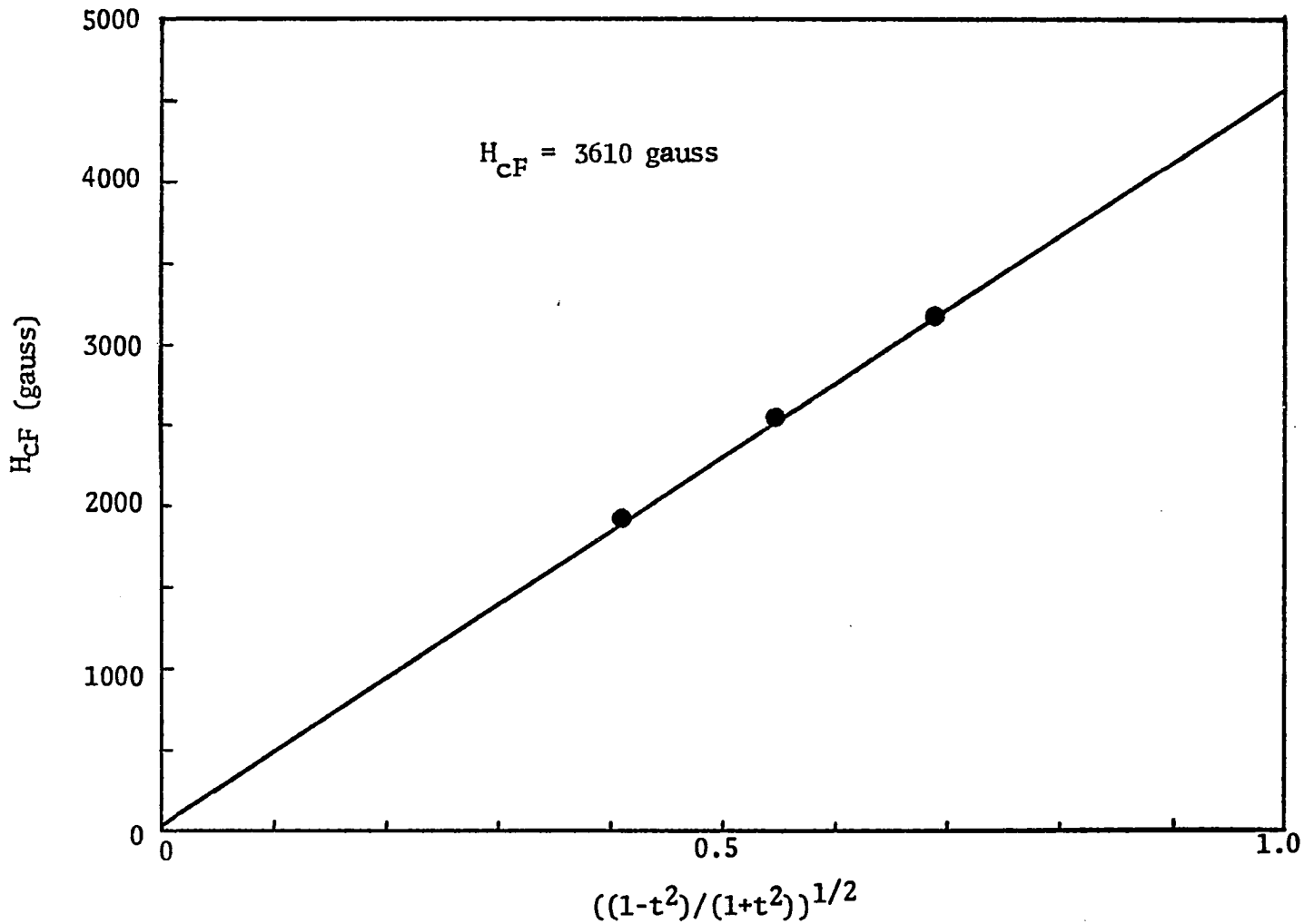

Figure 5 - 6. Data for sample R1 is plotted by Eq.(27) of the thin film approximation.

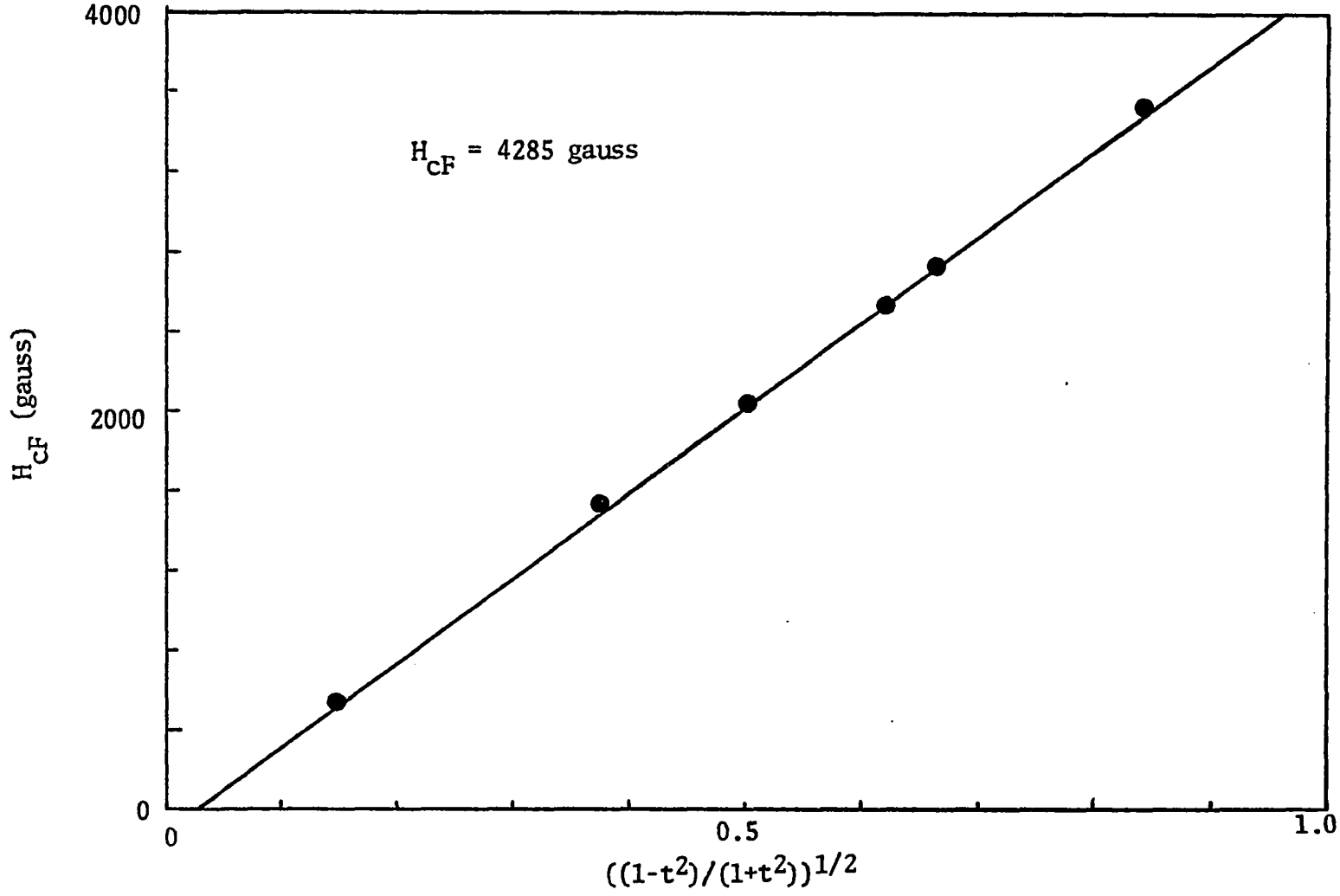

Figure 5 - 7. Data for sample S2 is plotted by Eq.(27) of the thin film approximation.

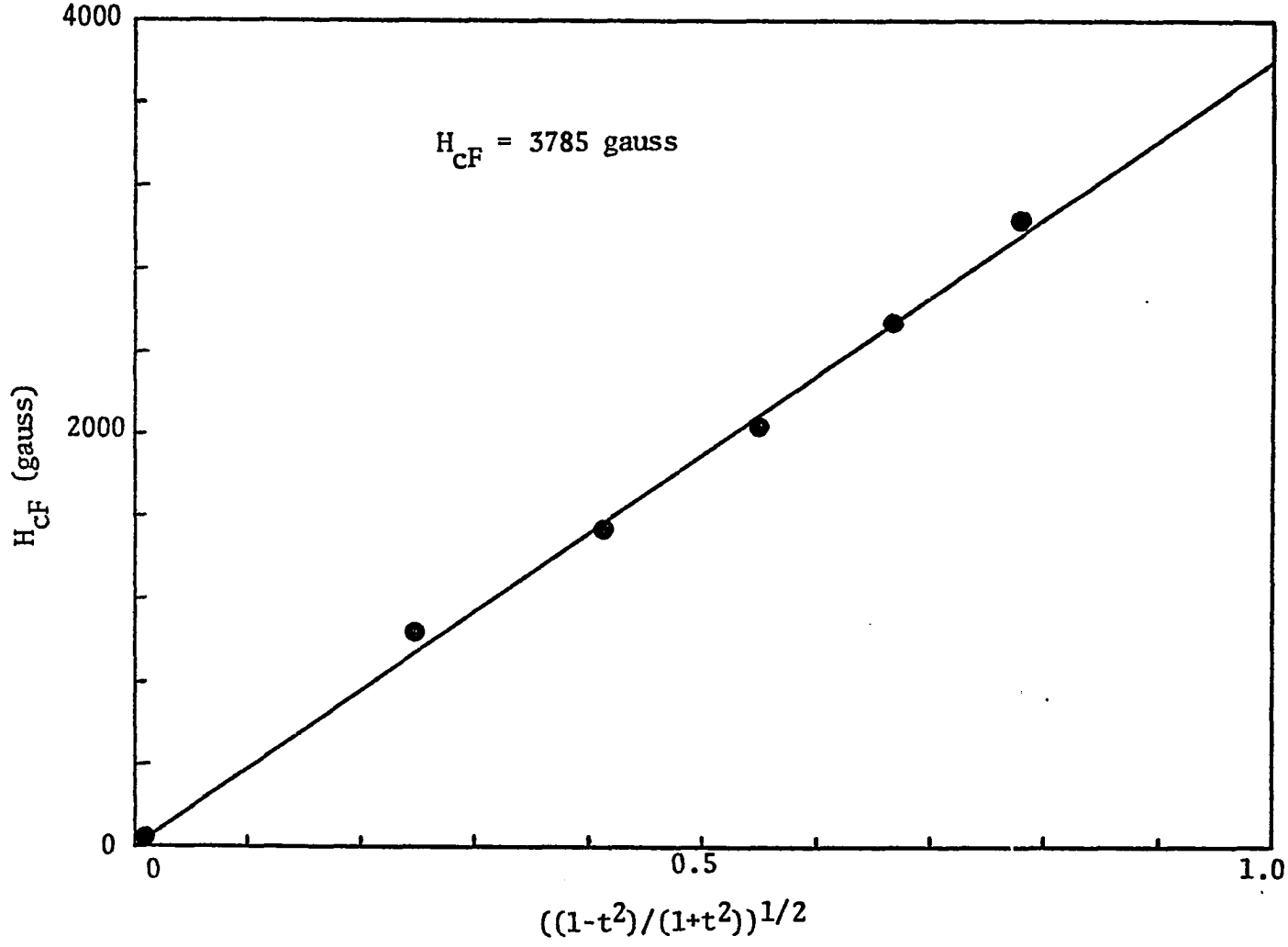

Figure 5 - 8. Data for sample S3 is plotted by Eq.(27) of the thin film approximation.

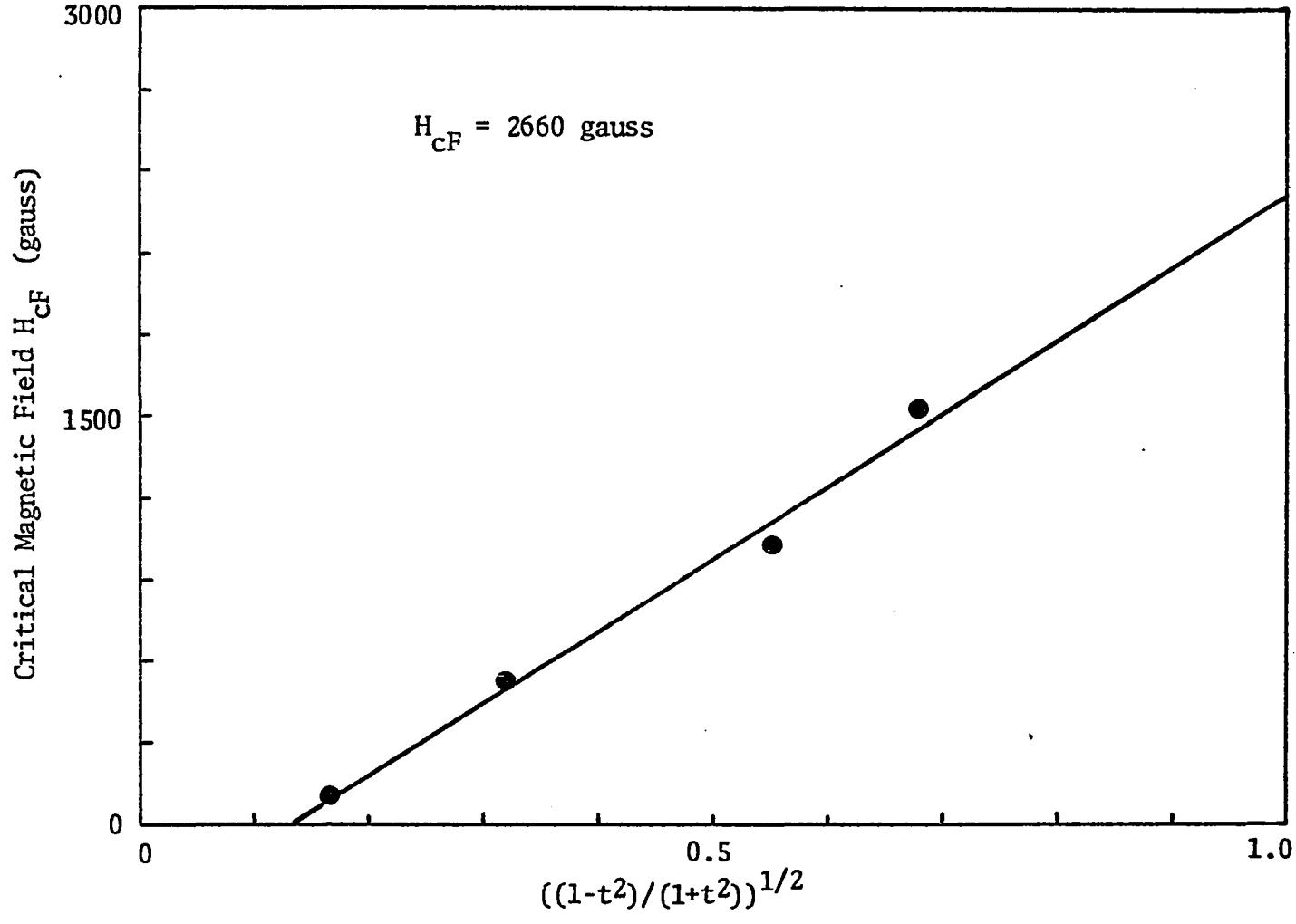

Figure 5 - 9. Data for sample S4 is plotted by Eq.(27) of the thin film approximation.

plotted by Equation (26) and Equation (27). They are shown in Figure 5-10(a) and Figure 5-10(b). The results of plotting show that sample S6, R6, S7 and S8 follow Equation (26) for thick films rather than Equation (27) for thin films. However, data of sample S5 follows both Equation (26) and Equation (27). This means that sample S5 may be a film with thickness around d_c. $H_{cF}(0)$ of sample S5 should be 1767 Oe by lower limit of thin film approximation, $2.2H_c(0)$, and 1164 Oe by the upper limit of thick film approximation, $1.45\ H_c(0)$, where $H_c(0)$ is 803 Oe. $H_{cF}(0)$ of sample S5 is 1580 Oe by Equation (27) of the thin film approximation, and 1570 Oe by Equation (26) of the thick film approximation. Therefore, the critical thickness in terms of the $H_c(0)$ is likely to be $2.2H_c(0)$ rather than $1.45H_c(0)$.

C. Determination of Film Thickness

The thickness of sample is determined by the sputtering time if the deposition rate is known. The deposition rate is determined by the weight and area of a film deposited, and the deposition time. The deposition rate for Pb is 3.57Å/sec. ± .96Å/sec. It is also determined by electrical resistance of films. It is given as

$$d = \frac{L}{w} \frac{\rho(295)}{R(295) - R(4.2)} \qquad (151)$$

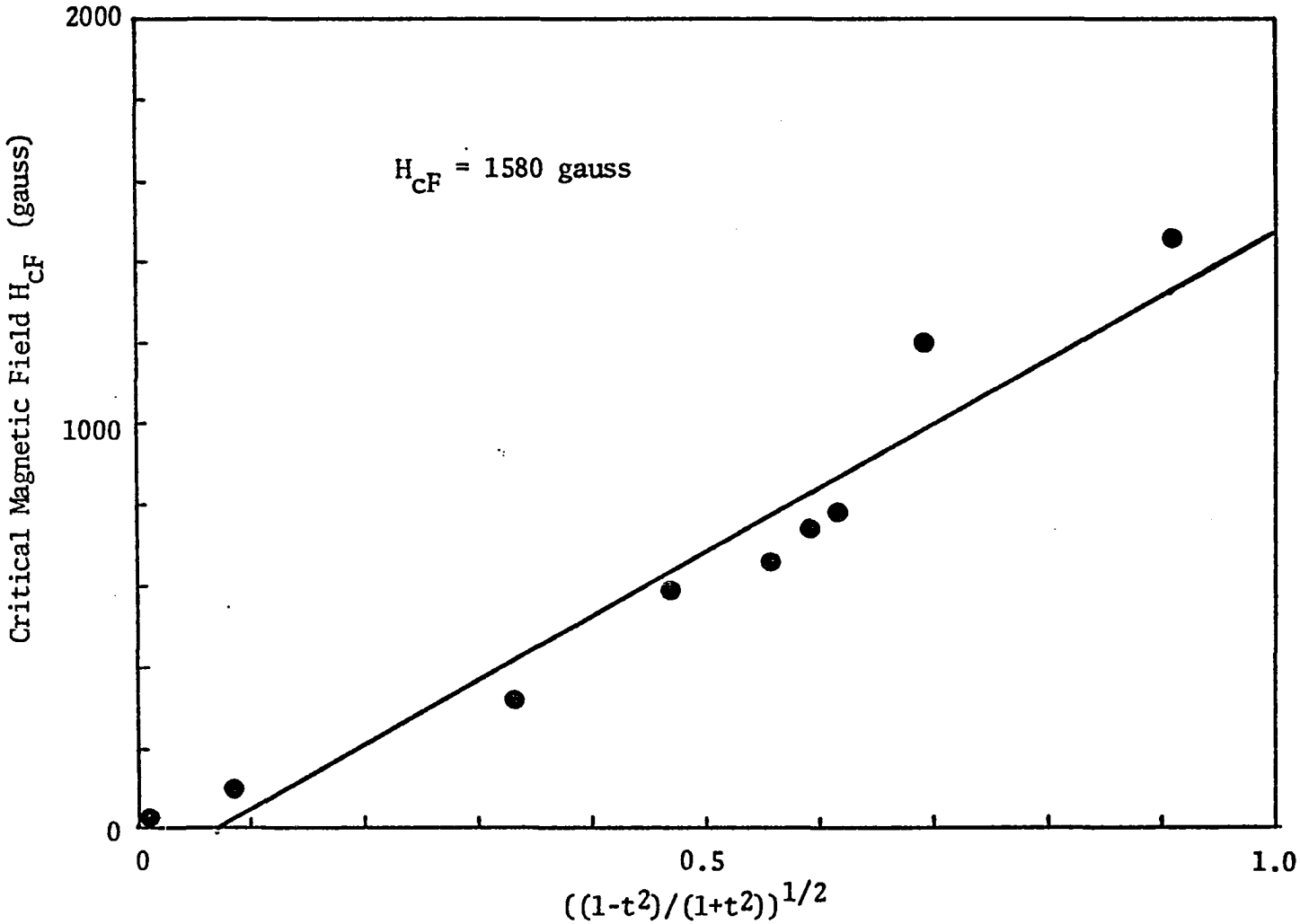

Figure 5 - 10(a). Data for sample S5 is plotted by Eq.(27) of the thin film approximation.

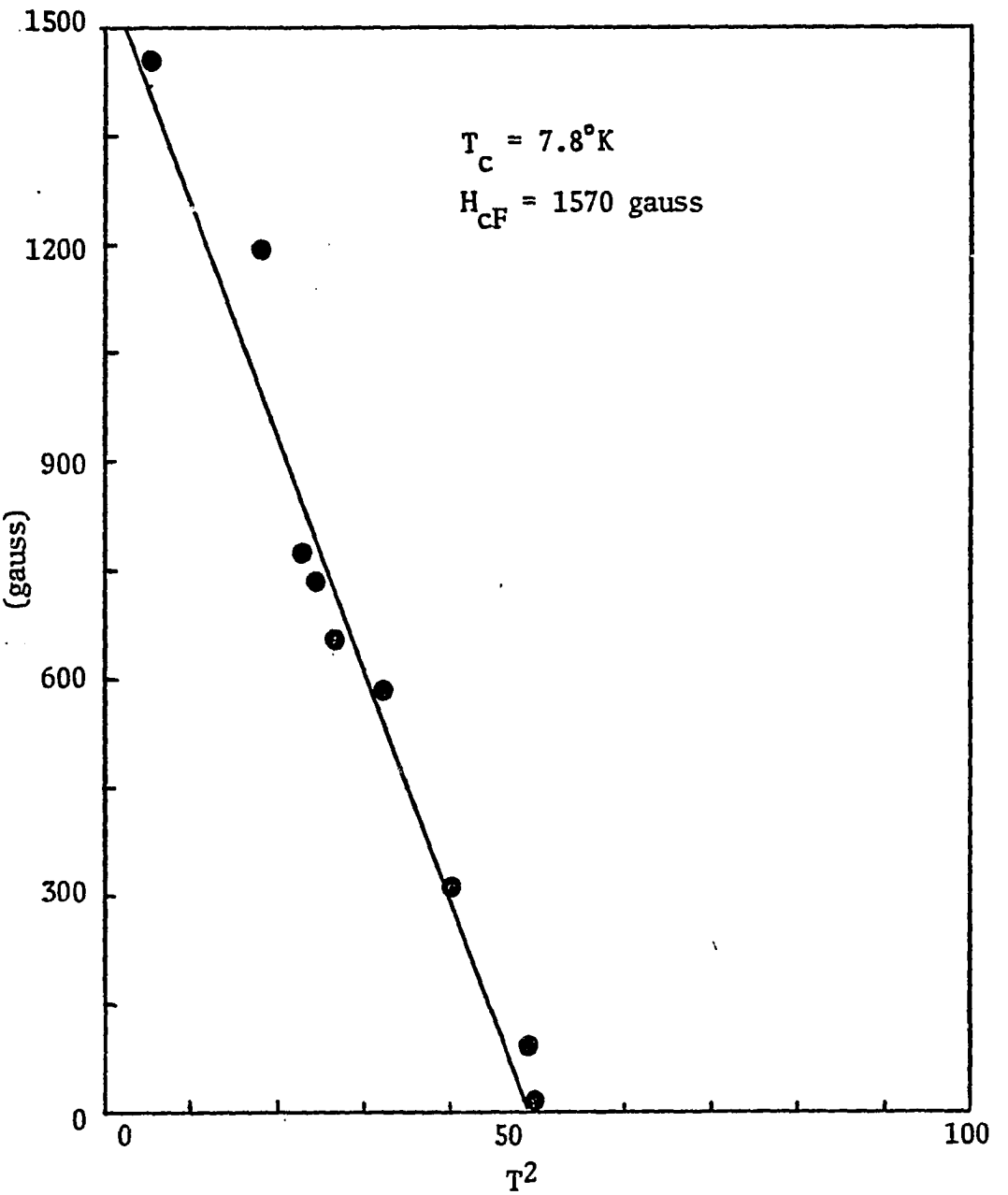

Figure 5 - 10(b). Data for sample S5 is plotted by Eq.(27) of the thin film approximation.

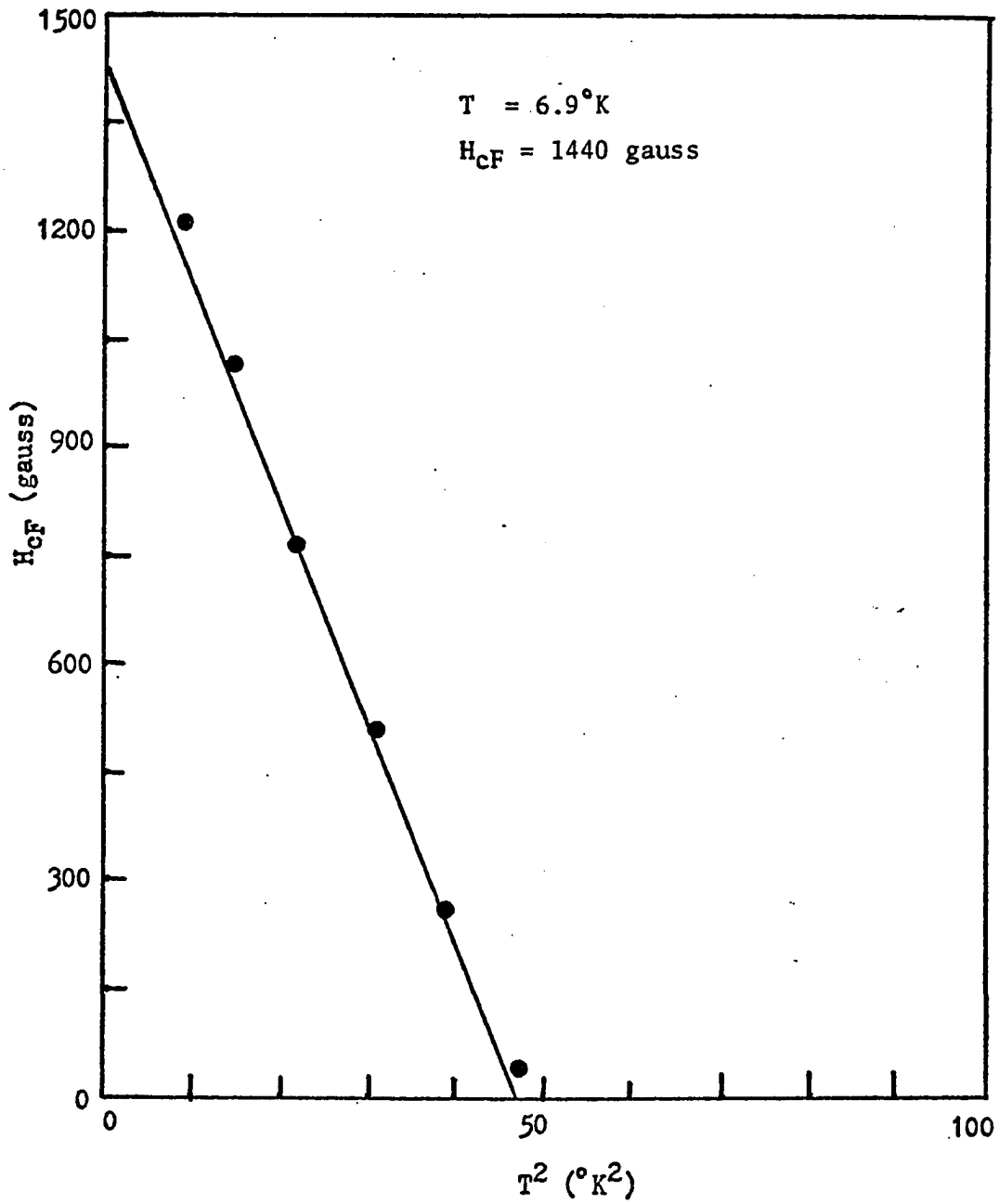

Figure 5 - 11(a). Data for sample S6 is plotted by Eq.(26) of the thick approximation.

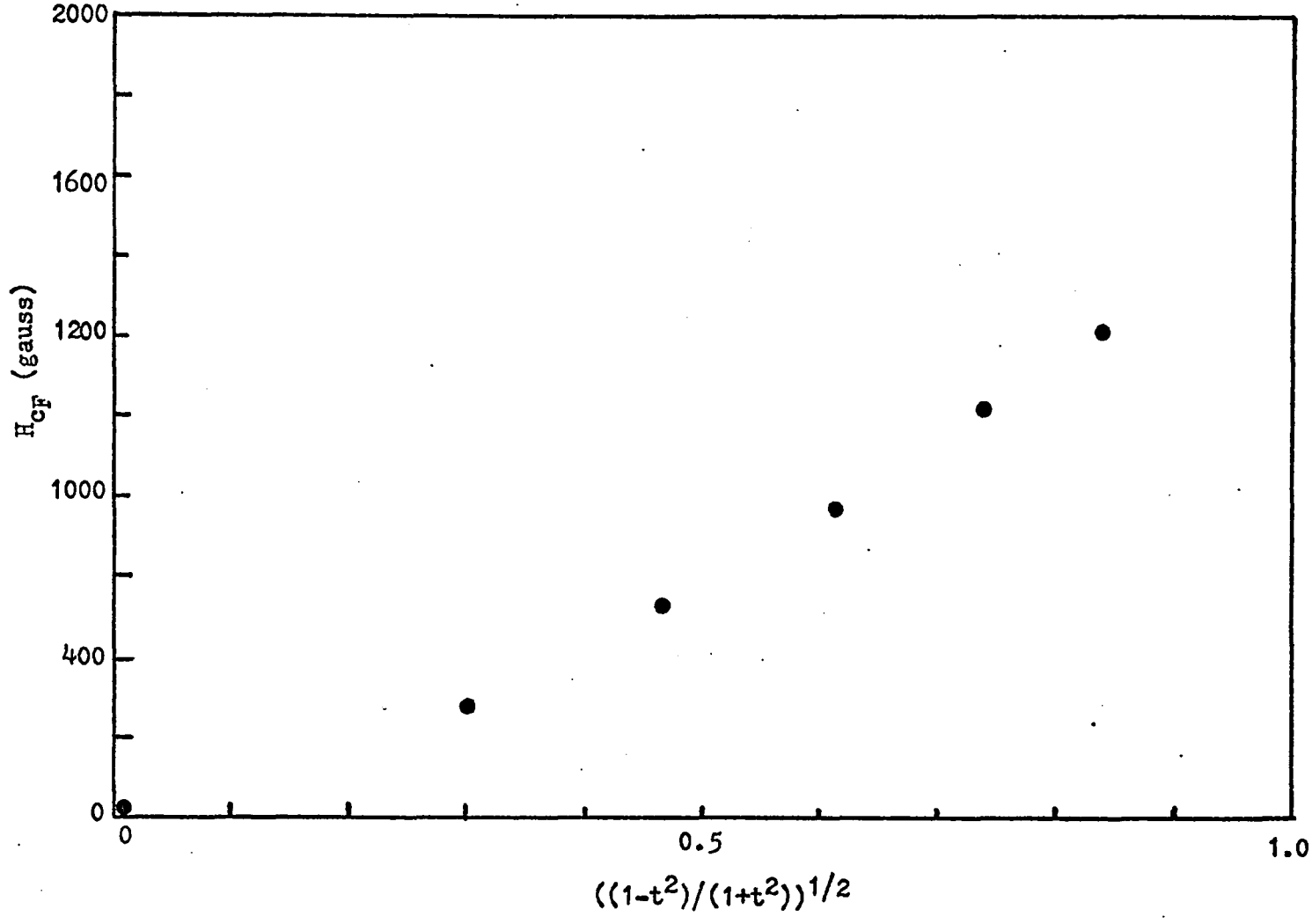

Figure 5 - 11(b). Data for sample S6 is plotted by Eq.(27) of the thin film approximation.

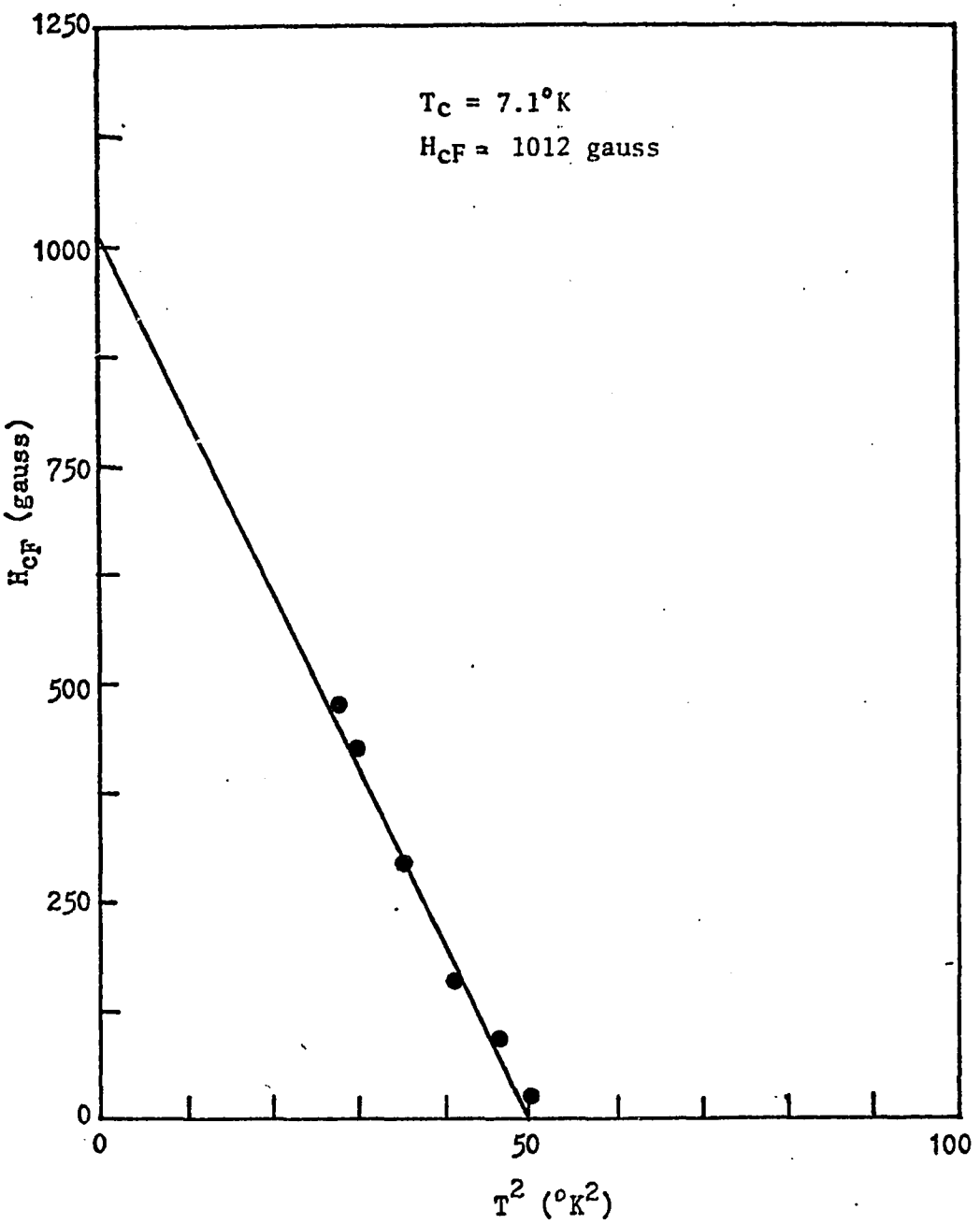

Figure 5-12(a).Data for sample R6 is plotted by Eq.(26) of the thick film approximation.

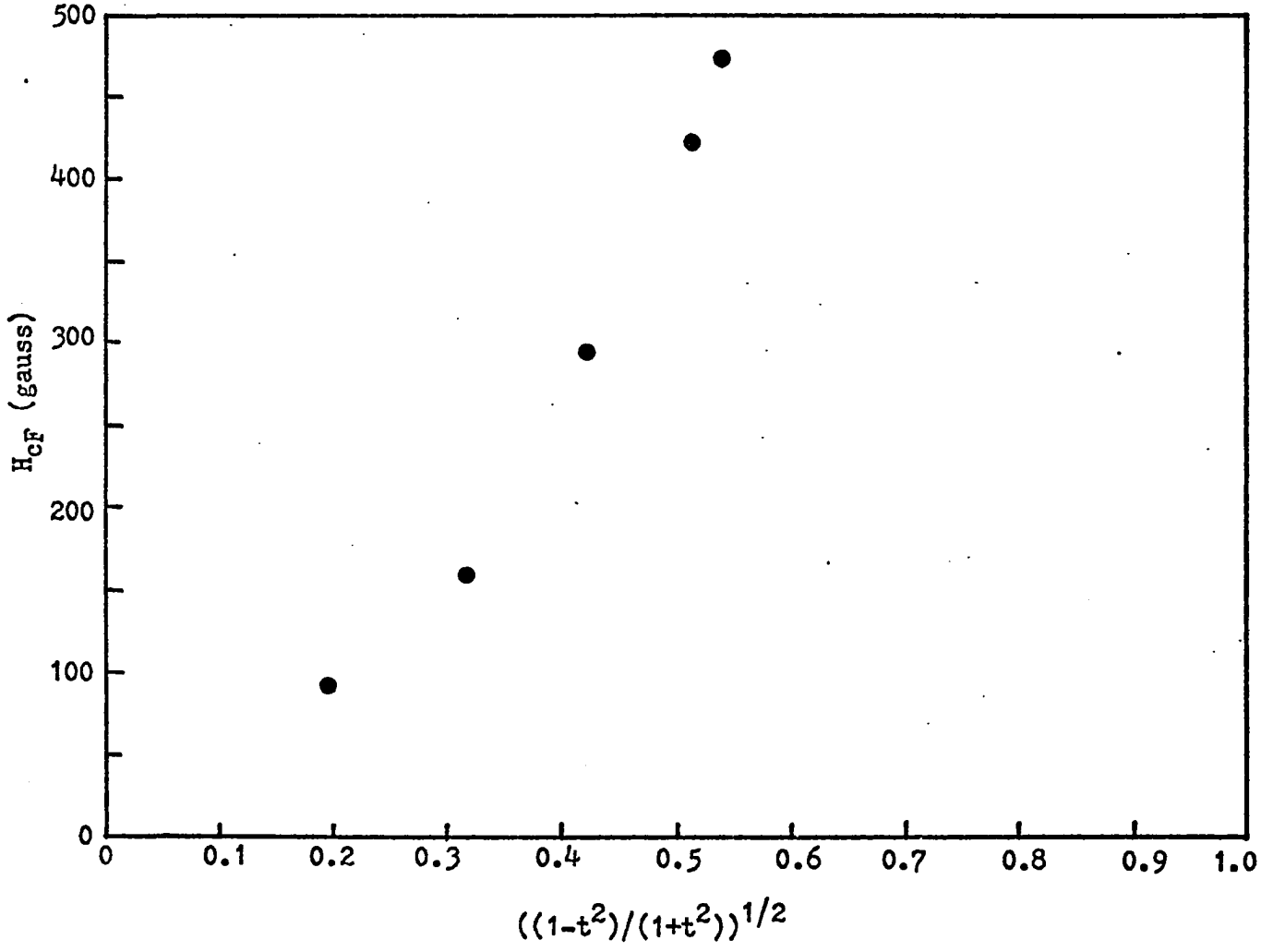

Figure 5 - 12(b). Data for sample R6 is plotted by Eq.(27) of the thin film approximation.

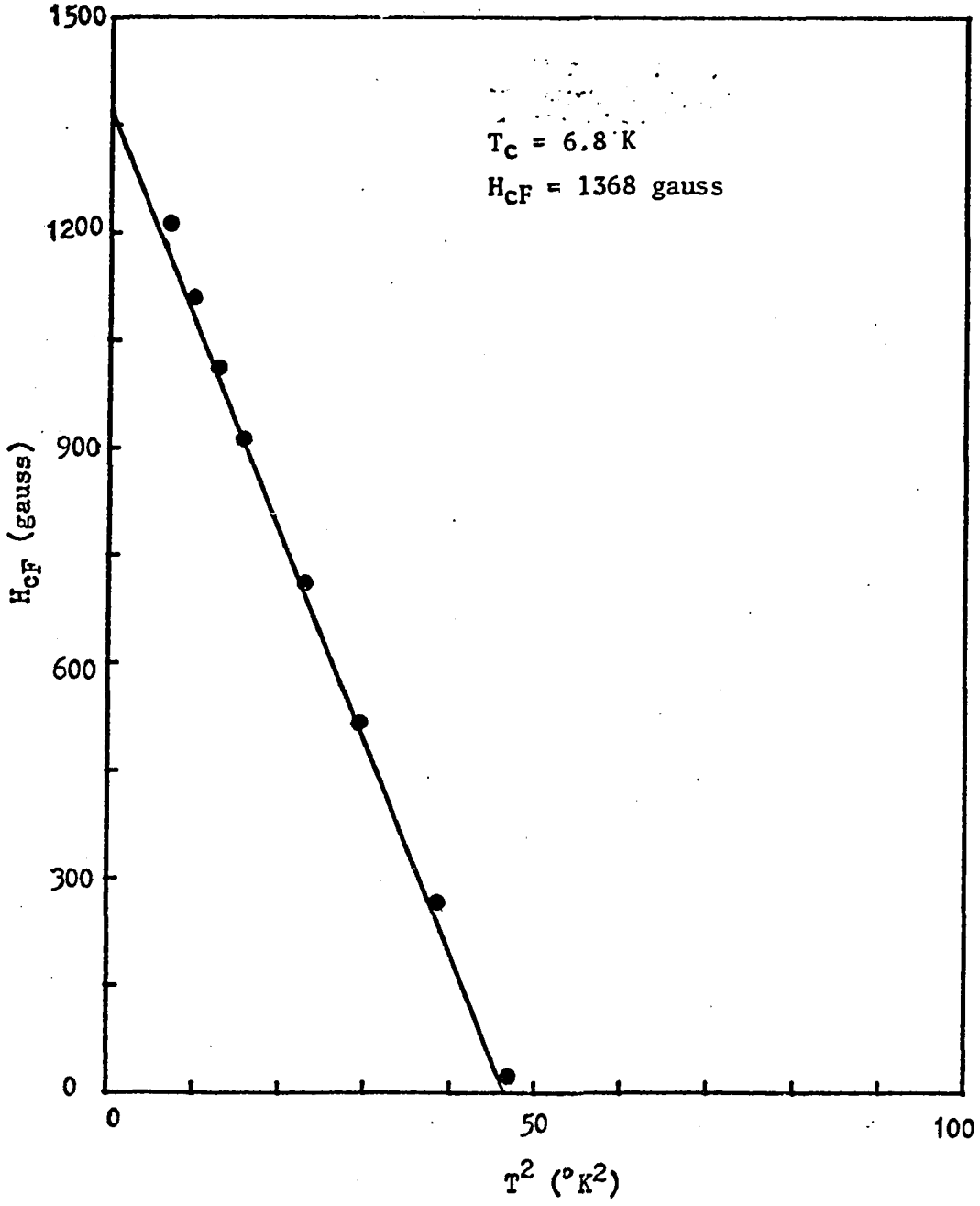

Figure 5 - 13(a). Data for sample S7 is plotted by Eq.(26) of the thick film approximation.

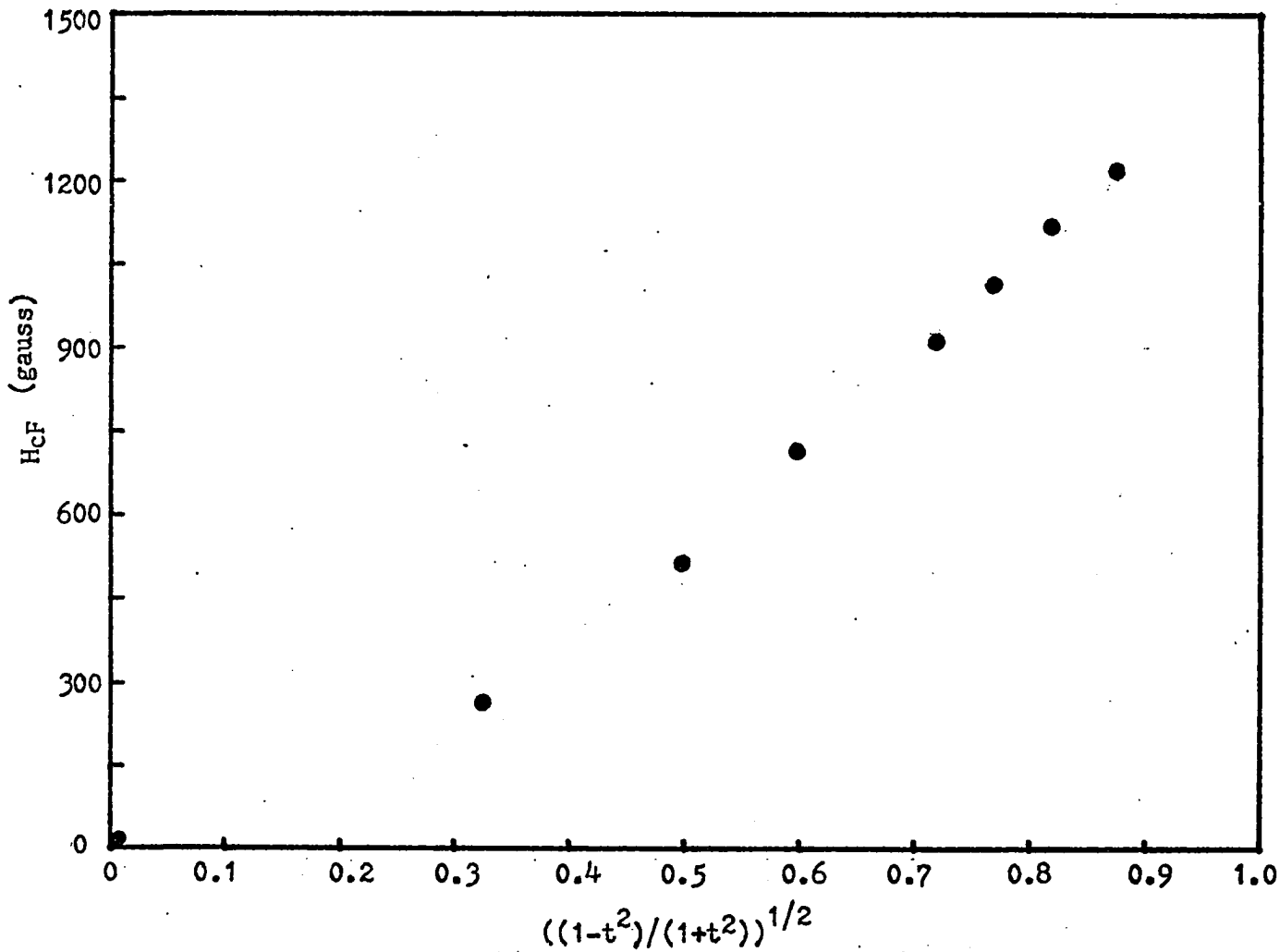

Figure 5 - 13(b). Data for sample S7 is plotted by Eq.(27) of the thin approximation.

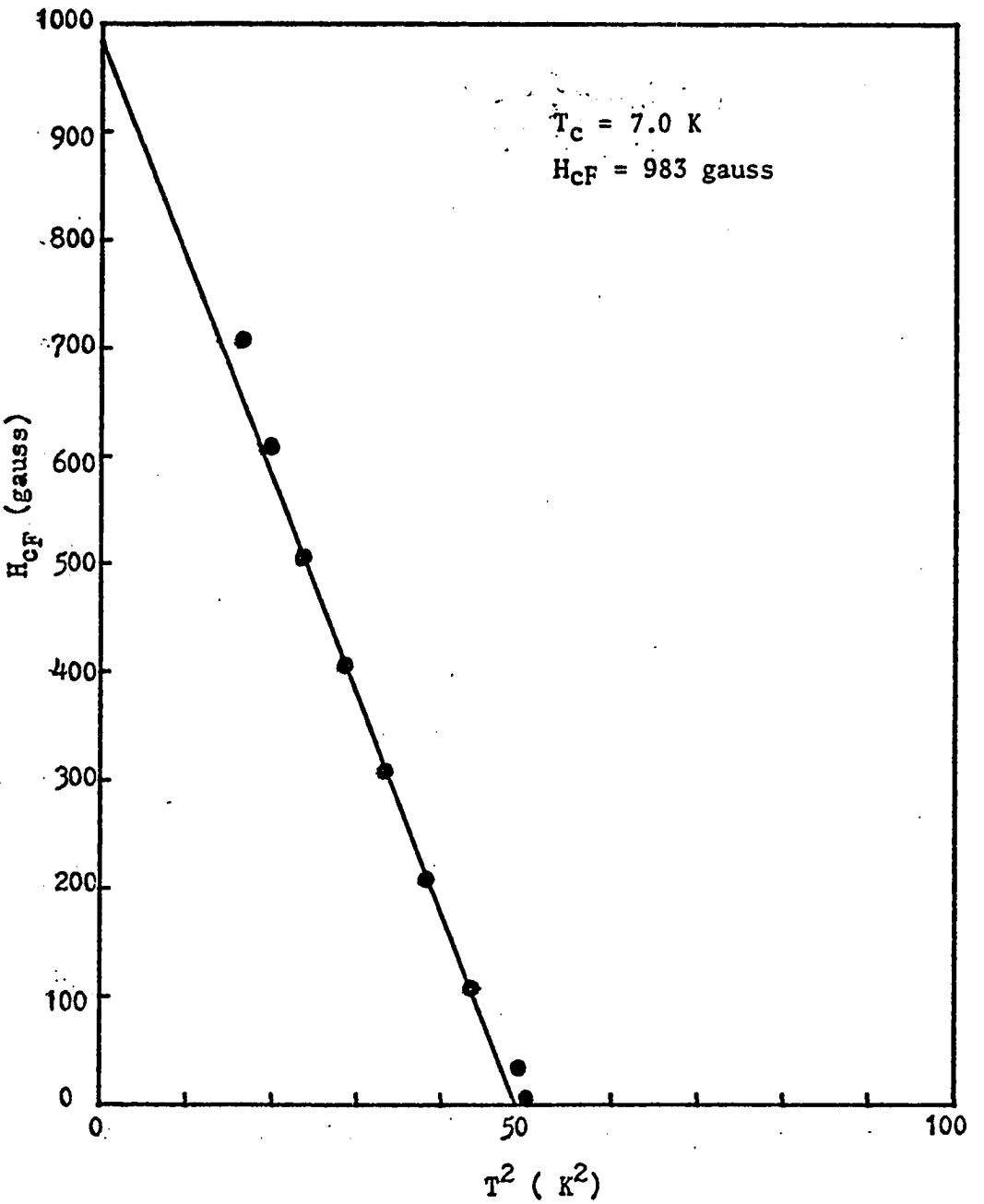

Figure 5 - 14(a). Data for sample S8 is plotted by Eq.(26) of the thick film approximation.

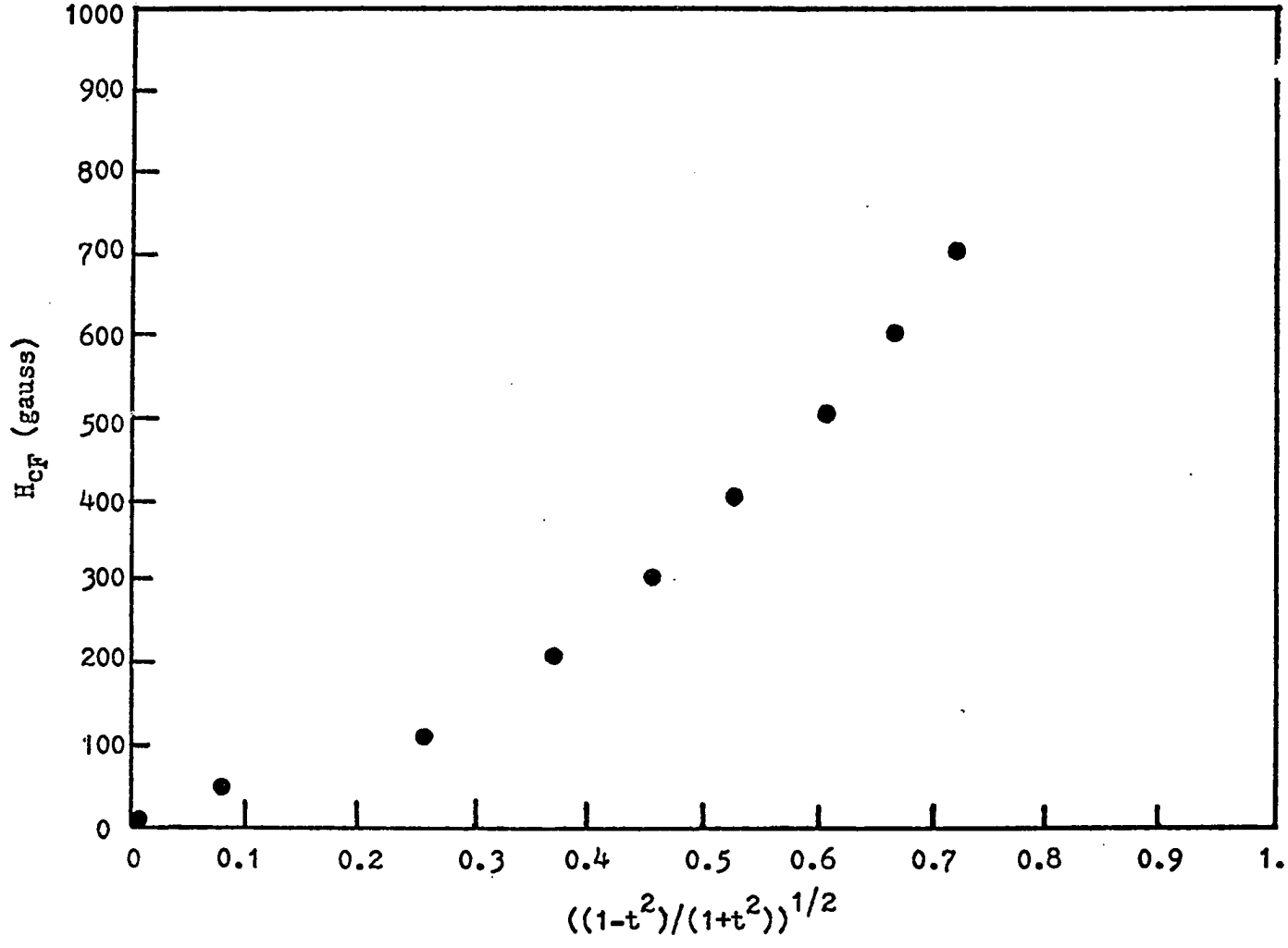

Figure 5 - 14(b). Data for sample S8 is plotted by Eq.(27) of the thin film approximation.

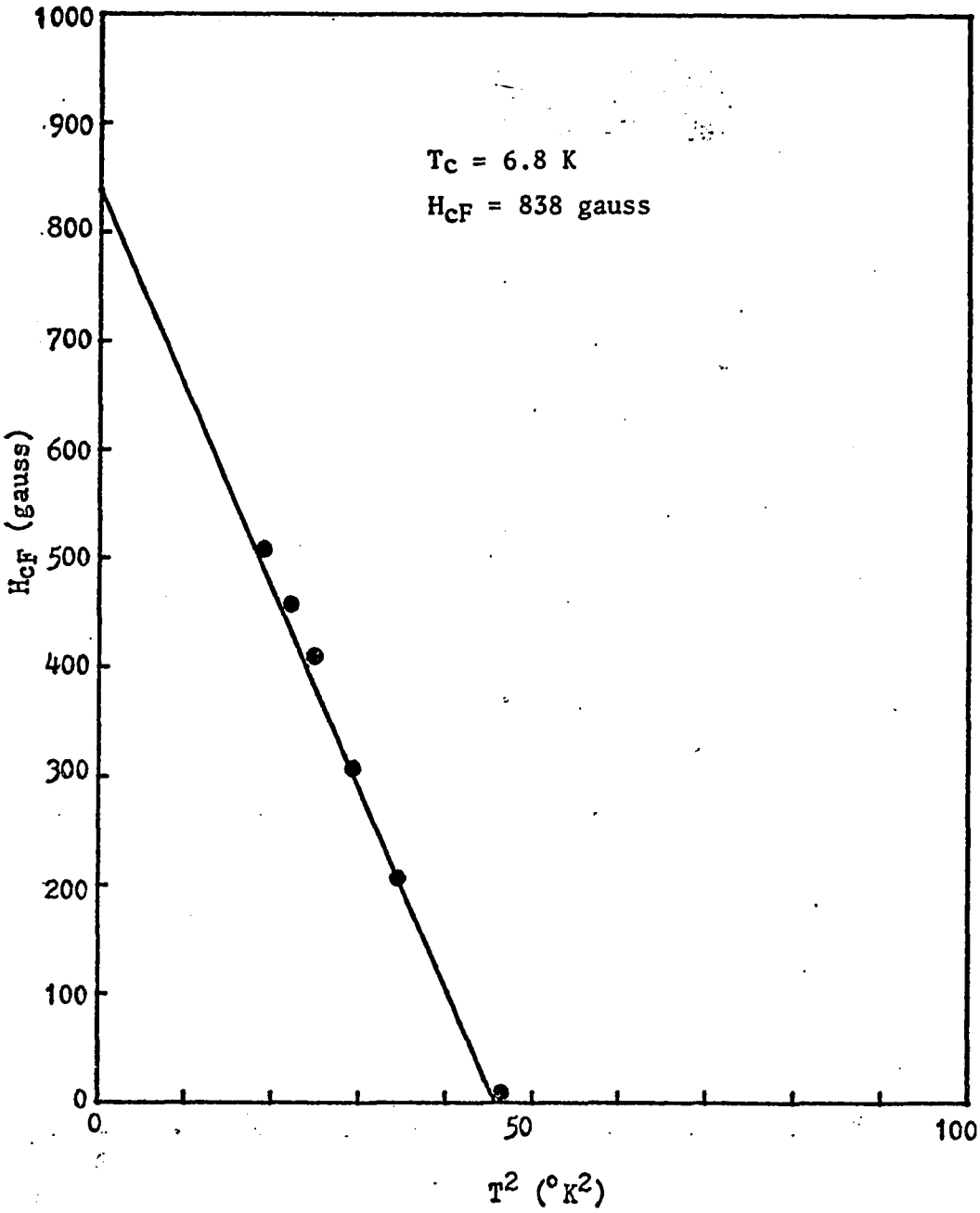

Figure 5 - 15. Data for sample R8 is plotted by Eq.(26) of the thick film approximation.

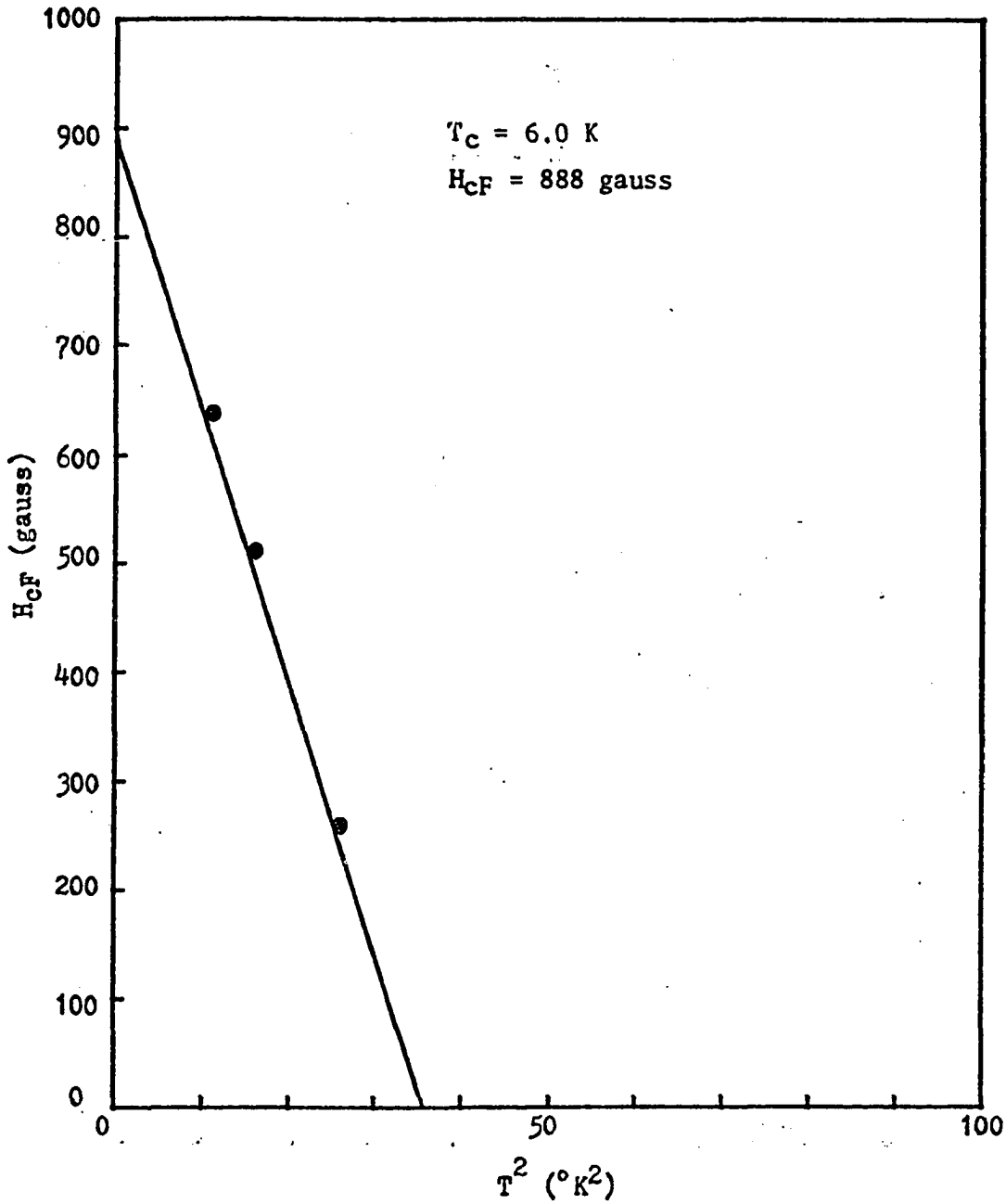

Figure 5 - 16. Data for sample S9 is plotted by Eq.(26) of the thick film approximation.

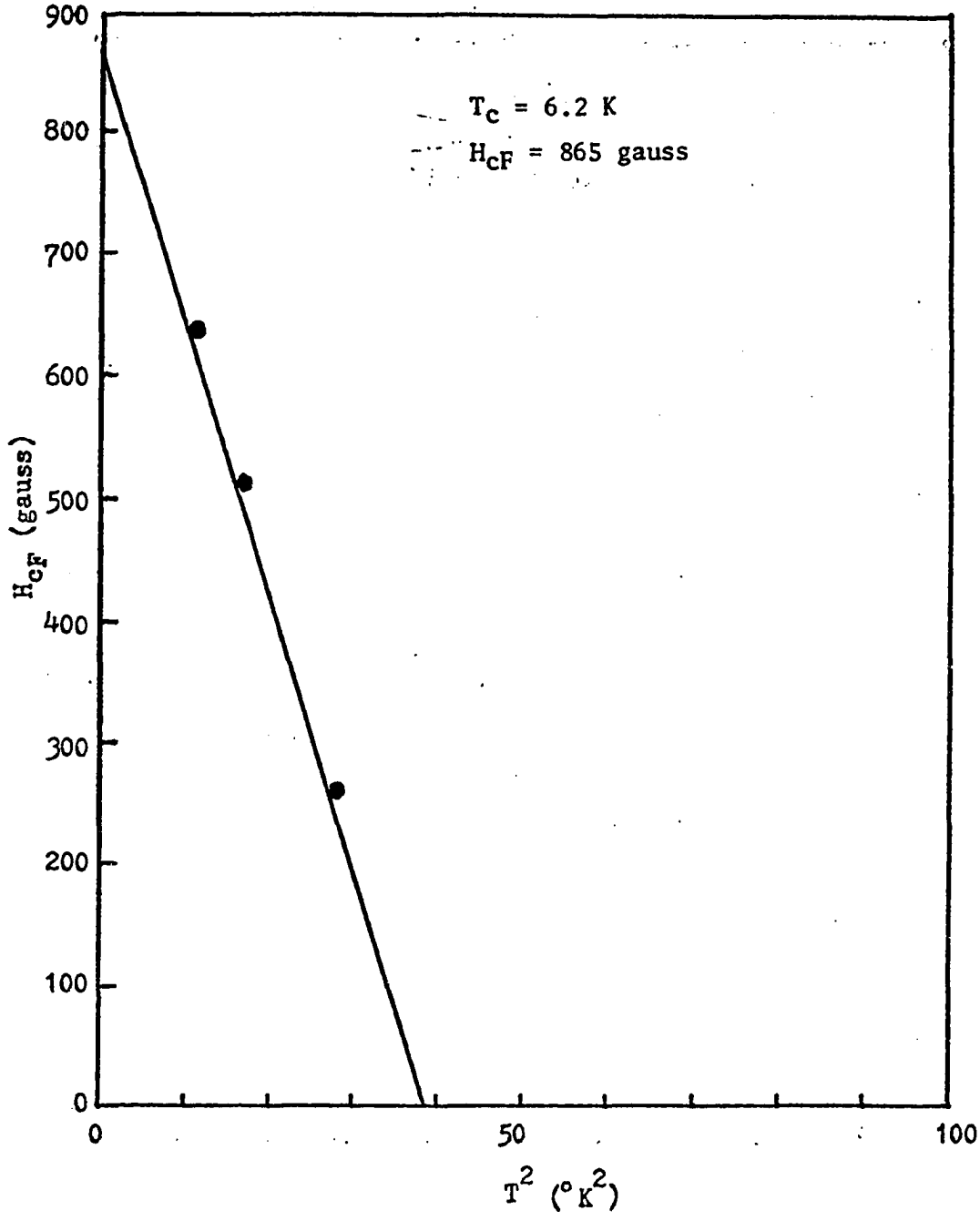

Figure 5 - 17. Data for sample R9 is plotted by Eq.(26) of the thick film approximation.

where L and W are length and width of a film, P(295), R(295) and R(4.2) are resistivity of a bulk specimen at 295°K, the resistance of the film at 295°K and the resistance of the film at 4.2°K. The thickness calculated by Equation (151) is in Table 5-2. The thickness calculated by electrical resistance tends to be less than one by the deposition rate. The thickness based on sputtering time has a degree of uncertainty. It is not known how accurately the mean sputtering rate applies for the first 100Å. Also, any oxidation which occurs will reduce the film thickness obtained by the electrical measurement since oxide layers of surfaces are not good electrical conductors. For these reasons, the thickness quoted here are considered the upper limits. For these samples the average room-temperature resistivity P(295) is 2.4×10^{-5} ohm-cm which is comparable to the value 2.1×10^{-5} ohm-cm of bulk specimen.

D. Roughness of Films

The films are deposited on smooth surface or rough surface of substrates. The surface profiles of smooth and rough surfaces are taken with a surface profilemeter and shown in Figure 5-18. The roughness is defined as the standard deviation at the surface profile from the mean surface. The smooth surface has roughness of 60Å and the rough surface has 700Å of roughness. Result of critical field measurements for films of different roughness are

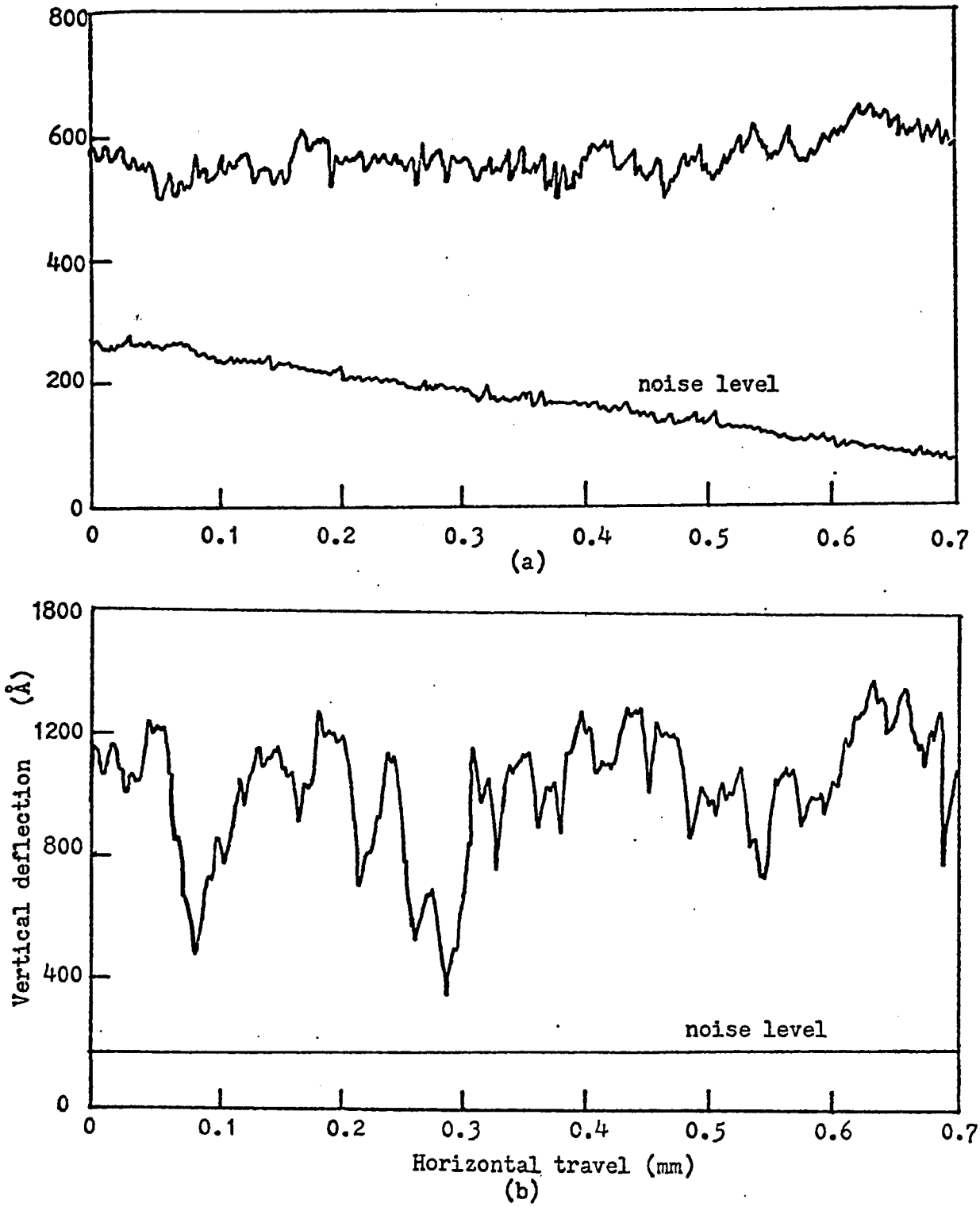

Figure 5 - 18

(a) A typical surface profile of the smooth side of a sapphire substrate. (b) A typical surface profile of the rough side of a sapphire substrate.

shown in Table 5-1. It is consistent that the critical magnetic field deposited on rough surface is always less than one deposited on smooth surface. To confirm the lowering of H_{cF} of a film deposited on a rough surface, the glass plates were made rough by sand paper of #80 and #350, and lead was deposited on each glass plate. The results are shown in Figure 5-4. The H_{cF} of the glass plate roughened by #350 is lower than the one by #180. Also, the glass plate are scatched parallel and perpendicular to the magnetic field, and this film deposited on glass plate which was scatched parallel to the applied magnetic field shows higher H_{cF} than that which was perpendicular to the applied magnetic field.

A possible approach to the explanation of the roughness effect is as follows. As roughness of film surface is known to have a Gaussian distribution, f(y), the Equations (26 and (27) are modified by f(y) as,

$$\langle H_{cF} \rangle = \int_{-\infty}^{\infty} H_c \left(1 + \frac{\lambda}{d}\right) f(y)\, dy \quad \text{for } d >> \lambda \qquad (152)$$

$$\langle H_{cF} \rangle \quad \int_{-\infty}^{\infty} \sqrt{24}\, H_c \frac{\lambda}{d} f(y)\, dy \quad \text{for } d << \lambda \qquad (153)$$

To calculate Equations (152) and (153) it is essential to calculate $\langle \frac{1}{d} \rangle$.

$$\langle \frac{1}{d} \rangle = \int_{-\infty}^{\infty} \frac{1}{d} f(y)\, dy = \int_{-\infty}^{\infty} \frac{1}{d_o + y} e^{-ay^2} dy \qquad (154)$$

Unfortunately, Equation 154 can not be calculated simply

Sample number	Thickness (Å)	H_{CF} (Oe)	T_c (°K)	$\lambda(0,d)$ (Å)	ξ_o (Å)	ξ_o' (Å)	ℓ (Å)
S1	389	4778	7.01	472	750		1011
R1	389	3610	6.20	357	-		
S2	460	4285	7.00	501	999		1190
S3	531	3785	7.13	487	1089		1368
S4	601	2660	6.67	406	859		1541
S5	814	1580	7.02	327	753		2059
		1570		778		8721	
S6	991	1440	6.86	786		10765	2478
R6	991	1012	7.03	258		-	
S7	1097	1360	6.82	761		10930	
S8	3611	991	7.01	845		40176	
R8	3611	838	6.75	157		-	
S9	6392	886	6.00	659		23115	8385
R9	6392	865	6.21	492			

Table 5 - 1

Measured values of thickness d , critical magnetic field H_{CF} and critical temperature T_c, and calculated values of penetration depth $\lambda(0,d)$, coherent length ξ_o for thin films and ξ_o' for thick films and mean free path ℓ of lead films.

Sample number	R(4.2°K) (ohm)	R(295°K) (ohm)	ρ(4.2°K) (μohm-cm)	ρ(295°K) (μohm-cm)	$\frac{R(295°K)}{R(4.2°K)}$	d(nominal) (Å)	d(electrical) (Å)
S1	4.40	60.0	2.0	27	14	354	262
S2	1.80	38.4	1.2	24	21	460	401
S3	0.92	24.5	0.79	21	27	531	623
S4	1.02	20.4	0.88	18	20	601	650
S5	0.62	21.3	0.72	25	34	814	710
S6	0.46	18.6	0.65	26	40	991	810
S7	0.27	18.1	0.42	28	67	1097	824
S8	0.04	4.1	0.21	21	103	3611	3619
S9	0.012	2.9	0.077	19	242	6372	5088

Table 5 - 2

Measured resistance R of lead films at 4.2°K and 295°K are given in second and third columns respectively. Resistivity ρ calculated from R and nominal thickness d by Eq.(151) are in fourth and fifth columns. Nominal thickness d in seventh column is from deposition rate. The last column gives the thickness d (electrical) calculated by Eq.(151).

analytically. However, this approach to the roughness effect may be proper. When the size of roughness is bigger than the thickness of a film, the configuration of the deposited film is not clear.

E. Influence of Gases on Critical Temperature

Auger spectra obtained by Auger Electron Spectrometer are shown in Figure 5-19, and 5-20. Figure 5-19 shows carbon peak of 267 ev and an oxygen peak at 520 ev. The large peaks at less than 267 ev are lead. The amount of carbon and oxygen are almost the same. Figure 5-20 was taken six months later. It shows a prominent peak of carbon, which is almost three times the peak of oxygen. The amount of oxygen also increased and became almost the same size as the peak of lead at 97 ev. At 380 ev, a nitrogen peak appeared. This means that the amount of oxygen increased six times and amount of carbon increased eighteen times in half a year. The critical temperature was depressed only slightly during that time. De Sorba reported that the presence of oxygen in niobium depressed the critical magnetic field. Rairden and Nevgebaver derived an empirical relationship from the experimental restuls of De Sorbo for the variation of T_c with the resistance ratio $(R_{100} - R_{10})/R_{10}$ due to the oxygen concentration in niobium. However, it is too risky to apply Rairdon and Nevgebaver's theory to a film with a heavy concentration of carbon.

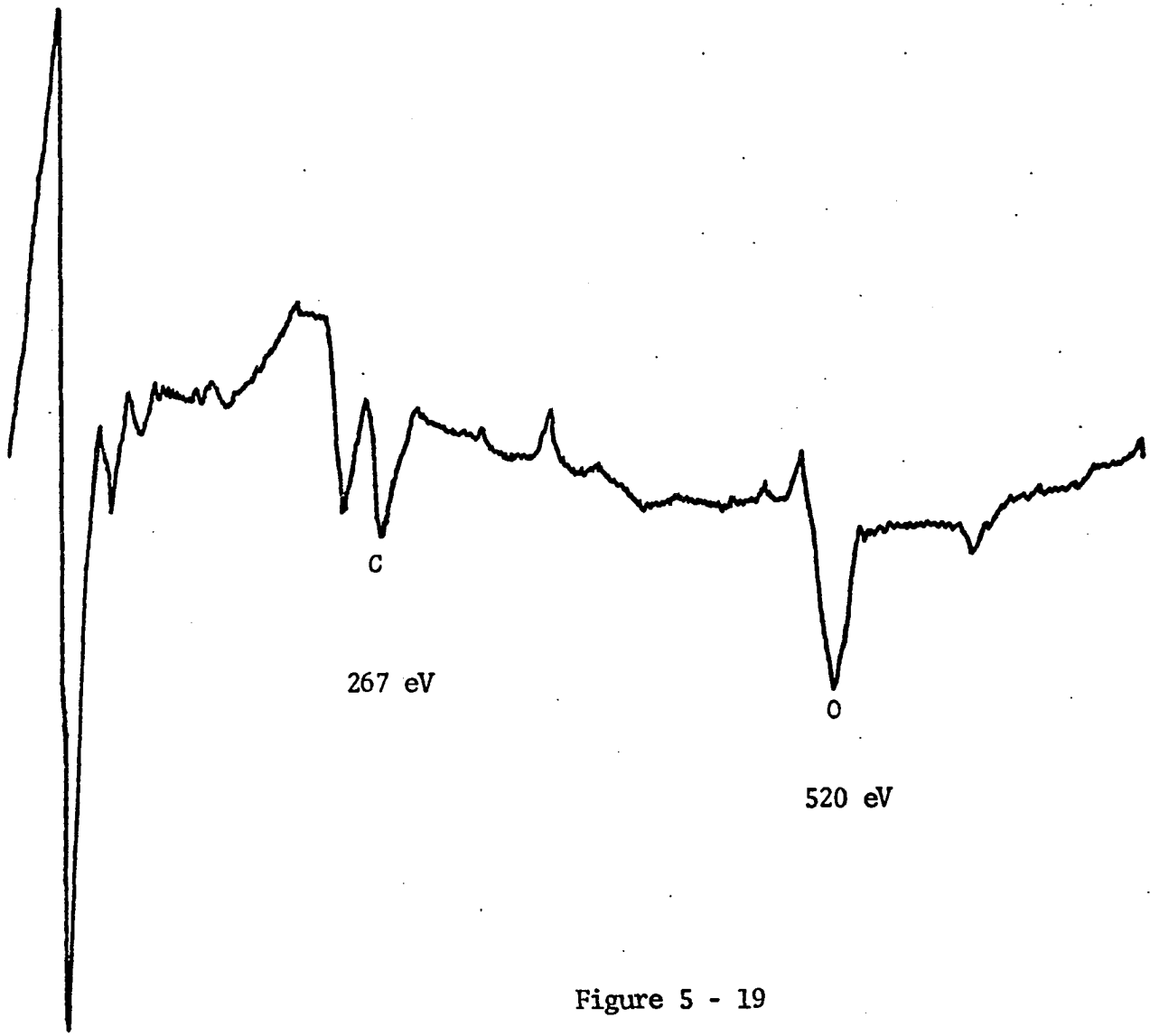

Figure 5 - 19

Auger Spectra of a lead film. The vertical axis is dN(E)/dE in arbitrary unit. The horizontal axis is energy in eV.

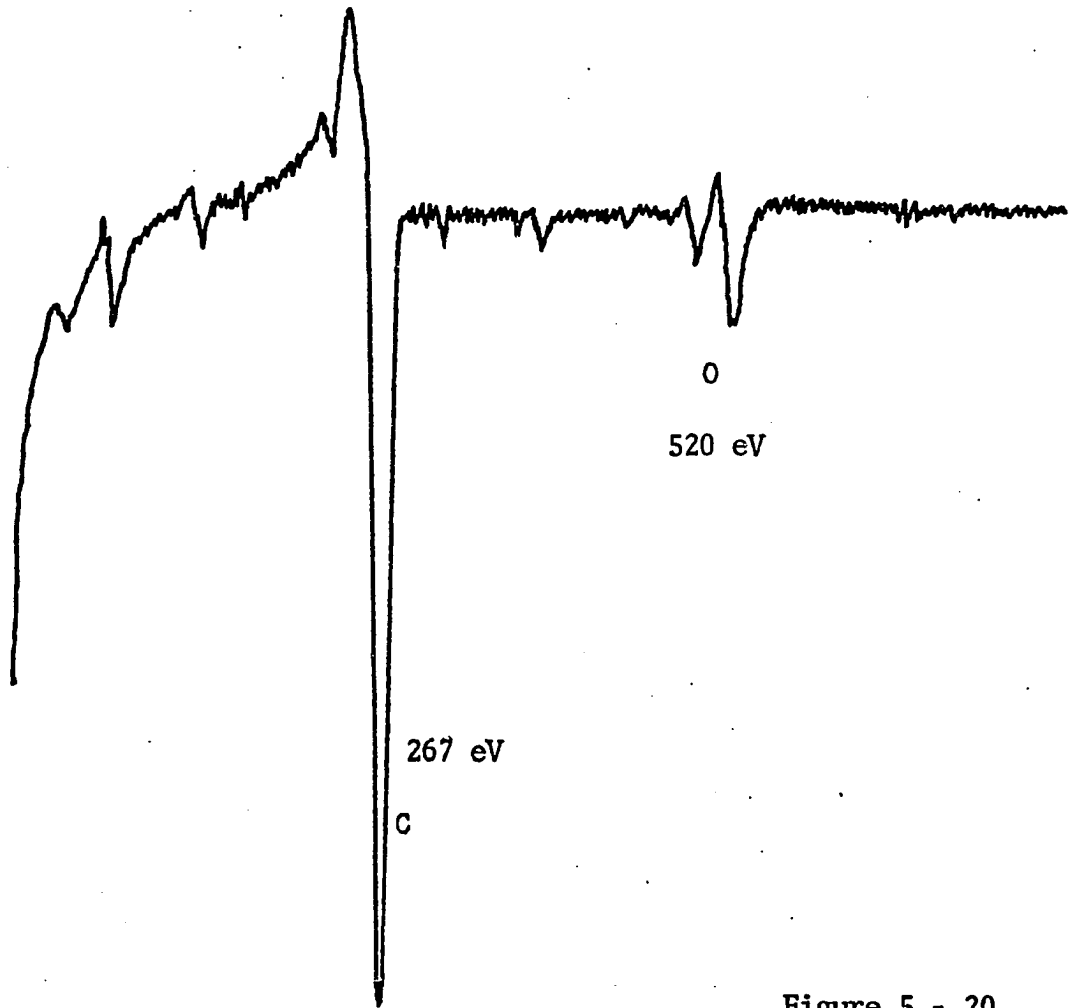

Figure 5 - 20

Auger Spectra of the lead film of Figure 5 - 19 taken six month later.

F. Critical Magnetic Field $H_{cF}(0)$, Penetration Depth $\lambda(0)$, and Coherence Length ξ_o

For the thin film region ($d<d_c$), H_{cF} is plotted against $[(1 - t^2)/(1 + t^2)]^{1/2}$, where t is T/T_c. Samples S1, R1, S2, S3, S4, S5 are plotted in Figure 5-5(a) through Figure 5-10(a). The linear dependence predicted by Equation (56) through the origin is observed. $H_{cF}(0)$ of a thin film can be obtained as the slope of lines. For the thick-film region ($d_c<d$), H_{cF} is plotted against t^2. Plots for samples S5, S6, R6, S7, S8, R8, S9 and R9 are shown in Figure 5-5(b) through Figure 5-10(b). The linear dependence predicted by Equation (55) is observed. $H_{cF}(0)$ of a thick film is obtained as the y-intercept of Equation (55). Samples S5, S6, R6, S7 and S8 are plotted by both Equations (55) and (56). Only data of S5 fit well to both equations.

The plot of $H_{cF}(0)$ versus d for thin film samples S1, S2, S3, S4 and S5 is shown in Figure 5-21 where the slope is seen to be -1.5. However, points of S1 are lower than this predicted line because the H_{cF} of S1 and S2 are lower than ones predicted. This is probably due to uncertainty of the thickness of these films. The plot of $H_{cF}/H_c - 1$ versus d for thick films S5, S6, S7, S8 and S9 is shown in Figure 5-22. Equation (55) predicts the slope of the Figure 5-22 to be -1. The observed slope -1.3. Figure 5-23 is the plot of $H_{cF}(0)$ versus d for thin and thick films together in a semi-log graph. (Cody and Miller use a

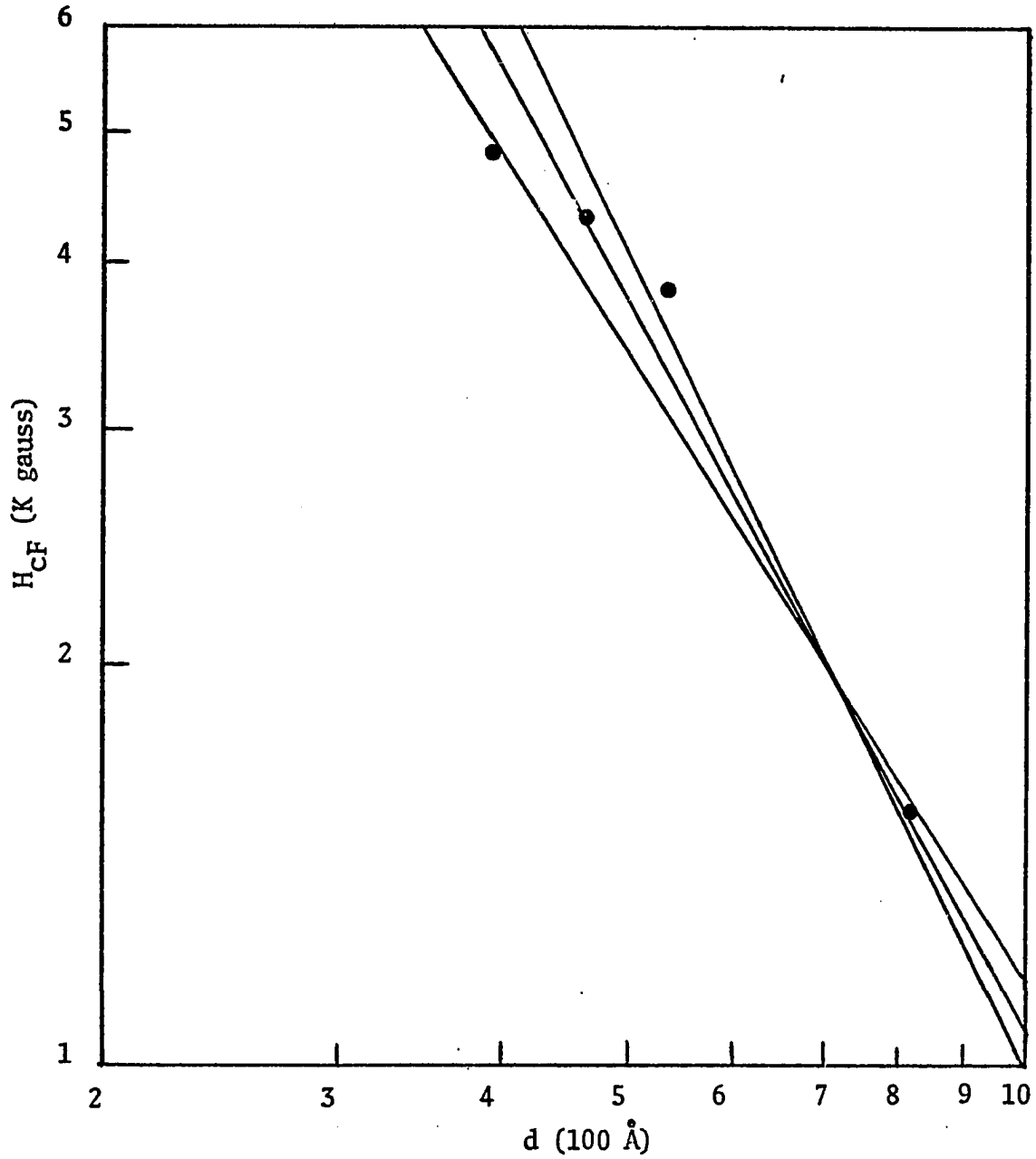

Figure 5 - 21

The critical magnetic field H_{CF} versus the film thickness d for thin films.

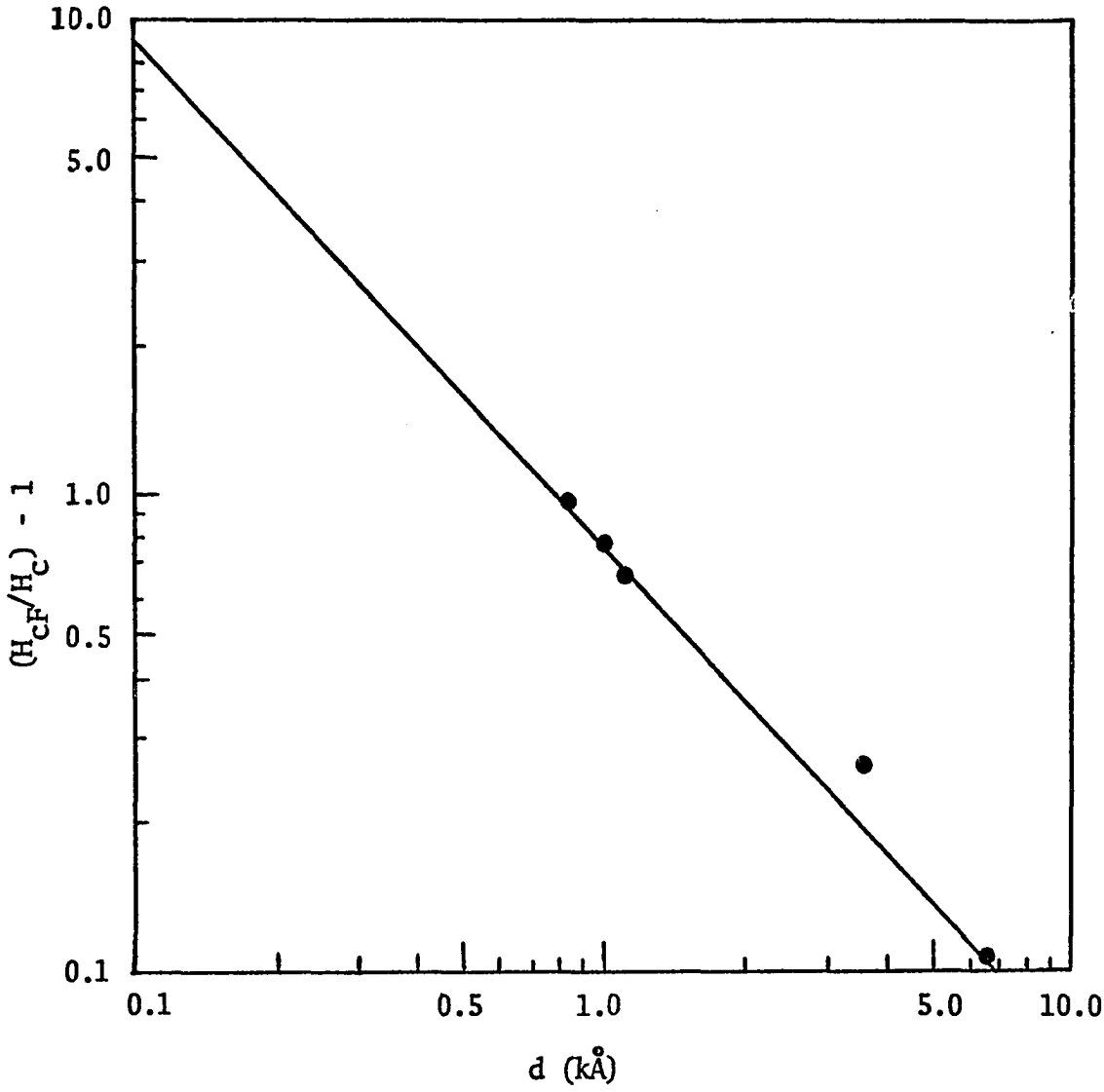

Figure 5 - 22

H_{cF}/H_c - 1 versus the film thickness d for thick films. H_c is the critical magnetic field for a bulk lead.

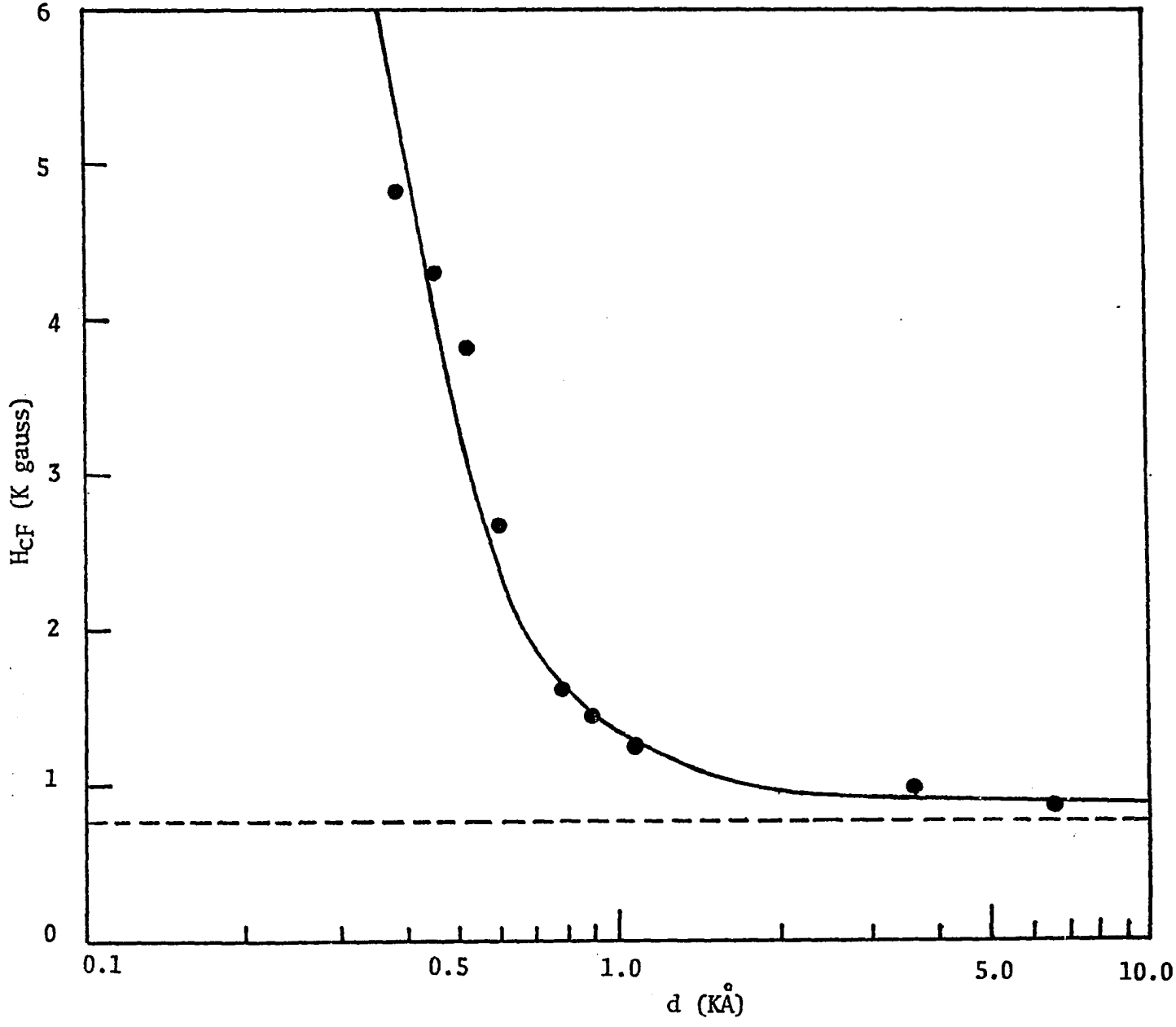

Figure 5 - 23. The critical magnetic field H_{CF} versus the film thickness.

similar plot for their $H_{cF}(0)$ data.) The fluctuation of the data in the thin film region can be seen.

The penetration depth $\lambda\ (0,d) = \lambda_L(\xi_o/d)^{1/2}$ is calculated by substituting values of $H_c(0)$ and d in the expression for the slopes of the linear curves of H_{cF} versus $[(1 - t^2)/(1 + t^2)]^{1/2}$. $\lambda(o,d)$ of thick films can be obtained by substituting values of $H_{cF}(0)$ and d in the expressions for the linear curves versus $1 - t^2$. Values of $\lambda(0,d)$ of films deposited on the rough surface of the substrate are a great deal lower than $\lambda(0,d)$ of those deposited on the smooth surface of substrate.

The coherence length, ξ_o, can be calculated for thin films by Equation (51) with $\lambda_L = 340\text{Å}$ which was calculated by Cody and Miller (See Table 5-3) for thick film region ($d_c<d$). Some values are listed in Table 5-1. However, it is difficult to determine which equation should be used to calculate ξ_o, the value of the mean free path should be known. ℓ for sample S6 is calculated by the equation for $d<\ell_B$.

$$\frac{1}{\ell} = \frac{4}{3d} \frac{1}{[\ell n\ (\frac{\ell_B}{d}) + 0.4228]} \qquad (155)$$

where ℓ_B is the mean free path of a bulk specimen, and ℓ_B of lead is about 40KÅ. Substituting ℓ_B and d of sample S6, 1097Å, yields the value of ℓ in order of a few cm. This result is not reasonable at all. The equation for

	Calculated London Values	Calculated BCS Values		Observed Values	
	$\lambda(0)$, Å	$\lambda(0)$, Å	ξ_o, Å	$\lambda(0)$, Å	ξ_o, Å
Bardeen & Schrieffer[134]	370	470	830, 900	390	
Cody & Miller[73]	340	440	800, 1000		
Lock[9]		390			
Hauser[135]			1000		510-600
Gasparovic & Mclean[136]	305		960		
Krätzig, Walther & Schilz[12]				819	

Table 5 - 3

Values of the penetration depth $\lambda(0)$ and the coherent length ξ_o calculated and observed by other groups.

$d > \ell_B$:

$$\frac{1}{\ell} = \frac{1}{\ell_B} + \frac{3}{8d}, \quad d > \ell_B \tag{156}$$

gives 2700Å as the value of ℓ. This is reasonable value. Substituting ℓ = 2700Å in Equation (48) yields 8800Å as the value of ξ_o. Values of ℓ calculated by Equation (156) are shown in Table 5-1. (Although the condition of Equation (156) $d > \ell_B$, is not proper at all for the thickness of some films in this present work, Cody and Miller, also applied Equation (156) to the thin-film region by neglecting the term $1/\ell_B$.) ξ_o' in Table 5-1 is the value of the coherence length calculated by ℓ and Equation (48). Values of ξ_o calculated by the thin film approximation and Equation (51) are within values those predicted on the basis of BCS theory (See Table 5-3), except for sample S3. However, the coherence length ξ_o', calculated by ℓ and Equation (48), tend to increase with film thickness.

G. Critical Current Versus Temperature

Critical current measured was plotted against temperatures. The error of critical current measurement is 1%. Critical current, I_c, was plotted against $1 - t^2$, and the value of the slope, 0.9 was obtained from the plotted line. According to Glover and Coffy, as described by Equation (84) and Equation (125), the critical current density, $J_c(t)$ is approximately proportional to $(1 - t^2)^{3/2}$ and consequently $I_c(t)$ is proportional to $(1 - t^2)/(1 + t^2)^{1/2}$. Using

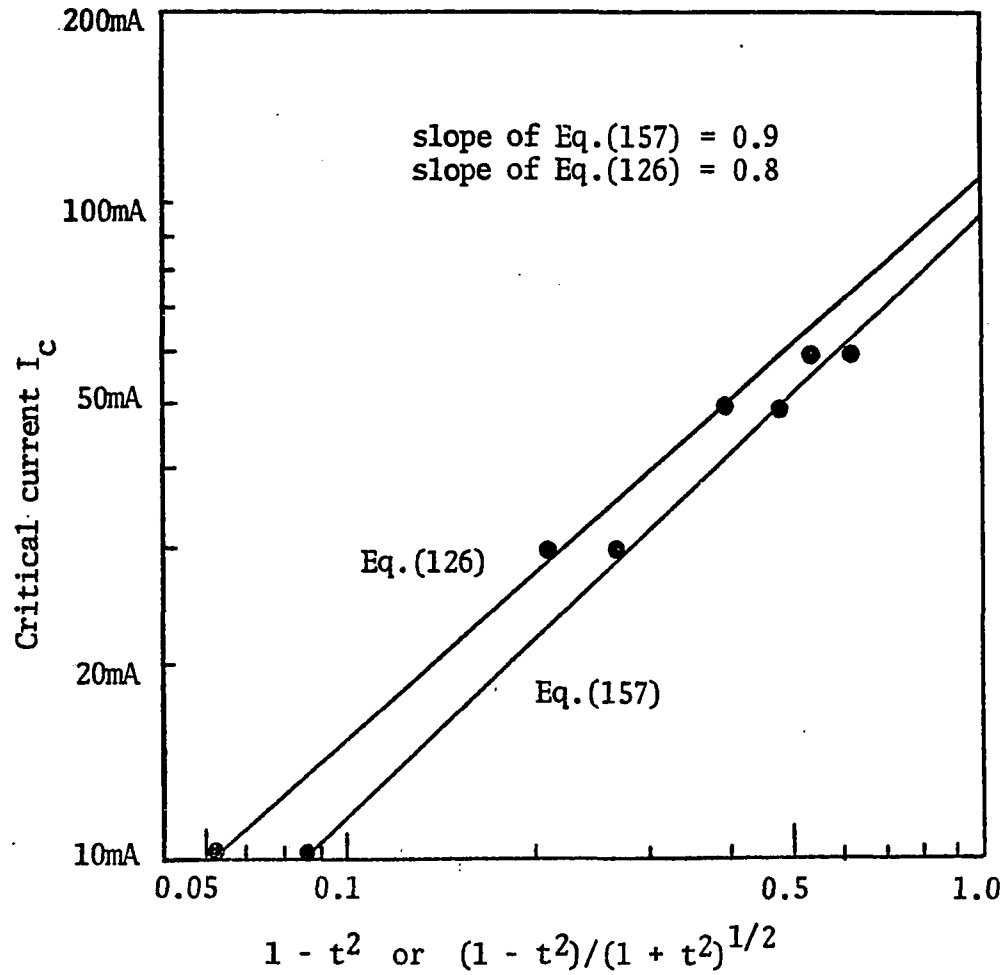

Figure 5 - 24

Critical current I_c versus temperature t where $t = T/T_c$.

Eq.(157) : $I_c(t) = I_c(0)(1-t^2)$

Eq.(126) : $I_c(t) = I_c(0)(1-t^2)/(1+t^2)^{1/2}$

equations of Glover and Coffey Mydosh and Meissner plotted $I_c(t)$ of tin against $(1 - t^2)/(1 + t^2)^{1/2}$ and obtained 1.0 as the value of the slope. They concluded that their data agreed, to a great degree with the equations derived by Glover and Coffey. However, Glover and Coffey's assumption that $J_c(t)$ is proportional to $(1 - t^2)^{3/2}$ is too simplified. As seen from Equations (84) and (95), $J_c(t)$ is proportional to $(1 - t^2)^{3/2}(1 + t^2)^{1/2}$. Substituting Equation (84) into Equation (124) without assuming that $(1 - t^2)^{3/2}$ is dominant, yields

$$I_c(t) = I_c(0)(1 - t^2) \qquad (157)$$

Instead of Equation (126) given as

$$I_c(t) = I_c(0) \frac{1 - t^2}{(1 + t^2)^{1/2}} \qquad (126)$$

The data of this present work which showed 0.9 as the value of the slope when I_c was plotted against $1 - t^2$, supports Equation (157) rather than Equation (126). However, it is dangerous to make such a conclusion that I_c follows Equation (157) rather than Equation (126) since data of this present work was measured from only one sample. Glover and Coffey's conclusion was based on $J_c(t)$ versus t in spite of the fact that $I_c(t)$ was actually measured, and then substituted for $J_c(t)$ by means of an equation. Mydosh and Meissner mentioned their data of planar films in an appendix without much detail. Therefore, further study is necessary

to determine whether $I_c(t)$ follows Equation (157) or Equation (126).

As for the distribution of critical current density such as Equation (123) and Equation (129), it does not matter whether $I_c(t)$ follows Equation (157) or Equation (126) are derived from Equation (124) which includes the current density distribution.

H. Current Versus Magnetic Field

Critical currents are measured in the presence of an applied magnetic field. The resistance versus magnetic field curve with a constant current was used to obtain the relationship between applied current and magnetic field at the critical field. Equation (138) was changed to

$$I^{2/3} = I_c^{2/3} - \left(\frac{I_c^{3/2}}{H_c^2}\right) H^2$$

and $I^{2/3}$ and H^2 were treated as variables y and x. Applying the least square method to this yields y-intercept B and slope M. Figure 5-25 and Figure 5-28 show data and the best fitting curve. From B and M, I_c and H_c are calculated.

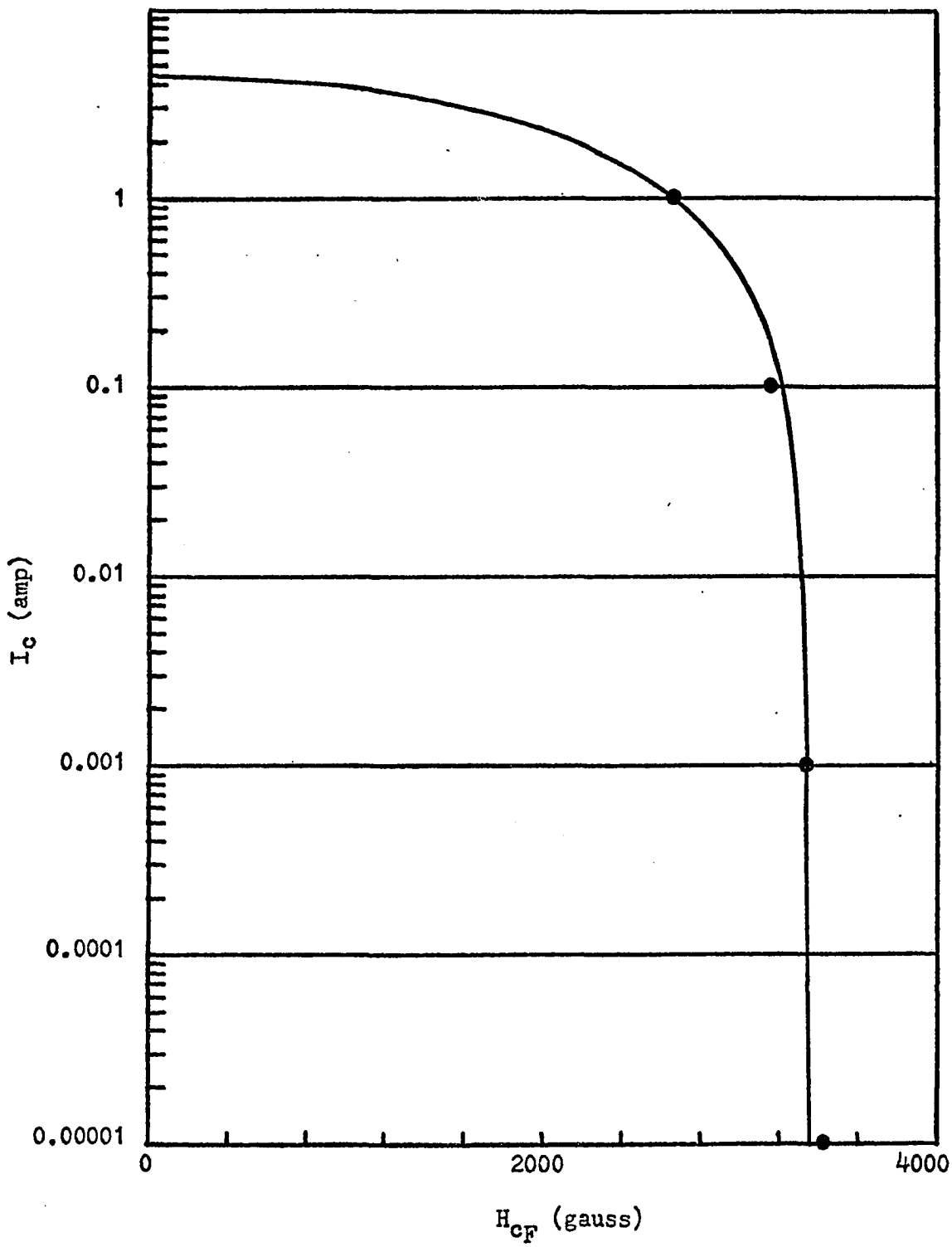

Figure 5 - 25. Critical current I_c versus critical magnetic field H_{cF} of sample S 10.

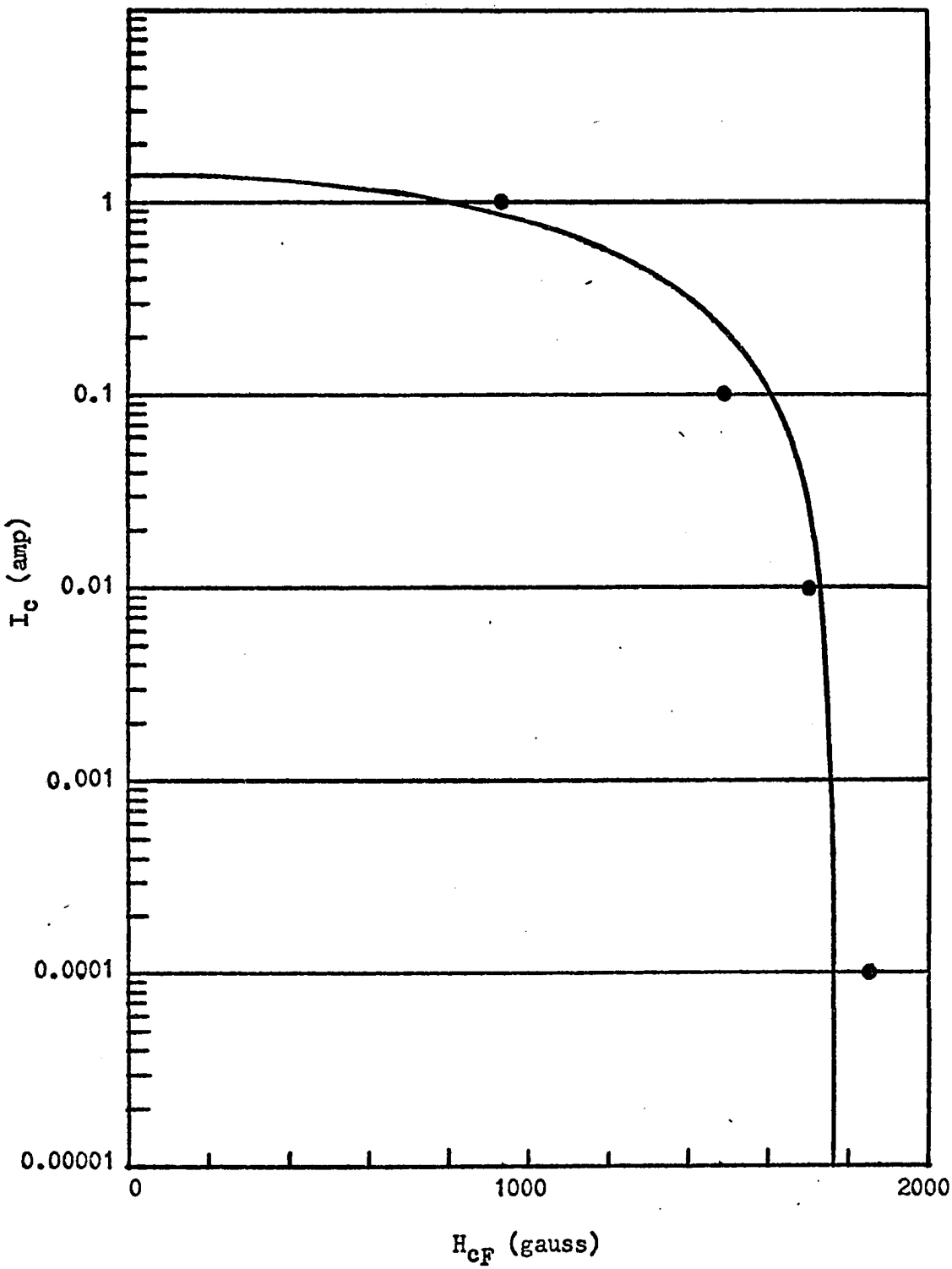

Figure 5 - 26(a). I_c vesus H_{cF} for sample S11.

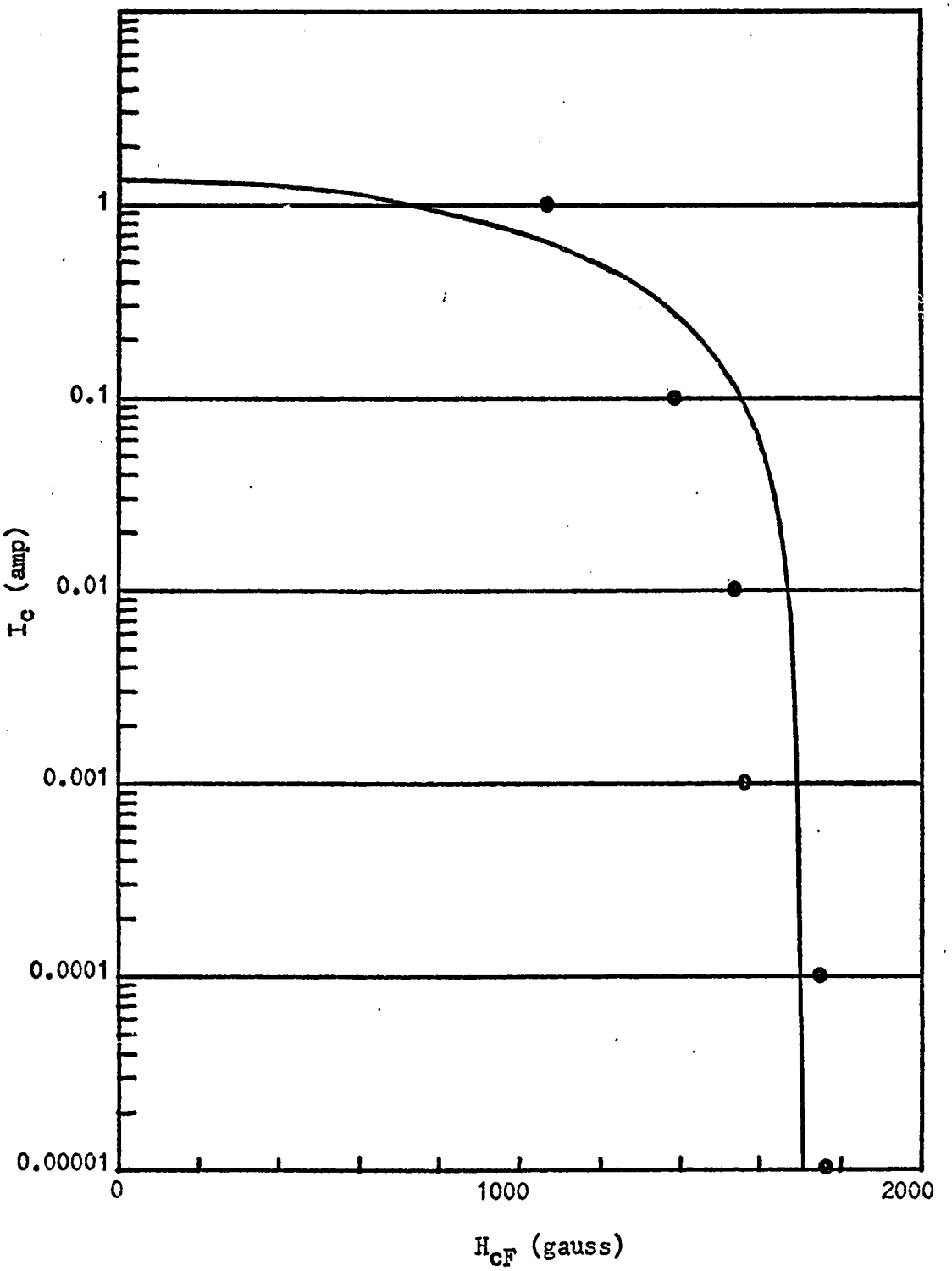

Figure 5 - 26(b). I_c versus H_{cF} for sample R 11.

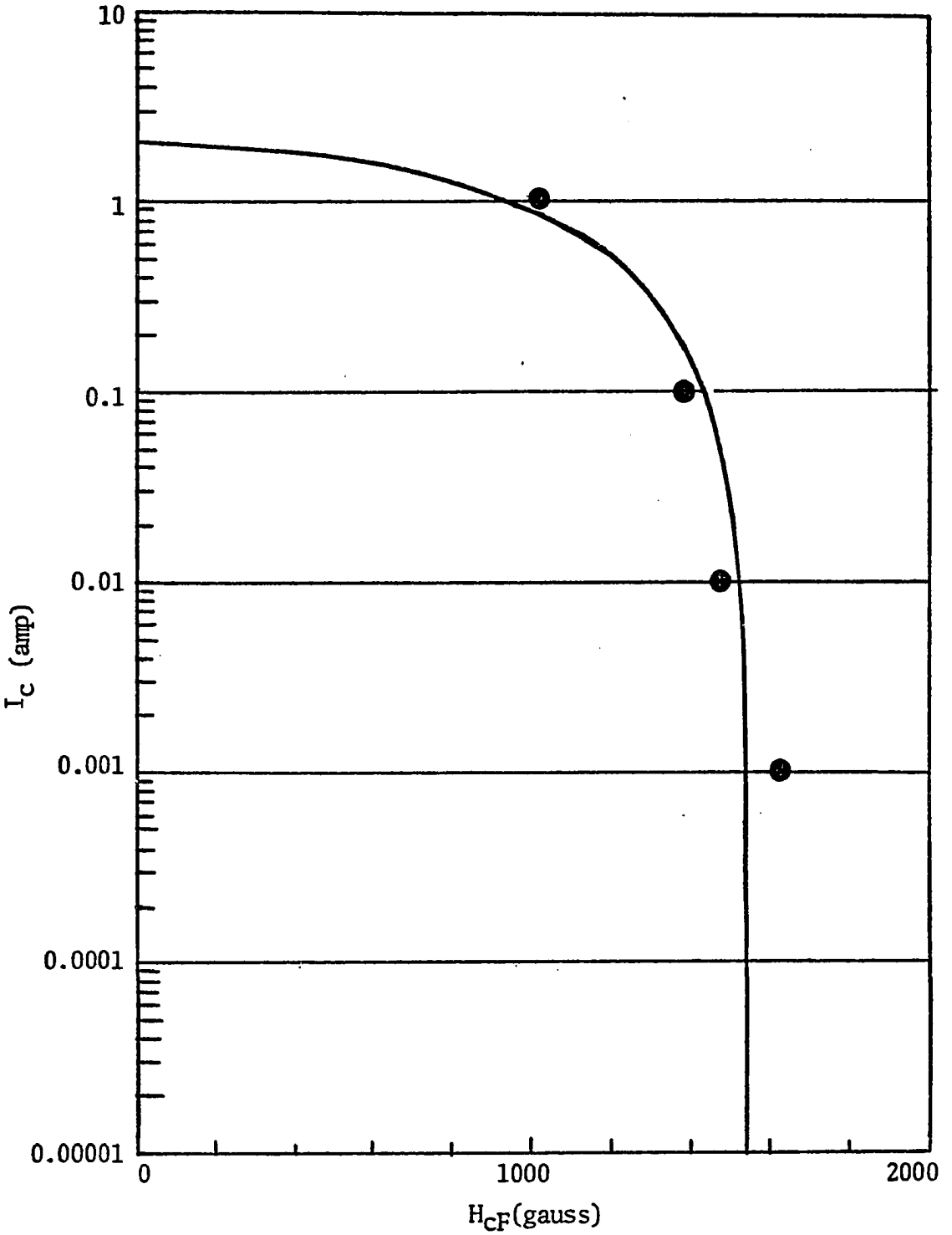

Figure 5 - 27(a). I_c versus H_{cF} for sample S13.

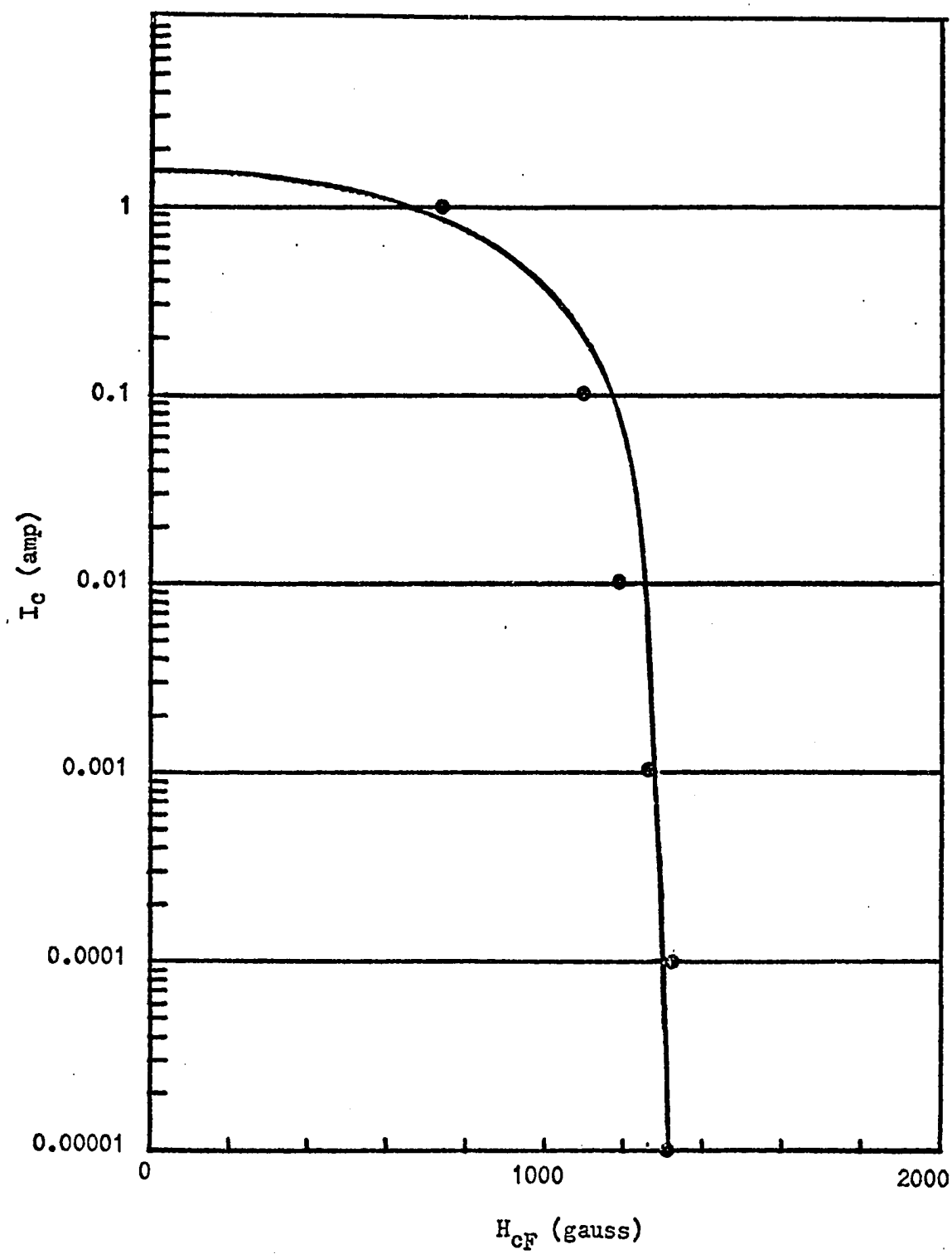

Figur 5 - 27(b). I_c versus H_{cF} for sample R12.

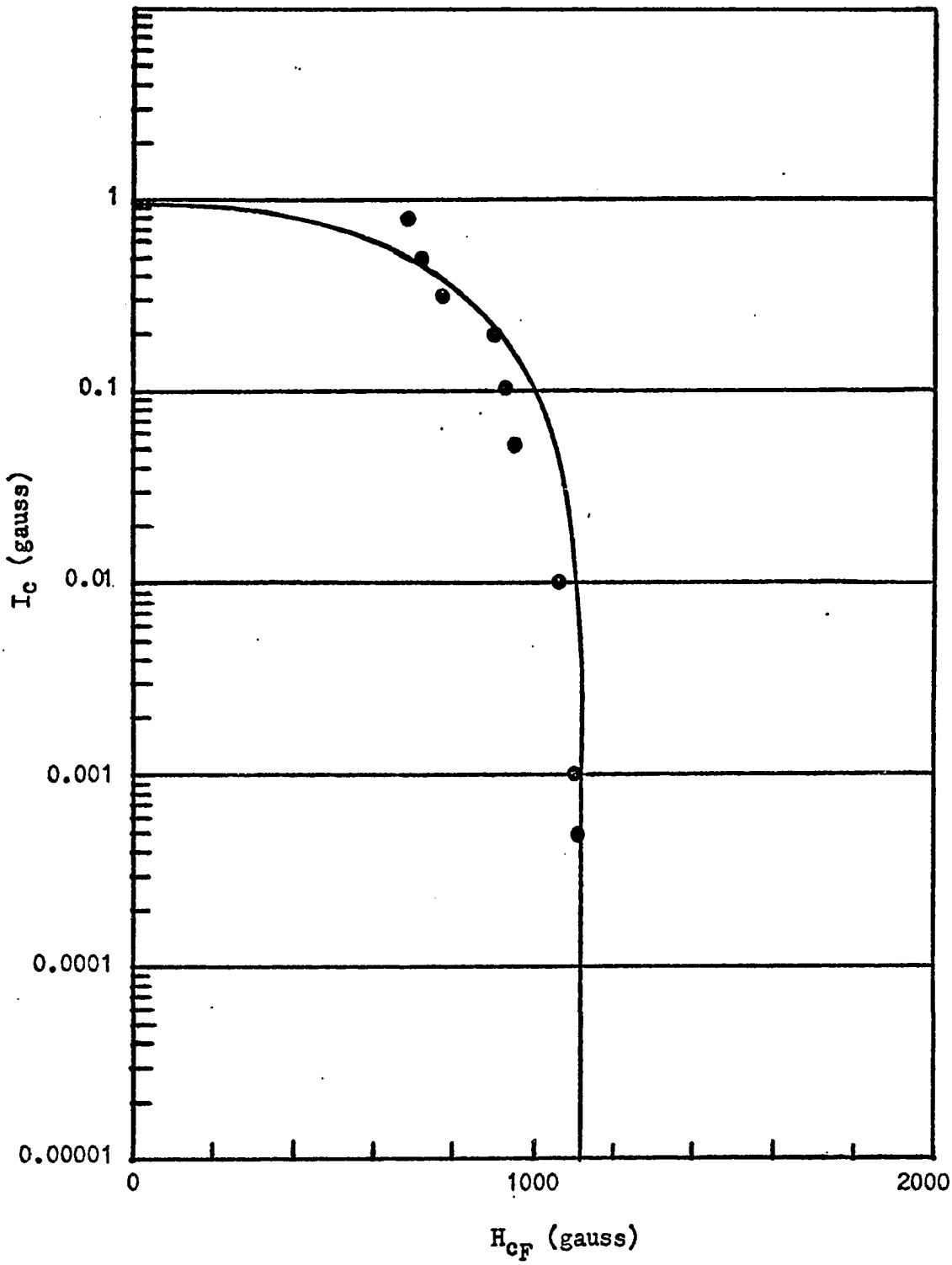

Figure 5 - 28(a). I_c versus H_{cF} for sample S 14.

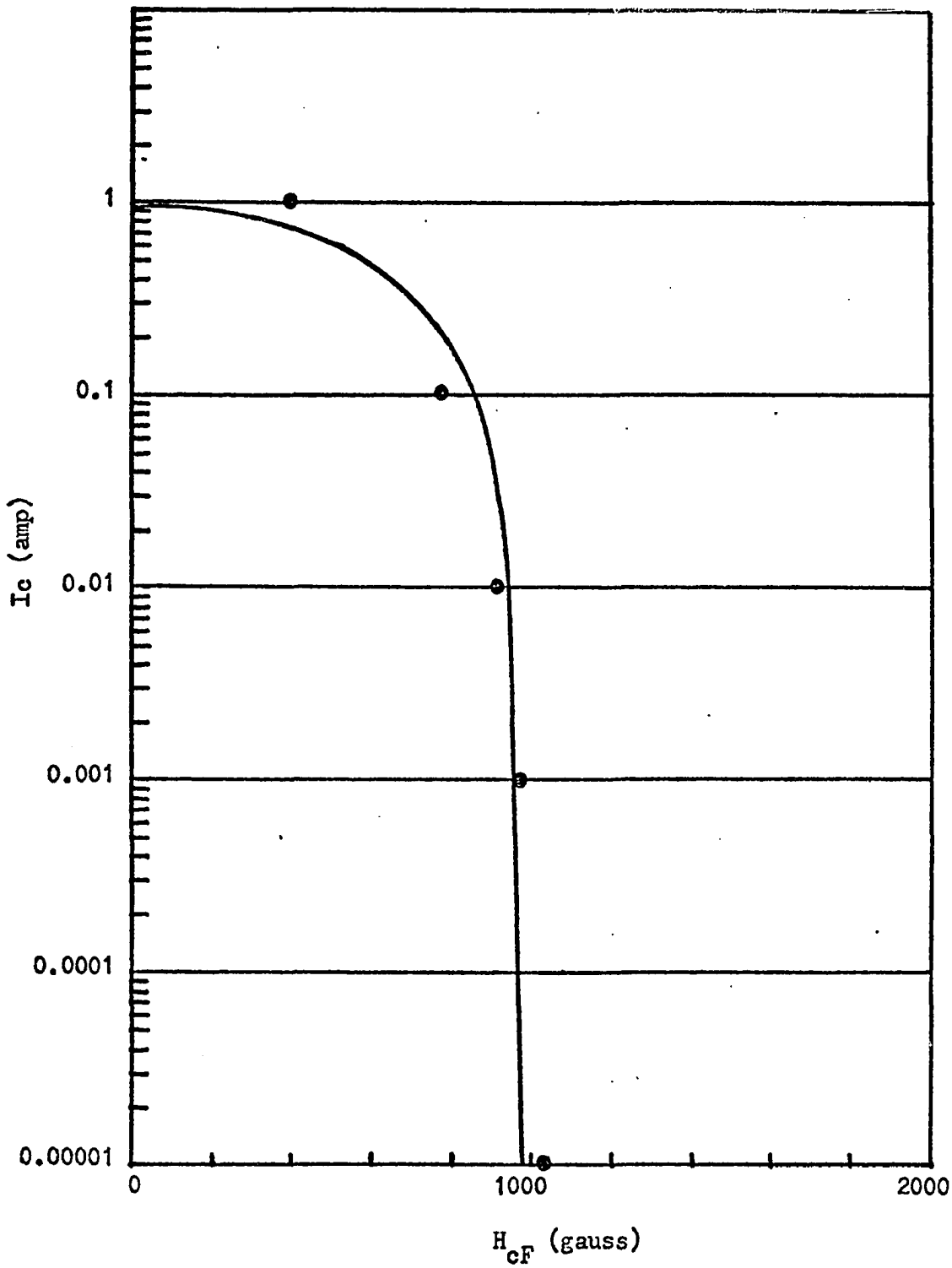

Figure 5 - 28(b). I_c vesus H_{cF} for sample R 14.

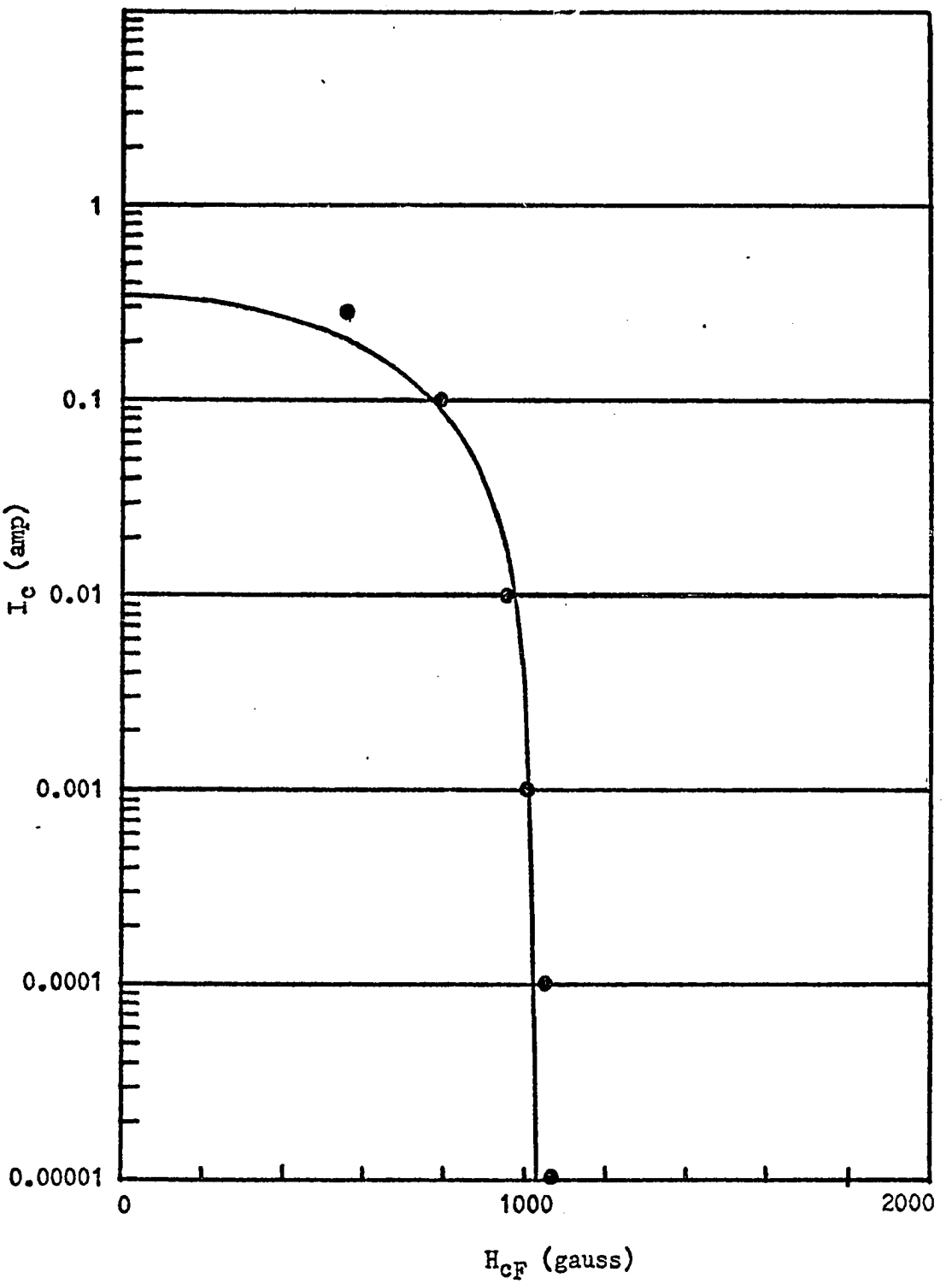

Figure 5 - 29. I_c versus H_{cF} for sample S15.

CHAPTER VI

CONCLUSIONS

1. The temperature dependence of the critical magnetic field of both thin and thick films was measured and these measurements are consistent with the models of London, Ginzburg-Landau, and BCS theories (Equations 55 and 56).

2. H_{CF} is predicted to be proportional to -1.5 power of d for thin film region. In this work, the observed value of the power of d ranges from -1.33 to -1.49. For a thick film region, H_{CF}/H_C -1 is predicted to be proportional to the -1 power of d. The observed value of the power of d is -1.3.

3. The predicted value of the penetration depth $\lambda(0)$ ranges from 305Å to 470Å (See Table 5-3). Observed values in this work are from 327Å to 845Å. Observed values in other work are from 390Å to 819Å.

4. It is expected that a thickness dependence of λ should be observed. However, in this work, it was not observed.

5. The predicted coherence lengths are from 800Å to 1000Å. The values in this work are from 753Å to 40KÅ. The only other observed value by Cody and Miller is around 500Å.

6. The influence of the roughness of the surfaces of substrates on which lead was deposited was observed. The results show that H_{cF} of films deposited on rough surfaces of substrates is lower than that of films deposited on smooth surfaces of substrates. The degree of lowering of H_{cF} by a rough surface is more in thin films than in thick films.

7. The temperature dependence of critical current was found to follow Equation (157) rather than the model of Glover and Coffey, (Equation 126).

8. When the applied magnetic field is perpendicular to the applied current and parallel to the film surface, the relationship between the critical values of magnetic field and current was found to follow themodel of Alphonse and Bergstein (Equation 138) for lead films (type I superconductor).

REFERENCES

1. D.J. Quinn and W.B. Ittner III, J. Appl. Phys. 33 748 (1962).

2. H.K. Onnes, Commun. Phys. Lab. Univ. Leiden, Suppl. no. 34 (1913).

3. A.C. Meta, P.M. Brester, A.C. Lawson, R.W. Fitzgerald and J.H. Bishop, Phys. Lett. 34A 160 (1971).

4. J.R. Gavaler, Appl. Phys. Lett. 23 160 (1971).

5. J. Bardeen, L.N. Cooper, and J.R. Schriffer, Phys. Rev., 108 1175 (1957).

6. H. London and F. London, Proc. Royal Soc. London, A149 71 (1935).

7. V.L. Ginzburg and J.D. Landau, Zh. Eksperim. i Teor. Fiz. 20 1 64 (1950).

8. V.L. Ginzburg, Zh. Eksp. Teor. Fiz. 34 113 (1958); Soviet Phys. JEPT 7 78 (1958).

9. J.M. Lock, Proc. Roy. Sec. London, A200 391 (1951).

10. J.A. Mydosh and H. Meissner, Phys. Rev., 140 A1568 (1965).

11. G.D. Cody, R.E. Miller, Phys. Rev. 173 481 (1968).

12. E. Kratzig, K. Walther and W. Schilz, Phys. Lett. 30A 411 (1969).

13. R.P. Huebener, Phys. Rev. B2 3540 (1970).

14. D.C. Hill, J.G. Kohr and R.M. Rose, Phys. Rev. Letters, 23 764 (1969).

15. H.J. Fink and W.C. H. Joiner, Phys. Rev. Letters, 23 120 (1969).

16. D.D. Morrison and R.M. Rose, Phys. Rev. Letters, 25 356 (1970).

17. P.H. Melville, J. Phys. C: Solid St. Phys., 4 2833 (1971); J. Phys. C: Solid St. Phys. 5 147 (1972).

18. R.M. Esson and P. Hlawicka, Brit. J. Appl. Phys. (J. Phys. D). J. Phys. C: Solid St. Phys. 5 147 (1972).

19. J.F. Bussiere and M. Suenaga, J. Appl. Phys.

20. V.L. Ginzburg, Doklady Akad. Nauk SSSR 118 464 (1958): Soviet Phys. Doklady 3 102 (1958).

21. G.A. Alphonse and L. Bergstein, J. Appl. Phys. 38 5097 (1967).

22. W. Meissner and R. Ochsenfeld, Naturwissenschaften, 21 787 (1933).

23. R. Becker, G. Heller, and F. Sauter, Z. Phys. 85 772 (1933).

24. M. von Laue, Ann. Phys., Lpz., 32 71 (1938).

25. R.B. Pontius, Phil. Mag. 24 787 (1937).

26. A.I. Shalnikov, Nature, 142 74 (1938).

27. E.T.S. Appleyard and A.C.B. Lovell, Proc. Roy. Sec. A158 718 (1937).

28. E.T.S. Appleyard and A.D. Misener, Nature, 142 474 (1938).

29. E.T.S. Appleyard, J.R. Bristow, and London, Nature 143 433 (1939).

30. E.T.S. Appleyard, J.R. Bristow, H. London, and A.D. Misener, Proc. Roy. Soc. London, A172 540 (1939).

31. N.E. Alekseyevsky, F. Phys. USSR 4 401 (1941).

32. D. Shoenberg, Proc. Roy. Soc. London, A175 49 (1940).

33. H.B.G. Casimir, Physica, 7 887 (1940); Common. Phys. Lab. Univ. Leiden, No. 261c (1940).

34. C.J. Gorter and H.B.G. Casimir, Phys. Z. 35 963 (1934).

35. E.R. Andrew, Proc. Phys. Soc. London, A194 80 (1941).

36. V.L. Ginzburg, J. Phys. USSR 9 305 (1945).

37. A.B. Pippard, Proc. Camb. Phil. Soc. 47 617 (1951).

38. E.R. Andrew, Proc. Phys. Soc. London, A62 88 (1949).

39. J.M. Lock. Proc. Roy. Soc. London, A208 391 (1951).

40. D. Shoenberg, (1952), "Superconductivity", 2nd ed. : Cambridge University Press, New York, (1960).

41. A.B. Pippard, Proc. Roy. Soc. London, A203 210 (1950).

42. A.B. Pippard, Proc. Roy. Soc. London, A216 547 (1953).

43. L.D. Landau, Phys. Z. Sowjet. 11 545 (1937).

44. L.P. Gorkov, Soviet Phys. JETP, 10 593 998 (1960).

45. D.H. Douglass, Jr., Phys. Rev. 124 735 (1961).

46. D.H. Douglass, Jr., and R.H. Blumberg, Phys. Rev. 127 2038 (1962).

47. P.G. de Gennes and M. Tinkham, Physics 1 107 (1964).

48. J. Bardeen, Rev. Mod. Phys. 34 667 (1962).

49. J.J. Hauser and E. Helfand. Phys. Rev. 127 386 (1962).

50. P.B. Miller, Phys. Rev. 113 1209 (1959).

51. M. Tinkham, Phys. Rev. 110 26 (1958).

52. N.V. Zavaritskii, Dokl., Akad. Nauk SSSR, 78 665 (1951).

53. N.V. Zavaritskii, Dokl., Akad. Nauk SSSR 85 749; 86 501 (1952).

54. I.S. Khukhareva, Zh. Eksperim. i Teor. Fiz. 41 728 (1961) Soviet Phys. JETP 14 1526 (1962).

55. A.M. Toxen, Phys. Rev. 127 382 (1962).

56. D.H. Douglass, Jr. and R. Meservet, Phys. Rev. 135 A19 (1964).

57. R.E. Glover III, in "Thin Films", P. 173, American Society for Metals, Metals Park, Ohio, 1964.

58. L.W. Shubnikov, V.I. Khotkevich, J.D. Shepelev, and J. N. Rjabinin, Phys. Z. Sowjet 10 165 (1936).

59. L.W. Shubnikov, V.I. Knotkevich, J.D. Shepelev, and J. N. Rjabinin, Zh. Eksperim. i Teor. Fiz. 7 221 (1937).

60. A.A. Abrikosov, Dokl. Akad. Nauk SSSR 86 43 (1952).

61. A.A. Abrikosov Zh. Eksperim. i Teor. Tiz. 32 1442 (1957).

62. B.B. Goodman, Phys. Rev. Letters 6 597 (1961).

63. J.E. Kunzler, Rev. Mod. Phys. 33 501 (1961).

64. D. Saint James and P.G. de Gennes, Phys. Letters 7 306 (1963).

65. M. Cardona and B. Rosenblum, Low Temp. Phys. IX th. Conf. 560 (1964), LT9.

66. E.H. Rhoderick, Prof. Roy. Soc. London A267 231 (1962).

67. J.P. Burger, G. Deutsher, E. Guyon, and A. Martinent, Phys. Rev. 137 A853 (1965).

68. T. Seidel and H. Meissner, Phys. Letter 17 100 (1965).

69. G.A. Alphonse and L. Bergstein, J. Appl. Ph s. 38 5097 (1967).

70. J.P. Baldwin, Phys. Letters 3 223 (1963).

71 R.D. Tilley, J.P. Baldwin, and G. Robinson, Proc. Phys. Soc. London 89 645 (1966).

72. G. Fischer, Phys. Rev. Letters 20 268 (1968).

73. G.D. Cody and R.E. Miller, Phys. Rev. 173 481 (1968).

74. R.E. Miller and G.D. Cody, Phys. Rev. 173 494 (1968).

75. G.D. Cody, R.E. Miller, Phys. Rev. B5 1834 (1972).

76. L.S. Khuskhareva, Zh. Eksperim. i Teor. Fiz. 43 1183 (1962); Soviet Phys. Jetp 16 828 (1963).

77. P.M. Tedrew and R. Meservey, Phys. Rev. B8 5098 (1973).

78. L.G. Hayler, L.M. Geppert, J.T. Chen, and Y.W. Kim, Phys. Rev. B 11 1924 (1975).

79. W. DeSorbe, Phys. Rev. 132 107 (1963).

80. C.A. Neugebauer and R.A. Ekvall, J. Appl. Phys. 35 547 (1964).

81. J. Sosniak and G.W. Hull, J. Appl. Phys. 38 4390 (1967).

82. P. Hlawiczka and J.M. Ross, Brit. J. Appl. Phys. (J. Phys. D), ser. 2, 1 995 (1968).

83. D.R. Tilley and R. Ward, J. Phys. C: Solid St. Phys. 3 2119 (1970).

84. H.K. Onnes, Commun. Phys. Lab. Univ. Leiden, Suppl. no. 34 (1913); Commun. Phys. Lab. Univ. Leiden, no. 133d (1913).

85. F.B. Silsbee, J. Wash. Acad. Sci., 6 597 (1916).

86. H. London, Proc. Roy. Soc. A, 152 650 (1935).

87. L.W. Schubnikow and N.E. Alekseyevsky, Nature, 138 804 (1936).

88. F. London, Une conceptuin nouvelle de la superconductibilite. Paris; Herman et Cie. (1937).

89. R.B. Scott, Bur. Stand. F. Rec., Wash., 41 581 (1948).

90. C.G. Kuper, Phil. Mag. 42 961 (1951).

91. B.V. Makei, J. Exp. Theor. Phys. USSR 34 312 (1958).

92. D.C. Baird and B.M. Mukherjee, Phys. Rev. B 3 1043 (1971).

93. D.C. Baird and B.K. Mukherjee, Phys. Letters 25A 137(1967).

94. R. Freud, C. Sulkewski, and B. Makiej, Phys. Letters 27A 187 (1968).

95. R.E. Glover, III Low Temperature Physics and Chemistry, edited by J.R. Dillinger (Univ. of Wisconsin Press, Madison, Wisconsin 1958) P. 330.

96. J.W. Bremer and V.L. Newhouse, Phys. Rev. Letters 1 282 (1958).

97. J.W. Bremer and V.L. Newhouse, Phys. Rev., 116 309 (1959).

98. C.R. Smallman, A.E. Slade and M.L. Cohen, Proc. I.R.E., 48 1562 (1960).

99. F.W. Schmidlin, A.J. Learn, E.C. Crittendeu, Jr., and L.N. Cooper, Solid-State Electron., 1 323 (1960).

100. P.M. Marcus, Proc. Seventh Intern. Cof. Low. Temp. Phys., 418 (University Press, Toronto, 1961).

101. R.E. Glover, Proc. Seventh Intern. Conf. Low. Temp. Phys., 421 (University Press, Toronto, 1961) (see discussion of paper by Marcus).

102. E.H. Rhoderick and E.M. Wilson, Nature, 194 1167 (1962).

103. R.F. Broom and E.H. Rhoderick, Proc. Phys. Soc., 79 586 (1964).

104. R.E. Glover, III and H.T. Coffey, Rev. Mod. Phys., 36 299 (1964).

105. J. Bardeen, Rev. Mod. Phys. 34 667 (1962).

106. R.P. Huebener and D.E. Gallus, Phys. Rev. B 7 4089 (1973).

107. L.A. Feigein and A.I. Shlnikov, Dokl. Akad. Nauk (USSR) 108 823; Soviet Phys. Dokl. 1 337 (1956).

108. N.I. Ginzburg and A.I. Shalnikov, Zh. Eksperim. i Teor. Fiz. 31 951 (1956).

109. N.E. Alekseevski and M.N. Mikheeva, Zh. Eksperim. i Teor. Fiz. 38 292 (1960); Soveit Phys. JETP 11 211 (1960).

110. H.H. Edwards and V.L. Newhouse, Phys. Rev. 33 868 (1962).

111. C.A. Neugebauer and R.A. Ekvall, J. Appl. Phys., 35 547 (1964).

112. P. Fowler, J. Appl. Phys., 34 3538 (1963).

113. A. El Bindari and M.M. Litvak, Rev. Mod. Phys. 36 102 (1964).

114. C.J. Gorter and H.B.G. Casimir Physica 2 341 (1935).

115. P.M. Marcus Phys. Rev. 88 373 (1952).

116. W.B. Ittner, III, Phys. Rev. 119 1591 (1960).

117. F. London, "Superfluids", Vol. 1, 2nd ed. New York: Dover.

118. J.R. Schriffer, Phys. Rev. 106 47 (1957).

119. K.T. Rober, Ph.D. dissertation, University of Illinois, 1960 (unpublished).

120. M. Tinkham, "Introduction to Superconductivity" McGraw-Hill (1975).

121. V.L. Ginzburg, Soviet Phys. Doklady 1 541 (1956).

122. J.A. Kok, Physica 1 1103 (1934).

123. M. Tinkham, Phys. Rev. 129 2413 (1963).

124. T.E. Faber and A.B. Pippard, Proc. Roy. Soc. A231 336 (1955).

125. J.P. Burger, G. Deutscher, E. Gvyon, and A. Martinet, Phys. Rev. 137 A853 (1965).

126. R.H. White, Phys. Rev. 142 241 (1966).

127. C.A. Rose-Innes and E.H. Rhoderick, "Introduction to Superconductivity" Pergamon Press (1969).

128. J. Bardeen, Phys. Rev. Letters 1 399 (1958).

129. V.L. Ginzberg and L.D. Landau, Zh. Eksperim. i Teor. Fix. 20 1 64 (1950).

130. R. Meservey and P.M. Tedrow, J. Appl. Phys. 40 2028 (1969).

131. L.N. Cooper, Proc. 7th Intern. Conf. Low Temp. Phys., 416 (University Press, Toronto).

132. V.L. Newhouse, "Applied Superconductivity" Wiley (1964).

133. R.W. Cohen and B. Abeles, Phys. Rev. 168 444 (1968).

134. J. Bardeen and J.R. Schrieffer, "Progress in Low Temperature Physics" 3 170, North Holland Pub. Co. (1961).

135. J.J. Hauser, Phys. Rev. b 10 2792 (1974).

136. R.F. Gasparovic and W.L. McLean, Phys. Rev. B 2 2519 (1970).

APPENDIX 1

Silsbee's method

The case of a wire

1) The wire with the radius $a >> \lambda$

At the surface of the wire, from Ampere's law

$$\oint H\, ds = \frac{4\pi I}{c}$$

$$2\pi a H = \frac{4\pi}{c} 2\pi a \lambda J$$

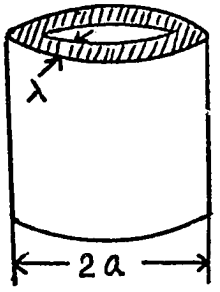

At the transition

$$H_c = \frac{4\pi}{c} \lambda J_c \quad \text{or} \quad J_c = \frac{c}{4\pi\lambda} H_c$$

Since $I = 2\pi a \lambda J$, the critical current by Silsbee's method, I_s is given as

$$I_s = 2\pi a \lambda J_c = \frac{ac}{2} H_c$$



2) The wire with the radius $a << \lambda$

$$2\pi a H = \frac{4\pi}{c} \pi a^2 J$$

At the transition

$$H_c = \frac{2\pi a}{c} J_c \quad \text{or} \quad J_c = \frac{c}{2\pi a} H_c$$

Since $I = \pi a^2 J$, I_s is gives as

$$I_s = \pi a^2 J_c = \frac{ac}{2} H_c$$

At the transition

$$J_c = \frac{c}{4\pi\lambda} H_c$$

Since $I = 2\pi a\lambda J$, the critical current by London's method I_L is

$$I_L = \frac{ac}{2} H_c = I_s$$

2) The wire with the radius $a<<\lambda$

At the transition

$$J_c = \frac{c}{4\pi\lambda} H_c$$

Since $I = \pi a^2 J$, I_L is given as

$$I_L = \left(\frac{a}{2\lambda}\right) \frac{acH}{2} = \left(\frac{a}{2\lambda}\right) I_s$$

The case of a flat film

1) The film with the thickness $d>>\lambda$

$$J_c = \frac{c}{4\pi\lambda} H_c$$

Since $I = \lambda WJ$, I_L is given as

$$I_L = \frac{cW}{4\pi} H_c = I_s$$

2) The film with the thickness $d<<\lambda$

$$J_c = \frac{c}{4\pi\lambda} H_c$$

Since $I = dWJ$, I_L is given as

$$I_L = \left(\frac{d}{\lambda}\right) \frac{Wc}{4\pi} H_c = \left(\frac{d}{\lambda}\right) I_s$$

The case of flat film

1) The film with the thickness $d \gg \lambda$

From Ampere's law

$$H \cdot 2L = \frac{4\pi\lambda}{c} 2LJ$$

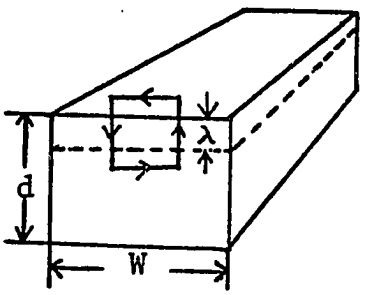

At the transition

$$H_c = \frac{4\pi\lambda}{c} J_c \quad \text{or} \quad J_c = \frac{c}{4\pi\lambda} H_c$$

since $I = W\lambda J$, I_s is given as

$$I_s = \frac{cW}{4\pi} H_c$$

when two sides of the film are penetrated by magnetic fields

$$I_s = \frac{cW}{2\pi} H_c$$

2) The film with the thickness $d \ll \lambda$

$$H \cdot 2L = \frac{4\pi}{c} d \cdot 2LJ$$

at the transition

$$H_c = \frac{4\pi\lambda}{c} J_c \quad \text{or} \quad J_c = \frac{c}{4\pi d} H_c$$

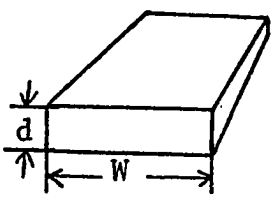

Since $I = WdJ$, I_s is given as

$$I_s = \frac{cW}{4\pi} H_c$$

London's method

The case of a wire

1) The wire with the radius $a \gg \lambda$

From Eq.(72)

$$J_c = \frac{cH_c}{4\pi\lambda}$$

APPENDIX 2

Surface current density on a flat superconducting film by H.H. H.H. Edwards[132]

The surface current density is obtained by carrying out a conformal transformation of the magnetic field around a superconducting cylinder. The magnetic potential lines ϕ for the cylinder are defined so that

$$\nabla\phi = - H = -\frac{2I}{cr}$$

$$\frac{1}{r}\frac{d\phi}{d\theta} = \nabla\phi$$

Hence

$$\phi = \frac{2I\theta}{c}$$

where I is the current carried by the cylinder. If the potential near the cylinder is reoresebted by the equation $Z = r\exp(i\theta)$, the cylinder is transformed to an ellipse by using the transformation.

$$W = \frac{1}{2}\left(Z + \frac{\alpha^2}{Z}\right) = u + iv$$

$$= \frac{1}{2}\left(r + \frac{\alpha^2}{r}\right)\cos\theta + \frac{i}{2}\left(r - \frac{\alpha^2}{r}\right)\sin\theta$$

For r = constant, w is an ellipse which reduces to a line for $\alpha \to r$. For the straight line, the surface field is

$$H = \frac{d\phi}{du} = \frac{d\phi}{d\theta}\frac{d\theta}{du}\Bigg|_{\alpha=r=w}$$

Now

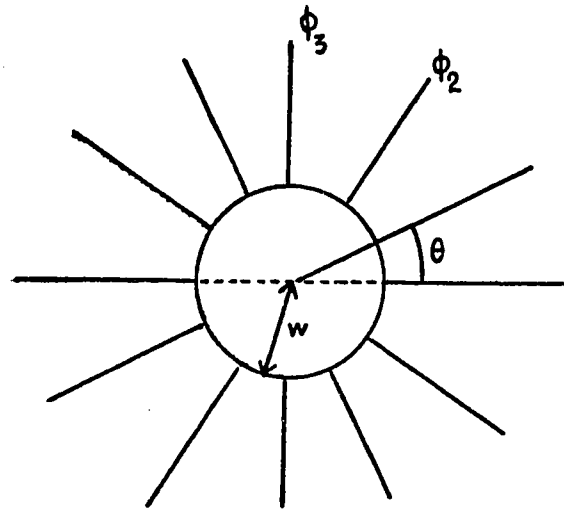

If $\alpha = r$, $u = w \cos\theta$ where w is the cylinder radius.

Hence

$$\frac{du}{d\theta} = w \sin\theta$$
$$= - (w^2 - u^2)^{1/2}$$

Hence at distance u from the center of a flat superconductor of width 2w, carrying a current I, the surface field is

$$H(u) = \frac{2I/c}{(w^2 - u^2)^{1/2}}$$

Hence the surface current density on each surface of the film is

$$J = \frac{H(u)}{4\pi} = \frac{I}{2\pi (w^2 - u^2)^{1/2}}$$